VOLUME 47, NUMBER 4, DECEMBER 2024

HADRONIC JOURNAL Volume 47, Number 4, December 2024

HADRONIC JOURNAL

Founded in 1978 by Prof. R. M. Santilli at Harvard University. Some of the past Editors include Professors S. L. Adler, A. 0. Barut, L. C. Biedenharn, N. N. Bogoliubov, M. Froissart, J.Lohmus, S. Okubo, Nobel Laureate Ilya Prigogine, M. L. Tomber, J. P.Vigier, J. Wess, Nobel Laureate Chen Ning Yang.

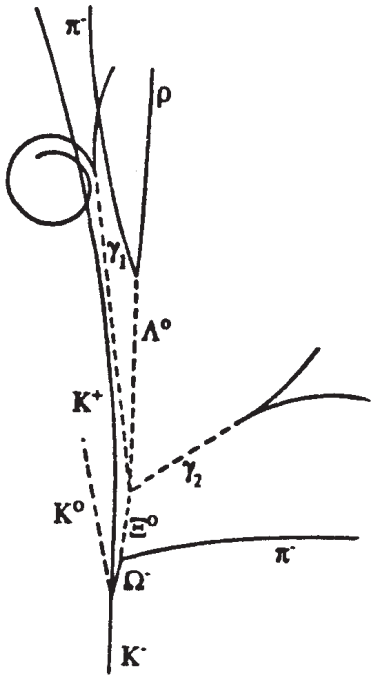

HADRONIC PRESS, INC.

HADRONIC JOURNAL

Established in 1978 by Prof. R. M. Santilli at Harvard University Hadronic Journal and Algebras, Groups and Geometries have been regularly published since 1978 without publication charges and are among the few remaining independent refereed journals.

This Journal publishes advances research papers and Ph. D. theses in any field of mathematics without publication charges.

For subscription, format and any other information please visit the website
http://www.hadronicpress.com

HADRONIC PRESS INC.
35246 U. S. 19 North Suite 215
Palm Harbor, FL 34684, U.S.A.
http://www.hadronicpress.com
Email: info@hadronicpress.com
Phone: +1-727-946-0427

HADRONIC JOURNAL

Founder and Editor in Chief
RUGGERO MARIA SANTILLI
The Institute for Basic Research
35246 U. S. 19 North Suite 215, Palm Harbor, FL 34684, U.S.A.
Email: resarch@i-b-r.org; TEL: +1-727-688-3992

ISSN: 0162-5519

HADRONIC JOURNAL Volume 47, Number 4, December 2024

Established in 1978 by Prof. R. M. Santilli at Harvard University Hadronic Journal and Algebras, Groups and Geometries have been regularly published since 1978 without publication charges and are among the few remaining independent refereed journals.

This Journal publishes advances research papers and Ph. D. theses in any field of mathematics without publication charges.

For subscription, format and any other information please visit the website http://www.hadronicpress.com

HADRONIC PRESS INC.
35246 U. S. 19 North Suite 215
Palm Harbor, FL 34684, U.S.A.
http://www.hadronicpress.com
Email: info@hadronicpress.com
Phone: +1-727-946-0427

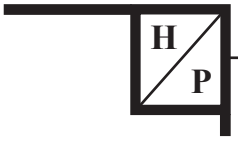

HADRONIC PRESS, INC.

HADRONIC JOURNAL

VOLUME 47, NUMBER 4, DECEMBER 2024

HADRONIC JOURNAL 47, 381 - 409 (2024)
DOI 10.29083/HJ.47.04.2024/SC381

THE PHYSICAL INTERPRETATION OF THE SPINOR CONDITIONS FOR THE WAVE EQUATION

Simon Davis
Research Foundation of Southern California
8861 Villa La Jolla Drive #13595
La Jolla, CA 92307
sbdavis@resfdnsca.org

Received April 26, 2024
Revised August 26, 2024

Abstract

The nonrelativistic equation may be derived from generalized commutation relations with a matrix form of the momentum operator. The four-component spinor may be reduced to two components by a Majorana or anti-Majorana condition, which produce different coefficients of the Laplacian. The condition on the Hermitian conjugate of a Majorana fermion field is the equivalent of the anti-Majorana spinor, and a theoretical explanation is given for the essentially vanishing positron current in system consisting of negative-energy electron states. The mass of the electron would result from its representation as a predominantly Majorana spinor. The transformations from Weyl spinors to Majorana spinors can be mapped isomorphically to a subset of an $SL(2;\mathbb{R})$ subgroup of $SL(2;\mathbb{C})$, which reflects the infinitesimal mass of the neutrino. The neutrino mass term can be transformed into another spinor bilinear through this transformation. After a transition to a quantum state with the coefficient derived from this expansion, an iteration of the algorithm yields a final state with after a finite sequence. The identification of these states in each fermion generation with the leptons provides a theoretical explanation of the Koide relation for leptons and neutrinos and a prediction for m_{ν_e}, m_{ν_μ} and m_{ν_τ}. A generalized wave equation is deduced from the Hamilton-Jacobi equation for the WKB wavefunction and the path integral for a new nonrelativistic action.

PACS: 03.65.Fd, 11.40.Dw, 14.60.Cd

Keywords: *Majorana spinors, vanishing bilinears, position current, spinor automorphism*

1. Introduction

The commutation relations of quantum mechanics can be given a functional form by equating the momentum operator with $-i\hbar\frac{d}{dx}$. The commutator of the position and momentum variables then would be $[x,p]=i\hbar$. By contrast, the Poisson bracket of these phase space coordinates in classical mechanics are $\{x,p\}_{P.B.}=1$, and there exists no classical limit of the quantum commutator without introducing a real term into the relations.

The condition of Hermiticity of the observables then requires that the real term is not a numerical multiple of $\frac{\partial}{\partial x}$. Instead, a matrix is added to the generalized momentum. In three dimensions, it would be $\tilde{p}_i=(\kappa_0\gamma^i-i\hbar)\frac{\partial}{\partial x_i}$ [2]. The adjoint equals $\tilde{p}_i^\dagger=(\kappa_0(\gamma^i)^\dagger+i\hbar)$

$\partial x_i\sim\kappa_0\gamma^i\frac{\partial}{\partial x^i}-i\hbar\frac{\partial}{\partial x_i}$. The equation for the energy

$$\frac{p^2}{2m}+V(x)=E \tag{1.1}$$

now becomes

$$\frac{1}{2m}\left(-\kappa_0^2\mathbb{I}-\hbar^2\right)\nabla^2\psi-i\frac{\kappa_0\hbar}{m}\gamma^i\nabla^2\psi+V\psi=E\psi, \tag{1.2}$$

which represents a coupled set of equations for the components $\psi_1,,\psi_4$.

The equations may be simplified by imposing a condition on the spinor of the form $\bar{\psi}=\pm\psi^TC$, where C is the charge conjugation matrix. When $\bar{\psi}=-\psi^TC$, and the components are real, the set of coupled equations reduces to the Schrödinger equation in one dimension

$$-\frac{\hbar^2}{2m}\frac{\partial^2\psi}{\partial y^2}+V(y)\psi=E\psi \tag{1.3}$$

when κ_0 is set equal to $\hbar$ after setting the derivatives with respect to the other coordinates equal to zero. However, if $\bar{\psi}=\psi^TC$ and the components are real, the nonrelativistic wave equation is altered to

$$-\frac{3\hbar^2}{2m}\frac{\partial^2\psi}{\partial y^2}+V(x)\psi=E\psi. \tag{1.4}$$

The effect of the new coefficient is generally a multiplicative factor in the energy levels.

The consequences of these spinor conditions will be investigated. The fermions in four-dimensional quantum field theories usually satisfy the relations $\bar{\psi}=\psi^\dagger\gamma=\psi^TC$. These actions generally are Lorentz invariant, and a generalization to the nonrelativistic equation for scalar and spin-$\frac{1}{2}$ fields is necessary. The modified equations have been developed [1][3] and a study of the Lagrangian field theories then would follow. The anti-Majorana condition

$\bar{\psi} = -\psi^T C$ also shall be examined with respect to its effect on transformations of spinor bilinears.

The vanishing of a set of bilinears for Majorana and anti-Majorana spinors is developed in a study of the positron current. The Hermitian adjoint of a Majorana fermion field is found to be compatible with the equivalent of an anti-Majorana spinor condition. The spinor bilinear representing the current constructed from the Hermitian adjoint then vanishes for these fermions. A theoretical explanation then may be given for the nearly vanishing positron current in the system of negative energy electron states.

The electron would be a predominantly Majorana spinor field, which causes the observation of particles with the effective mass reduced by a factor of 3 in cosmic rays. The neutrino is essentially a chiral spinor, which is a nearly massless field. Both the electron and the neutrino occur in an $SU(2)$ isospin doublet in the theory of the electroweak interactions. A connection between the mass terms of the lepton and the neutrino is established by demonstrating the existence of a transformation between the Weyl spinor and the Majorana or anti-Majorana spinors. Both mass terms require a combination of different types of spinors to be nonvanishing. The neutrino spinor bilinear may be expanded to give two bilinears consisting of Majorana and anti-Majorana spinors. The first vanishes, while the second has a coefficient that is increased by a factor of 2, After a transition to a different set of four-component spinors that are embedded in an eight-component spinor similarly to the chiral spinors, an iteration of the transformation yields a sequence of scalar bilinears of quantum states. The sequence continues until a finite quantum state, which has a coefficient representing the mass of this state. The mass coincides with that of the electron in the first fermion generation. The proportionality of the mass of the lepton and the neutrino is demonstrated to be valid in the second and third fermion generations by the Koide relation. The masses of these neutrinos are predicted from the proportionality and the masses of the muon and tau lepton.

The Schrödinger equation may be deduced from a Hamilton-Jacobi equation and also the path integral. The first method consists of an equality between the wavefunction and the exponential of the WKB phase factor. The second follows from a definition of the expansion of the path integral over an infinitesimal time interval. A generalized Lagrangian in the path integral results in a modified Schrödinger equation.

2. The Effect of the Spinor Conditions in Quantum Field Theory

Beginning with the nonrelativistic matrix wave equation in component form

$$(2.1)\quad -\frac{(\kappa_0^2+\hbar^2)}{2m}\nabla^2\begin{pmatrix}\psi_1\\ \psi_2\\ \psi_3\\ \psi_4\end{pmatrix}$$

$$(2.2)\quad -\frac{i\kappa_0\hbar}{m}\begin{pmatrix}0 & 0 & \partial_3^2 & \partial_1^2-i\partial_2^2\\ 0 & 0 & \partial_1^2+i\partial_2^2 & -\partial_3^2\\ -\partial_3^2 & -\partial_1^2+i\partial_2^2 & 0 & 0\\ -\partial_1^2-i\partial_2^2 & \partial_3^2 & 0 & 0\end{pmatrix}\begin{pmatrix}\psi_1\\ \psi_2\\ \psi_3\\ \psi_4\end{pmatrix}$$

$$+V(x)\begin{pmatrix}\psi_1\\ \psi_2\\ \psi_3\\ \psi_4\end{pmatrix}=E\begin{pmatrix}\psi_1\\ \psi_2\\ \psi_2\\ \psi_3\\ \psi_3\\ \psi_4\end{pmatrix}$$

with $\kappa_0=\hbar$,

$$(2.3)\quad \begin{aligned}
&-\frac{\hbar^2}{m}\nabla^2\psi_1-i\frac{\hbar^2}{2m}\partial_3^2\psi_3-i\frac{\hbar^2}{2m}\partial_1^2\psi_4-\frac{\hbar^2}{2m}\partial_2^2\psi_4+V(x)\psi_1=E\psi_1\\
&-\frac{\hbar^2}{m}\nabla^2\psi_2-i\frac{\hbar^2}{2m}\partial_1^2\psi_3+\frac{\hbar^2}{2m}\partial_2^2\psi_3+i\frac{\hbar^2}{2m}\partial_3^2\psi_4+V(x)\psi_4=E\psi_4\\
&-\frac{\hbar^2}{m}\nabla^2\psi_3+i\frac{\hbar^2}{2m}\partial_3^2\psi_1+i\frac{\hbar^2}{2m}\partial_1^2\psi_2+\frac{\hbar^2}{2m}\partial_2^2\psi_2+V(x)\psi_3=E\psi_3\\
&-\frac{\hbar^2}{m}\nabla^2\psi_4+i\frac{\hbar^2}{2m}\partial_1^2\psi_1-\frac{\hbar^2}{2m}\partial_2^2\psi_1-i\frac{\hbar^2}{2m}\partial_3^2\psi_2+V(x)\psi_4=E\psi_4.
\end{aligned}$$

The spinor now will be required to satisfy the condition $\bar{\psi} = \psi^T C$, where $C = \begin{pmatrix} 0 & & & \\ & -i\sigma^2 & & \\ & & -i\sigma^2 & \\ & & & 0 \end{pmatrix}$ is the charge conjugation matrix in the Dirac representaion. Then $\psi_1^* = \psi_4$ and $\psi_2^* = -\psi_3$ and

$$
\begin{aligned}
(2.4) \qquad -\frac{3\hbar^2}{2m}\partial_2^2\psi_1 + V(x)\psi_1 &= E\psi_1 \\
-\frac{3\hbar^2}{2m}\partial_2^2\psi_2 + V(x)\psi_2 &= E\psi_2.
\end{aligned}
$$

The anti-Majorana condition $\bar{\psi} = -\psi^T C$ has the solutions $\psi_1^* = -\psi_4$ and $\psi_2^* = \psi_3$. The set of coupled differential equations [2] then is

$$
\begin{aligned}
(2.5) \qquad -\frac{\hbar^2}{m}\nabla^2\psi_1 - i\frac{\hbar^2}{2m}\partial_3^2\psi_2 + i\frac{\hbar^2}{2m}\partial_1^2\psi_1^* + \frac{\hbar^2}{2m}\partial_2^2\psi_1^* + V(x)\psi_1 &= E\psi_1 \\
-\frac{\hbar^2}{m}\nabla^2\psi_2 - i\frac{\hbar^2}{2m}\partial_1^2\psi_2^* + \frac{\hbar^2}{2m}\partial_2^2\psi_2^* - i\frac{\hbar^2}{2m}\partial_3^2\psi_1^* + V(x)\psi_2 &= E\psi_2 \\
-\frac{\hbar^2}{m}\nabla^2\psi_2^* + i\frac{\hbar^2}{2m}\partial_3^2\psi_1 + i\frac{\hbar^2}{2m}\partial_1^2\psi_2 + \frac{\hbar^2}{2m}\partial_2^2\psi_2 + V(x)\psi_2^* &= E\psi_2^* \\
\frac{\hbar^2}{m}\nabla^2\psi_1^* + i\frac{\hbar^2}{2m}\partial_1^2\psi_1 - \frac{\hbar^2}{2m}\partial_2^2\psi_1 - i\frac{\hbar^2}{2m}\partial_3^2\psi_2 - V(x)\psi_1^* &= E\psi_1^*.
\end{aligned}
$$

The fourth equation is the negative of the conjugate of the first, and the third equation is the conjugate of the second. For a real spinor, with $\partial_1\psi = \partial_3\psi = 0$,

$$
\begin{aligned}
(2.6) \qquad -\frac{\hbar^2}{2m}\partial_2^2\psi_1 + V(x)\psi_1 &= E\psi_1 \\
-\frac{\hbar^2}{2m}\partial_2^2\psi_1 + V(x)\psi_2 &= E\psi_2.
\end{aligned}
$$

which is the Schrödinger equation in one dimension if the potential is a function only of x^2.

The generalization of the momentum operator then may be extended to relativistic scalar fields and fermions. the analogue of the Klein-Gordon equation [3] is

$$
(2.7) \qquad -3\frac{\partial^2\phi}{\partial t^2} - 5\nabla^2\phi + m^2\phi = 0
$$

and the square root [1] is given by

$$(\sqrt{3}\gamma^0\partial_0 - \sqrt{5}\gamma^i\partial_i - m)\psi = 0. \tag{2.8}$$

It may be recalled that the relativistic formula

$$E = \sqrt{c^2|\vec{p}|^2 + m^2c^4} \tag{2.9}$$

can be expanded as

$$E = mc^2 + \frac{|\vec{p}|^2}{2m} - \frac{|\vec{p}|^4}{8m^3c^2} + \dots . \tag{2.10}$$

Incorporating the rest mass energy mc^2 into $V(x)$, the classical approximation $E_{tot} = \frac{|\vec{p}|^2}{2m} + V(x)$ would be valid to $O\left(\frac{v^4}{c^4}\right)$ when $v \ll c$.

Therefore, the nonrelativistic equation must be recovered in this limit. It is consistent, therefore, to consider the spinor conditions in the relativistic field theories. First, when $\bar{\psi} = \psi^T C$, the equation of motion for the fermion is given by Eq.(2.9), derived from from the modified Klein-Gordon equation (2.8), which is equivalent to the energy formula

$$\tilde{E}^2 \sim \frac{5}{3}c^2|\vec{p}_\ell|^2 + \frac{m^2c^4}{3} \tag{2.11}$$

where the energy is defined with respect to the Euclidean coordinate τ, with $t = i\tau$. The momentum vector $p^\mu = (p^0\vec{p})$ is a Lorentz four-vector, and yet the derivatives in the classical mechanics may defined with respect to a time coordinate that is independent of the spatial coordinates. Furthermore, with the magnitude of momentum $|\vec{p}|^2 = m\left|\frac{d\vec{x}}{dt}\right|$

$= m\left|-i\frac{d\vec{x}}{d\tau}\right|^2 = m\left|\frac{d\vec{x}}{d\tau}\right|^2$, and the entire formula (2.12) can be interpreted with a single time variable. It is clearly a modification of the standard relation between energy and momentum which occurs also in the formula obtained from the nonrelativistic wave equation (2.5) with a coefficient of 3.

The fermion action giving rise to Eq.(2.9) is

$$S_{ferm.} = \int d^4x\bar{\psi}\left[\sqrt{3}\gamma^0\partial_0 - \sqrt{5}i\gamma^i\partial_i - m\right]\psi. \tag{2.12}$$

and the quantum propagator [1] equals

$$S_{F\alpha\beta} = 25i\frac{((1+i\gamma_5)(\gamma\cdot p + m))_{\alpha\beta}}{5E^2 + 3|\vec{p}|^2 + m^2}. \tag{2.13}$$

in units with $\hbar = 1$. The scattering cross sections for various reactions near the classical scales then may be computed through the diagrammatic expansion of the S-matrix,

Now suppose that the conjugate of the fermion field is $\bar{\psi} = -\psi^T C$. The Schrödinger equation is recovered in the nonrelativistic limit, and the quantization of the relativistic action then could be developed with the standard energy formula without matrix operators. The Klein-Gordon and Dirac equations would be derived. Both the action and the perturbation series would be similar to the standard expressions except that the spinor bilinears would be defined to be $\bar{\psi}\gamma^{\mu_1}...\gamma^{\mu_r}\chi = -\psi^T C\gamma^{\mu_1}...\gamma^{\mu_r}\chi$.

Consider spinor bilinears $\bar{\psi}$ and $\bar{\psi}\gamma^\mu\psi$, where the Dirac and Majorana conjugates are equal, $\bar{\psi} = \psi^\dagger\gamma^0 = \psi^T C$. While

For an anti-Majorana spinor

$$\begin{aligned}(2.14)\qquad \bar{\psi}\psi &= -\psi^T C\psi = -(\psi^T C\psi)^T = -\psi^T C^T\psi \\ &= \psi^T C\psi = -(-\psi^T C)\psi - -\bar{\psi}\psi\end{aligned}$$

and $\bar{\psi}\psi$ must equal zero, while

$$\begin{aligned}(2.15)\qquad \bar{\psi}\gamma^\mu\psi &= -\psi^T C\gamma^\mu\psi = -\psi^T(-\gamma^\mu)^T C\psi \\ &= \psi^T(\gamma^\mu)^T C\psi = (\psi^T(\gamma^\mu)^T C\psi)^T = \psi^T C^T\gamma_\mu\psi \\ &= -\psi^T C\gamma^\mu\psi \\ &= \bar{\psi}\gamma^\mu\psi.\end{aligned}$$

Again, the current density can be nonvanishing. The other bilinears are

$$\begin{aligned}(2.16)\qquad \bar{\psi}\gamma_5\psi &= -\psi^T C\gamma_5\psi = -\psi^T\gamma_5^T C\psi \\ &= -(\psi^T\gamma_5^T C\psi)^T = -\psi^T C^T\gamma_5\psi \\ &= \psi^T C\gamma_5\psi - = -\bar{\psi}\gamma_5\psi\end{aligned}$$

$$\begin{aligned}(2.17)\qquad \bar{\psi}\gamma^{[\mu}\gamma^{\nu]}\psi &= -\psi^T C\gamma^{[\mu}\gamma^{\nu]}\psi = -\psi^T(-\gamma^{[\mu T})(-\gamma^{\nu]T})C\psi \\ &= -\psi^T\gamma^{[\nu\ T}\gamma^{\mu]T}C\psi = -(\psi^T\gamma^{[\nu\ T}\gamma^{\mu]T}C\psi)^T \\ &= -\psi^T C^T\gamma^{[\nu}\gamma^{\mu]}\psi = -\psi^T(-C)(-\gamma^{[\mu}\gamma^{\nu]})\psi \\ &= -\psi^T C\gamma^{[\mu}\gamma^{\nu]}\psi = \bar{\psi}\gamma^{[\mu}\gamma^{\nu]}\psi\end{aligned}$$

and

$$\begin{aligned}(2.18)\qquad \bar{\psi}\gamma^\mu\gamma_5\psi &= -\bar{\psi}^T C\gamma^\mu\gamma_6\psi = -\psi^T(-\gamma^{\mu\ T}C\gamma_5\psi \\ &= \psi^T\gamma^{\mu\ T}\gamma_5^T C\psi = (\psi^T\gamma^{\mu\ T}\gamma_5^T C\psi)^T = \psi^T C^T\gamma_5\gamma^\mu\psi \\ &= -\psi^T C\gamma_5\gamma^\mu\psi = \psi^T C\gamma^\mu\gamma_5\psi \\ &= -\bar{\psi}\gamma^\mu\gamma_5\psi.\end{aligned}$$

Consequently, $\bar{\psi}\gamma_5\psi$ and $\bar{\psi}\gamma^\mu\gamma_5\psi$ would equal zero and there are no Lagrangian field theories consisting of a fermion field satisfying the anti-Majorana spinor condition with axial currents.

3. Particle and Antiparticle Currents

The expansion of a fermion field psi is

$$(3.1)\qquad \psi(x) = \frac{1}{(2\pi)^3}\int\frac{d^3p}{2p^0}\sum_s [a_s^\dagger(\vec{p})e^{-ip\cdot x}u_s(p) + b_s^\dagger(\vec{p})e^{ip\cdot x}v_s(p)]$$

where $a_s(\vec{p})$ is annihilation operator of a particle state, $b_s^\dagger(\vec{p})$ is a creation operator of an anti-particle state of momentum $\vec{p}$ and helicity s, and $u_s(\vec{p})$ and $v_s(\vec{p})$ are two-component spinors normalized by $u_r^\dagger(\vec{p})u_s(\vec{p}) = v_r^\dagger(\vec{p})v_s(\vec{p}) = 2E_p\delta_{rs}$. Both sets of terms represent the equivalent of the annilhilation of a single fermion state, since the creation of the antiparticle is interpreted to be the removal of an electron. The hermitian adjoint of this field is

$$(3.2)\qquad \psi^\dagger(x) = \frac{1}{(2\pi)^3}\int\frac{d^3p}{2p^0}\sum_s [a_s^\dagger(\vec{p})e^{ip\cdot x}]u_s^\dagger(\vec{p}) + b_s(\vec{p})e^{-ip\cdot x}v_s^\dagger(\vec{p})]$$

there describes the expansion of the antiparticle field. Nevertheless, the formulation of these integrals is consistent with ψ annihilating particle states and $\psi^\dagger$ creating particle states. Suppose that $\psi(x)$ is a Majorana spinor. Then

$$(3.3)\qquad \overline{\bar{\psi}^\dagger} = (\psi^T C)^\dagger = (C^T)^*(\psi^{dag})^T = -C(\psi^\dagger)^T$$

which is the equivalent of the anti-Majorana condition. From §2, $\bar{\chi}\gamma^\mu\chi$ is not required to be zero when χ is an anti-Majorana spinor. However, given that ψ is a Majorana spinor and $\psi^\dagger$ is an anti-Majorana spinor,

$$(3.4)\qquad \begin{aligned}\psi^\dagger &= \bar{\psi}\gamma^0 = \psi^T C\gamma^0 \\ \bar{\psi}^\dagger &= (\psi^\dagger\gamma^0)^\dagger = \gamma^0\psi\end{aligned}$$

where C is the charge conjugation matrix with $C^{-1} = C^T = -C$, $C^* = C$, and

$$
\begin{aligned}
(3.5) \qquad \psi_A^\dagger \gamma^\mu \overline{\psi_A^\dagger} &= -\psi_A^T C \gamma^0 \gamma^\mu \gamma^0 \psi_M = -\psi_A^T C (\gamma^\mu)^\dagger \psi_M \\
&= -\psi_M^T (\gamma^\mu)^* C^T \psi_A = -(\psi^\dagger \gamma^0 C^{-1})_M (\gamma^\mu)^* C^T \gamma^0 \bar{\psi}_A^\dagger \\
&= \psi_A^\dagger \gamma^0 C^{-1} (\gamma^\mu)^* C \gamma^0 \bar{\psi}_A^\dagger = \psi_A^\dagger \gamma^0 (-\gamma^\mu)^\dagger \gamma^0 \bar{\psi}_A^\dagger \\
&= -\psi_M^\dagger \gamma^\mu \overline{\psi_A^\dagger},
\end{aligned}
$$

wherer ψ_M is the Majorana fermion and $\psi_A^\dagger$ is the anti-Majorana anti-fermion. The difference between this bilinear and Eq.(2.20) is the role of ψ as a Majorana spinor, which yields the identity $\psi^\dagger = \psi^T \gamma^0 C^{-1}$. Consequently, the current $\psi^\dagger \gamma^\mu \overline{\psi^\dagger}$ vanishes.

The physical effect of this vanishing current may be related to the filling of the negative energy electron states [5]. The zero-energy state, with no positive energy electrons, generally would be regarded as inert without any movement or interactions. The scattering off a system in this zero-energy state releases an electron from one of the negative energy states, which cannot be reached from positive energies by the exclusion principle, and creates a positron. It is evident that the energy is imparted to the electron externally with positron remaining nearly static internally within the initially zero-energy system. Consequently, the electrons may generate a current, while there may be essentially no positron current.

Positrons have been identified with electrons moving backwards in time [7]. If an electron wavefunction is represented as $u_s(\vec{p}) e^{-ip\cdot x} = u_s(\vec{p}) e^{-iE_p t + i\vec{p}\cdot\vec{x}}$, the reversal of time would transform the positive frequency mode to $e^{iE_p t + i\vec{p}\cdot\vec{x}}$ or equivalently $e^{-i(-E_p)t + i\vec{p}\cdot\vec{x}}$, which has negative energy. Therefore, the positron state can be viewed alternatively as a negative energy electron state.

The zero-energy state then consists of a continuum of positrons without only negligible motion. The positron current then would be almost zero. By contrast, it is possible for a nonvanishing electron current externally to this state. The vanishing of the current for $\psi^\dagger$ then verifies the dynamics of this physical model of the electron as a predominantly Majorana spinor field.

A general fermion field ψ can be written as a linear combination of a Majorana spinor ψ_1 and an anti-Majorana spinor ψ_1 since

$$\psi = k_1\psi_1 + k_2\psi_2 = k_1 \begin{pmatrix} \psi_{11} \\ \psi_{12} \\ -\psi_{12}^* \\ \psi_{11}^* \end{pmatrix} + k_2 \begin{pmatrix} \psi_{21} \\ \psi_{22} \\ \psi_{22}^* \\ -\psi_{21}^* \end{pmatrix} \tag{3.6}$$

because there are eight equations for twelve unknowns $Re\ k_1$, $Im\ k_1$, $Re\ k$, $Im\ k_2$, $Re\ \psi_{11}$, $Im\ \psi_{11}$, $Re\ \psi_{12}$, $Im\ \psi_{12}$, $Re\ \psi_{21}$, $Im\ \psi_{21}$, $Re\ \psi_{22}$ and $Im\ \psi_{22}$. It follows that

$$\bar{\psi}\gamma^\mu\psi = |k_1|^2\bar{\psi}_1\gamma^\mu\psi_1 + k_1^*k_2\bar{\psi}_1\gamma^\mu\psi_2 + k_1k_2^*\bar{\psi}_2\gamma^\mu\psi_2k_1k_2^* + |k_2|^2\bar{\psi}_2\gamma^\mu\psi_2. \tag{3.7}$$

Since

$$\begin{aligned} \bar{\psi}_1\gamma^\mu\psi_2 &= \psi_1^TC\gamma^\mu\psi_2 = \psi_1^T(-\gamma^\mu)^TC\psi \\ &= (-\psi_1^T\gamma^{\mu\ T}C\psi)^T = -\psi_1^TC^T\gamma^\mu\psi_1 \\ &= \psi_2^TC\gamma^\mu\psi_1 = -\bar{\psi}_2\gamma^\mu\psi_1, \end{aligned} \tag{3.8}$$

$$\bar{\psi}\gamma^\mu\psi = |k_1|^2\bar{\psi}_1\gamma^\mu\psi_1 + |k_2|^2\bar{\psi}_2\gamma^\mu\psi_2 + (k_1^*k_2 - k_1k_2^*)\bar{\psi}_1\gamma^\mu\psi_2 \tag{3.9}$$

Currents consist of coupling of Majorana spinors or anti-Majorana spinors only when $arg\ k_1 = arg\ k_2$ or $arg\ k_1 = arg\ k_2 + \pi$. Furthermore,

$$\begin{aligned} (\bar{\psi}_1\gamma^\mu\psi_2)^* &= (\psi_1^\dagger\gamma^0\gamma^\mu\psi_2)^* = \psi_1^T\gamma^0\gamma^{\mu\ *}\psi_2^* = (\psi_1^T\gamma^0(\gamma^{\mu\ *}\psi_2)^T \\ &= \psi_1^T(\gamma^\mu)^\dagger\gamma^\mu\psi_1 = \bar{\psi}_2\gamma^\mu\psi_1 \end{aligned} \tag{3.10}$$

Therefore, $\bar{\psi}_1\gamma^\mu\psi_2$ is imaginary and

$$k_1^*k_2\bar{\psi}_1\gamma^\mu\psi_2 + k_1k_2^*\bar{\psi}_2\gamma^\mu\psi_1 = 2\ Re\ [k_1^*k_2\bar{\psi}_1\gamma^\mu\psi_2] \tag{3.11}$$

is always real. It again vanishes when $arg\ k_1 = arg\ k_2$ and $arg\ k_1 = arg\ k_2 + \pi$.

The mass term in the Lagrangian equals

$$m\bar{\psi}\psi = m(|k_1|^2\bar{\psi}_1\psi_1 + |k_2|^2 + k_1^*k_2\bar{\psi}_1\psi_2 + k_1k_2^*\bar{\psi}_2\psi_1. \tag{3.12}$$

By §2, $\bar{\psi}_1\psi_1 = \bar{\psi}_2\psi_2 = 0$, while

$$\bar{\psi}_1\psi_2 = \psi_1^TC\psi_2 = (\psi_1^TC\psi_2)^T = \psi_2^TC^T\psi_1 = -\psi_2^TC\psi_1 = \bar{\psi}_2\psi_1. \tag{3.13}$$

and

$$(\bar{\psi}_1\psi_2)^* = \bar{\psi}_1^*\psi_2^* = (\psi_1^\dagger\gamma^9)^*(\psi_2^\dagger)^T \tag{3.14}$$
$$= \psi_1^T\gamma^0(\psi_2^\dagger)^T = (\psi_1^T\gamma^0(\psi_2^\dagger)^T)^T$$
$$= \psi_2^\dagger\gamma^0\psi_1 = \bar{\psi}_2\psi_1.$$

The mass term equals

$$(k_1^*k_2 + k_1k_2^*)\bar{\psi}_1\psi_2 = 2\ Re[k_1^*k_2\ \bar{\psi}_1\psi_2]. \tag{3.15}$$

Since $\bar{\psi}_1\psi_2$ is real, this expression is real if $arg\ k_1 = arg\ k_2$ or $arg\ k_1 = arg\ k_2 + \pi$.

The kinetic term equals

(3.16)
$$i\bar{\psi}\gamma^\mu\partial_\mu\psi = i[|k_1|^2\bar{\psi}_1\gamma^\mu\partial_\mu\psi_1 + |k_2|^2\bar{\psi}_2\gamma^\mu\partial_\mu\psi_2 + k_1^*k_2\bar{\psi}_1\gamma_\mu^\partial\psi_2 + k_1k_2^*\bar{\psi}_2\gamma^\mu\partial_\mu\psi_1].$$

Since

$$i\int_M d^4x\ [k_1^*k_2\bar{\psi}_1\gamma^\mu\partial_\mu\partial_\mu\psi_2 + k_1k_2^*\bar{\psi}_2\gamma^\mu\partial_\mu\psi_1] \tag{3.17}$$
$$= i\int_M d^4x[k_1^*k_2\bar{\psi}_1\gamma^\mu\partial_\mu\psi_2 - k_1k_2^*\overline{\partial_\mu\psi_1}\gamma^\mu\psi_2]$$
$$= i\int_M d^4x\ [k_1k_2^*\bar{\psi}_1\gamma^\mu\partial_\mu\psi_2 - k_1k_2^*\partial_\mu(\bar{\psi}_1\gamma^\mu\psi_2) + k_1k_2^*\bar{\psi}_1\gamma^\mu\partial_\mu\psi_2]$$
$$= i\int_M d^4x(k_1^*k_2 + k_1k_2^*)\bar{\psi}_1\gamma^\mu\partial_\mu 2 - ik_1k_2^*\int_{\partial M} d^3\Sigma_\mu\bar{\psi}_1\gamma^\mu\psi_2,$$

and the boundary integral vanishes when $\psi_1,\ \psi_2 \sim \frac{1}{r^{\frac{3}{2}+\epsilon}}$, $\epsilon > 0$, under these conditions, the kinetic action equals

$$i\int_M d^4x\ [|k_1|^2\bar{\psi}_1\gamma^\mu\partial_\mu\psi_1 + |k_2|^2\bar{\psi}_2\gamma^\mu\partial_\mu\psi_2 + (k_1^*k_2 + k_1k_2^*)\bar{\psi}_1\gamma^\mu\partial_\mu\psi_2]. \tag{3.18}$$

The complex conjugate of $i\bar{\psi}_1\gamma_\mu^\partial\psi_1$

$$(i\bar{\psi}_1\gamma^\mu\partial_\mu\psi_1)^* = -i(\psi_1^\dagger\gamma^0)^\mu\ {}^*\partial_\mu\psi_1^* = -i\psi_1^T\gamma^0\gamma^\mu\ {}^*\partial_\mu\psi_1^* \tag{3.19}$$
$$= -i\partial_\mu\psi_1^\dagger\gamma^{\mu\dagger}\gamma^0\psi_1 = -i\partial_\mu\psi_1^\dagger\gamma^{\gamma\mu}\psi_1$$

can be integrated to give

$$-i\int_M d^4x\ \partial_\mu\psi_1^T\gamma^0\gamma^\mu\psi_1 = -i\int_M d^4x\ [\partial_\mu(\psi_1^\dagger\gamma^0\gamma^\mu\psi_1) - \psi_1^\dagger\gamma^0\gamma^\mu\partial_\mu\psi_1] \tag{3.20}$$
$$= i\int_M d^4x\ \bar{\psi}_1\gamma^\mu\partial_\mu\psi_1 - i\int_M d^4x\ \bar{\psi}1\gamma^\mu\psi_1.$$

The boundary integral again vanishes under the same dependence on the distance near spatial infinity, and

$$\left(i\int_M d^4x\ \bar{\psi}_1\gamma^\mu\partial_\mu\psi_1\right)^* = i\int_M d^4x\ \bar{\psi}_1\gamma^\mu\partial_\mu\psi_2. \tag{3.21}$$

Similarly,

$$\left(i\int_M d^4x\ \bar{\psi}_2\gamma^\mu\partial_\mu\psi_2\right)^* = i\int d^4x\ \bar{\psi} + 2\gamma^\mu\partial_\mu\psi_2. \tag{3.22}$$

The complex conjugate of $i\bar{\psi}_1\gamma^\mu\partial_\mu\psi_2$ is

$$\begin{aligned}(i\bar{\psi}_1\gamma^\mu\partial_\mu\psi_2)^* &= -i(\psi_1^\dagger\gamma^0\gamma^\mu\partial_\mu\psi_2)^* = -i\psi^T\gamma^0(\gamma^\mu)^*\partial_\mu\psi_2^* \\ &= -i\partial\psi_2^\dagger(\gamma^\mu)^\dagger\gamma^0\psi_1 == i\partial_\mu\psi_2^\dagger(\gamma^\mu)^\dagger\gamma^\mu\psi_1 \\ &= -i\partial_\mu\psi_2^\dagger\gamma^0\gamma^\mu\psi_1.\end{aligned} \tag{3.23}$$

which is integrated to

$$\begin{aligned}-i\int_M d^4x\ \partial\bar{\psi}_2\gamma^\mu\psi_1 &= -i\int_M d^4x\ [\partial_\mu(\bar{\psi}_2^\mu\psi_1) - \bar{\psi}_2\gamma^\mu\partial_\mu\psi_1] \\ &= i\int_M d^4x\bar{\psi}_2\gamma^\mu\partial_\mu\psi_1 - i\int_{\partial M} d\Sigma_\mu\ \bar{\psi}_2\gamma^\mu\psi_1\end{aligned} \tag{3.24}$$

and

$$\left(i\int d^4x\bar{\psi}_1\gamma^\mu\partial_\mu\psi_2\right)^* = i\int d^4x\bar{\psi}_1\gamma^\mu\partial_\mu\psi_2. \tag{3.25}$$

Therefore, the fermion action is real if $arg\ k_1 = arg\ k_2$ or $arg\ k_1 = arg\ k_2 + \pi$.

When $|k_1| \gg |k_2|$, the fermion field is predominantly a Majorana spinor, the mass is proportional to $Re(k_1^* k_2)$, and the current is nearly equal to $|k_1|^2\, i\int d^4x\ \bar{\psi}_1\gamma^\mu\partial_\mu\psi_1$. The current then can be large even for an infinitesimal mass. Since the electron does have a non-zero mass, $k_1(e^-) \gg k_2(e^-) > 0$. It would be a field with a mainly Majorana spinor and an infinitesimal anti-Majorana spinor component.

4. A Transformation from Weyl Spinors to Majorana Spinors

The neutrino is generally described by a left-handed Weyl spinor ν_L. This field and the electron form an $SU(2)$ doublet in the standard model. Experimental data from cosmic rays reflect the occurence of a reaction $e^- \to W^-\nu_e$, with the effective mass of the W^- boson being reduced by an effective factor of 3 [4][12]. A study of the nonrelativistic form of the wave equation for a real

Majorana spinors demonstrates that the wavefunction would be a solution to a Schrödinger equation

$$-\frac{3\hbar^2}{2m}\partial_y^2\psi + V(y)\psi = i\hbar\frac{\partial\psi}{\partial t}. \tag{4.1}$$

with an effective mass reduced by a factor of 3. Consequently, the electron may be regarded as a primarily Majorana spinor.

Since $\begin{pmatrix} e \\ \nu_L \end{pmatrix}$ is an SU(2) isospin doublet, the existence of a rotation from a Weyl to a Majorana spinor may be examined. The gamma matrices will be defined in the chiral representation in the remainder of this section. With the matrix $\gamma_5 = \begin{pmatrix} -I & 0 \\ 0 & I \end{pmatrix}$, the chirality conditions $(1-\gamma_5)\psi_L = 0$ and $(1+\gamma_5)\psi_R = 0$ have the solutions

$$\psi_R = \begin{pmatrix} \psi_1 \\ \psi_2 \\ 0 \\ 0 \end{pmatrix} \sim \begin{pmatrix} \psi_{11} & \psi_{12} \\ \psi_{21} & \psi_{22} \\ 0 & 0 \\ 0 & 0 \end{pmatrix} \qquad \psi_L = \begin{pmatrix} 0 \\ 0 \\ \psi_3 \\ \psi_4 \end{pmatrix} \sim \begin{pmatrix} 0 & 0 \\ 0 & 0 \\ \psi_{31} & \psi_{32} \\ \psi_{41} & \psi_{42} \end{pmatrix} \tag{4.2}$$

Consider first the transformation from ψ_R to the Majorana spinor

$$\psi_M = \begin{pmatrix} \psi_1 \\ \psi_2 \\ -\psi_2^* \\ \psi_1^* \end{pmatrix} \equiv \begin{pmatrix} \psi_{11} & \psi_{12} \\ \psi_{21} & \psi_{22} \\ -\psi_{21} & \psi_{22} \\ \psi_{11} & -\psi_{12} \end{pmatrix}, \tag{4.3}$$

where $\psi_1 \equiv \psi_{11} + i\psi_{12}$ and $\psi_2 = \psi_{21} + i\psi_{22}$. The matrix equation

$$A\psi_R = \psi_M, \tag{4.4}$$

has the solution

(4.5)
$$a_{11} = 1 \qquad a_{12} = 0$$
$$a_{21} = 0 \qquad a_{22} = 1$$
$$a_{31} = -\frac{2\psi_{21}\psi_{22}}{det\ \Psi_2} \qquad a_{32} = \frac{\psi_{11}\psi_{22} + \psi_{12}\psi_{21}}{det\ \Psi_2}$$
$$a_{41} = \frac{\psi_{11}\psi_{22} + \psi_{12}\psi_{21}}{det\ \Psi_2} \qquad a_{42} = -\frac{2\psi_{11}\psi_{12}}{det\ \Psi_2}$$
$$\Psi_{2R} = \begin{pmatrix} \psi_{11} & \psi_{12} \\ \psi_{21} & \psi_{22} \end{pmatrix}.$$

The remaining elements are undetermined. The matrix can be completed to

(4.6)
$$A = \begin{pmatrix} I_2 & 0 \\ A_2 & -I_2 \end{pmatrix}$$
$$A_2 = \frac{1}{det\ \Psi_2} \begin{pmatrix} -2\psi_{21}\psi_{22} & \psi_{11}\psi_{22} + \psi_{12}\psi_{21} \\ \psi_{11}\psi_{22} + \psi_{12}\psi_{22} & -2\psi_{11}\psi_{12} \end{pmatrix},$$

with the identities

(4.7)
$$det\ A_2 = -1$$
$$A^2 = I_4$$
$$det\ A = 1.$$

This formula is consistent with an automorphism of a doublet. The matrix $\mathbb{A}$ belongs to a $\mathbb{Z}_2$ subgroup of $\mathrm{SL}(4;\mathbb{C})$. In the complex formulation,

(4.8)
$$A_2^{\mathbb{C}} \begin{pmatrix} \psi_1 \\ \psi_2 \end{pmatrix} = \begin{pmatrix} -\psi_2^* \\ \psi_1^* \end{pmatrix}$$

and $A_2^{\mathbb{C}}$ preserves the norm of vectors in $\mathbb{C}^2$. Since $|det\ A_2^{\mathbb{C}}| = 1$, and there is a bijective correspondence between the matrices of the form $A \in \mathrm{SL}(4;\mathbb{R})$, $A_2^{\mathbb{C}} \in \mathrm{SL}(2;\mathbb{C}) \cup \mathrm{SL}^-(2;\mathbb{C})$, where $\mathrm{SL}^-(2;\mathbb{C})$ is the set of special linear transformations in $\mathbb{C}^2$ with determinant -1. Since $A \in SL(4;\mathbb{R})$ and $det\ A_2 = -1$, $A_2 \in \mathrm{SL}^-(2;\mathbb{R}) \subset \mathrm{SL}^-(2;\mathbb{C})$. Multiplication by $\begin{pmatrix} 0 & 1 \\ 1 & 0 \end{pmatrix}$ gives an element of $\mathrm{SL}(2;\mathbb{R}) \subset \mathrm{SL}(2;\mathbb{C})$

(4.9)
$$\hat{A}_2 = A_2 \begin{pmatrix} 0 & 1 \\ 1 & 0 \end{pmatrix} = \frac{1}{det\ \Psi_{2R}} \begin{pmatrix} \psi_{11}\psi_{22} + \psi_{12}\psi_{21} & -2\psi_{21}\psi_{22} \\ -2\psi_{11}\psi_{12} & \psi_{11}\psi_{22} + \psi_{12}\psi_{21} \end{pmatrix}.$$

There is a bijection from the set $\{A\gamma_5\}$ to $\left\{ \begin{pmatrix} I & 0 \\ \hat{A}_2 & I \end{pmatrix} \right\}$, and a subset of an $SL(2;\mathbb{R})$ subgroup of $SL(2;\mathbb{C})$.

A solution to the equation

$$B\psi_L = \psi_M = \begin{pmatrix} \psi_4^* \\ -\psi_3^* \\ \psi_3 \\ \psi_4 \end{pmatrix} \tag{4.10}$$

is

$$B = \begin{pmatrix} -I_2 & B_2 \\ 0 & I_2 \end{pmatrix} \tag{4.11}$$

$$B_2 = \frac{1}{det\ \Psi_{2L}} \begin{pmatrix} \psi_{41}\psi_{42} \\ -(\psi_{31}\psi_{42} + \psi_{32}\psi_{41}) \\ -(\psi_{31}\psi_{42} + \psi_{32}\psi_{41}) \\ 2\psi_{31}\psi_{41} \end{pmatrix}$$

$$\Psi_{2L} = \begin{pmatrix} \psi_{31} & \psi_{32} \\ \psi_{41} & \psi_{42} \end{pmatrix}.$$

It follows that

$$\begin{aligned} det\ B_2 &= -1 \\ B^2 &= I_4 \\ det\ B &= 1. \end{aligned} \tag{4.12}$$

There is a bijective correspondence between the set of matrices $\{-B\gamma_5\}$ in $SL(4;\mathbb{R})$ and a subset of $SL(2,\mathbb{R})$.

Similarly, the transformations from the chiral spinors to an anti-Majorana spinor

$$\begin{aligned} A'\psi_R &= \psi_A \\ B'\psi_L &= \psi_A \end{aligned} \tag{4.13}$$

are given by

$$A' = \begin{pmatrix} I_2 & 0 \\ A_2' & -I_2 \end{pmatrix} \tag{4.14}$$

$$A_2' = -A_2$$

and

$$B' = \begin{pmatrix} -I_2 & B_2' \\ 0 & I_2 \end{pmatrix} \tag{4.15}$$

$$B_2' = -B_2$$

The sets $\{A'\gamma_5\}$ and $\{-B'\gamma_5\}$ can be mapped bijectively to subsets of $\mathrm{SL}(2;\mathbb{R})$.

The bilinears $\bar{\psi}_R\psi_R$ and $\psi_L\psi_L$ vanish, and chiral spinors describe massless fields. Suppose that the nearly chiral spinor is $\nu = \kappa_1\nu_L + \kappa_2\nu_R$, where $\kappa_1 \gg \kappa_2$. Then

$$m\bar{\nu}\nu = m[\kappa_1^*\kappa_2\bar{\nu}_L\nu_R + \kappa_1\kappa_2^*\bar{\nu}_R\nu_L] = 2Re[\kappa_1^*\kappa_2\bar{\nu}_L\nu_R]. \tag{4.16}$$

The initial set of solutions to Eq.(4.11) yields

$$\bar{\nu}_L^\dagger\gamma^0 \to \nu_M^\dagger(B^{-1})^\dagger\gamma^0 = \nu_M^\dagger B^T\gamma^0 = \bar{\nu}_M\gamma^0 B^T\gamma^0. \tag{4.17}$$

If

$$\nu_R \to (B')^{-1}\nu_A = B'\nu_A. \tag{4.18}$$

$$\bar{\nu}_L\nu_R \to \bar{\nu}_M\gamma^0 B^T\gamma^0 B'\nu_A \tag{4.19}$$

From

$$\gamma^0 B^T\gamma^0 B' = -I_4, \tag{4.20}$$

it follows that

$$\bar{\nu}_L\nu_R \to -\bar{\nu}_M\nu_A. \tag{4.21}$$

When the solutions $\{A, B, C, D\}$ are replaced by $\{A\gamma_5, -B\gamma_5, C\gamma_5, -D\gamma_5\}$,

$$\bar{\nu}_L \to -\nu_M^\dagger(B^{-1})^T\gamma_5\gamma^0 = -\bar{n}u_M\gamma^0(B^{-1})^T\gamma_5\gamma^0, \tag{4.22}$$

$$\nu_R \to -\gamma_5(B'^{-1})\nu_A \tag{4.23}$$

and

(4.24)

$$\bar{\nu}_L\nu_R \to = -\bar{\nu}_M\gamma^0(B^{-1})^T\gamma_5\gamma^0(-\gamma_5(B')^{-1})\nu_A = -\bar{\nu}_M\gamma^0(B^{-1})^T\gamma^0(B')^{-1}\nu_A.$$

Since

(4.25)

$$-\gamma^0(B^{-1})^T\gamma_5\gamma^0(B')^{-1} = -\begin{pmatrix} 0 & I_2 \\ I_2 & 0 \end{pmatrix}\begin{pmatrix} -I_2 & 0 \\ -B_2 & I_2 \end{pmatrix}\begin{pmatrix} 0 & I_2 \\ I_2 & 0 \end{pmatrix}\begin{pmatrix} -I_2 & B_2 \\ 0 & I_2 \end{pmatrix}$$

$$= \begin{pmatrix} I_2 & 2B_2 \\ 0 & I_2] \end{pmatrix},$$

$$\bar{\nu}_L \nu_R \rightarrow \bar{\nu}_M \nu_A + 2\bar{\nu}_M \begin{pmatrix} 0 & B_2 \\ 0 & 0 \end{pmatrix} \nu_A. \tag{4.26}$$

It may be noted that ν_L and ν_R can be derived from two different spinors. If $\nu_L = \frac{1}{2}(1-\gamma_5)\nu$ and $\nu_R = \frac{1}{2}(1+\gamma_5)\nu$,

$$\bar{\nu}_L \nu_R = (0\ 0\ \nu_3^*\ \nu_4^*) \begin{pmatrix} 0 & I_2 \\ I_2 & 0 \end{pmatrix} \begin{pmatrix} \nu_1 \\ \nu_2 \\ 0 \\ 0 \end{pmatrix} \tag{4.27}$$

$$= \nu_3^* \nu_1 + \nu_4^* \nu_1.$$

When the spinors ν_M and ν_A are set equal to $\begin{pmatrix} \nu_1 \\ \nu_2 \\ -\nu_2^* \\ \nu_1^* \end{pmatrix}$ and $\begin{pmatrix} \nu_1 \\ \nu_2 \\ \nu_2^* \\ -\nu_1^* \end{pmatrix}$, respectively, in the mass term $m\bar{\nu}_M \nu_R$ vanishes because $\bar{\nu}_M \nu_A = 0$.

A coincidence of the spinors generating ν_M and ν_A will be necessary for the reduction of any remaining bilinears. Given that

$$B_2 = \frac{1}{det\ V_{2L}} \begin{pmatrix} 2\nu_{31}\nu_{42} & -(\nu_{31}\nu_{42} + \nu_{32}\nu_{41}) \\ -(\nu_{31}\nu_{42} + \nu_{32}\nu_{41} & 2\nu_{31}\nu_{42} \end{pmatrix} \tag{4.28}$$

$$V_{2L} = \begin{pmatrix} \nu_{31} & \nu_{32} \\ \nu_{41} & \nu_{42} \end{pmatrix},$$

$$\bar{\nu}_M \begin{pmatrix} 0 & B_2 \\ 0 & 0 \end{pmatrix} \nu_A = (\nu_{34}^{\nu *}) B_2 \begin{pmatrix} \nu_3 \\ \nu_4 \end{pmatrix}. \tag{4.29}$$

Expressing the complex component of the spinor as two real components, the above matrix product can be written in the form

(4.30)
$$\frac{1}{det\ V_{2L}}\begin{pmatrix} \nu_{31} & \nu_{41} \\ -\nu_{32} & -\nu_{42} \end{pmatrix}\begin{pmatrix} 2\nu_{41}\nu_{42} & -(\nu_{31}\nu_{42}+\nu_{32}\nu_{41}) \\ -(\nu_{31}\nu_{42}+\nu_{32}\nu_{41}) & 2\nu_{31}\nu_{32} \end{pmatrix}$$
$$= \frac{1}{det\ V_{2L}}\begin{pmatrix} \nu_{31} & \nu_{41} \\ -\nu_{32} & \nu_{42} \end{pmatrix} det(V_{2L}) \begin{pmatrix} \nu_{41} & -\nu_{42} \\ -\nu_{31} & \nu_{32} \end{pmatrix}$$
$$= \begin{pmatrix} 0 & -det\ V_{2L} \\ det\ V_{2L} & 0 \end{pmatrix} = \begin{pmatrix} 0 & -1 \\ 1 & 0 \end{pmatrix} det\ V_{2L},$$

The bilinear $\bar{\nu}_M\nu_A$ is real because it equals the complex conjugate $(\bar{\nu}_M\nu_A)^* = \bar{\nu}_A\nu_M$. By contrast,

(4.31)
$$\left(\bar{\nu}_M\begin{pmatrix} 0 & B_2 \\ 0 & 0 \end{pmatrix}\nu_A\right)^* = \left(\nu_M^\dagger\gamma^0\begin{pmatrix} 0 & B_2 \\ 0 & 0 \end{pmatrix}\nu_A\right)^*$$
$$= \left(\nu_M^T\gamma^0\begin{pmatrix} 0 & B_2 \\ 0 & 0 \end{pmatrix}\nu_A^*\right)^T$$
$$= \nu_A^\dagger\begin{pmatrix} 0 & 0 \\ B_2 & 0 \end{pmatrix}\gamma^0\nu_M = \bar{\nu}_M\gamma^0\begin{pmatrix} 0 \\ B_2 \\ 0 \end{pmatrix}\gamma^0\nu_M$$

Since

(4.32)
$$\gamma^0\begin{pmatrix} 0 & 0 \\ B_2 & 0 \end{pmatrix}\gamma^0 = \begin{pmatrix} 0 & B_2 \\ 0 & 0 \end{pmatrix},$$

(4.33)
$$\left(\bar{\nu}_M\begin{pmatrix} 0 & B_2 \\ 0 & 0 \end{pmatrix}\nu_A\right)^* = \bar{\nu}_A\begin{pmatrix} 0 & B_2 \\ 0 & 0 \end{pmatrix}\nu_M.$$

However,

(4.34)
$$\bar{\nu}_M\begin{pmatrix} 0 & B_2 \\ 0 & 0 \end{pmatrix}\nu_A = \nu_M^T C\begin{pmatrix} 0 & B_2 \\ 0 & 0 \end{pmatrix}\nu_A = \left(\nu_M^T C\begin{pmatrix} 0 & B_2 \\ 0 & 0 \end{pmatrix}\nu_A\right)^T$$
$$= \nu_A^T\begin{pmatrix} 0 & 0 \\ B_2 & 0 \end{pmatrix}C^T\nu_M = -\nu_A^T\begin{pmatrix} 0 & B_2 \\ 0 & 0 \end{pmatrix}C\nu_M$$

With the matrix products

$$\begin{pmatrix} 0 & B_2 \\ 0 & 0 \end{pmatrix}\begin{pmatrix} i\sigma^2 & 0 \\ 0 & -i\sigma^2 \end{pmatrix} = \begin{pmatrix} 0 & -iB^2\sigma^2 \\ 0 & 0 \end{pmatrix} \tag{4.35}$$

$$\begin{pmatrix} i\sigma_2 & 0 \\ 0 & -i\sigma^2 \end{pmatrix}\begin{pmatrix} 0 & B_2 \\ 0 & 0 \end{pmatrix} = \begin{pmatrix} 0 & i\sigma^2 B_2 \\ 0 & 0 \end{pmatrix},$$

(4.36)

$$\begin{aligned} -\nu_A^T \begin{pmatrix} 0 & B_2 \\ 0 & 0 \end{pmatrix} C\nu_M &= -\nu_A^T C \begin{pmatrix} 0 & B_2 \\ 0 & 0 \end{pmatrix}\nu_M - \nu_A^T \begin{pmatrix} 0 & -i[B_2,\sigma_2] \\ 0 & 0 \end{pmatrix}\nu_M \\ &= \bar{\nu}_A \begin{pmatrix} B_2 \\ 0 \\ 0 \end{pmatrix}\nu_M - \nu_A^T \begin{pmatrix} 0 & -i[B_2,\sigma^2] \\ 0 & 0 \end{pmatrix}\nu_M \end{aligned}$$

Therefore, $\bar{n}u_M \begin{pmatrix} 0 & B_2 \\ 0 & 0 \end{pmatrix}\nu_A$ is a complex number and

$$Im\left[\bar{\nu}_M \begin{pmatrix} 0 & B_2 \\ 0 & 0 \end{pmatrix}\nu_A\right] = -\frac{1}{2i}\nu_A^T \begin{pmatrix} 0 & -i[B_2,\sigma^2] \\ 0 & 0 \end{pmatrix}\nu_M \tag{4.37}$$

The commutator equals

$$\begin{aligned} [B_2, -i\sigma^2] &= \left[B_2, \begin{pmatrix} 0 & -1 \\ 1 & 0 \end{pmatrix}\right] \\ &= -\frac{1}{det\ V_{2L}}\left[\begin{pmatrix} \nu_{31}\nu_{42}+\nu_{32}\nu_{41} & -2\nu_{31}\nu_{32} \\ 2\nu_{41}\nu_{42} & -(\nu_{31}\nu_{42}+\nu_{32}\nu_{41}) \end{pmatrix}\right. \\ &\quad \left. -\begin{pmatrix} -(\nu_{31}\nu_{42}+\nu_{32}\nu_{41} & 2\nu_{31}\nu_{32} \\ -2\nu_{41}\nu_{42} & \nu_{31}\nu_{32}+\nu_{32}\nu_{41} \end{pmatrix}\right] \\ &= -\frac{2}{detV_{2L}}\begin{pmatrix} {}_{31}\nu_{42}+\nu_{32}\nu_{41} \\ -2\nu_{31}\nu_{32} \\ 2\nu_{41}\nu_{42} \\ -(\nu_{31}\nu_{42}+\nu_{32}\nu_{41} \end{pmatrix}. \end{aligned} \tag{4.38}$$

and

(4.39)

$$Im\left[\bar{\nu}_M \begin{pmatrix} 0 & B_2 \\ 0 & 0 \end{pmatrix} \nu_A\right] = -\frac{i}{det\ V_{2L}} \nu_A^T \begin{pmatrix} \nu_{31}\nu_{42} + \nu_{32}\nu_{41} & -2\nu_{31}\nu_{32} \\ 2\nu_{41}\nu_{42} & -(\nu_{31}\nu_{42} + \nu_{32}\nu_{41}) \end{pmatrix} \nu_M$$

$$= -\frac{i}{det\ V_{2L}} (-\nu_4^*\ \nu_3^*) \begin{pmatrix} \nu_{31}\nu_{42} + \nu_{32}\nu_{41} & -2\nu_{31}\nu_{32} \\ 2\nu_{41}\nu_{42} & -(\nu_{31}\nu_{42} + \nu_{32}\nu_{41}) \end{pmatrix} \begin{pmatrix} \nu_3 \\ \\ \nu_4 \end{pmatrix}.$$

Expressing the complex components as two real components,

(4.40)

$$Im\left[\bar{\nu}_M \begin{pmatrix} 0 & B_2 \\ 0 & 0 \end{pmatrix} \nu_A\right]$$

$$= -\frac{i}{det\ V_{2L}} \begin{pmatrix} -\nu_{41} & \nu_{31} \\ \nu_{42} & -\nu_{32} \end{pmatrix} \begin{pmatrix} \nu_{31}\nu_{42} + \nu_{32}\nu_{41} & -2\nu_{31}\nu_{32} \\ 2\nu_{41}\nu_{42} & -(\nu_{31}\nu_{42} + \nu_{32}\nu_{41}) \end{pmatrix} \begin{pmatrix} \nu_{31} & \nu_{32} \\ \nu_{41} & \nu_{42} \end{pmatrix}$$

$$= -\frac{i}{det\ V_{2L}} \begin{pmatrix} -\nu_{41} & \nu_{31} \\ \nu_{42} & -\nu_{32} \end{pmatrix} det(V_{2L}) \begin{pmatrix} \nu_{31} & -\nu_{32} \\ \nu_{41} & -\nu_{42} \end{pmatrix}$$

$$= -i \begin{pmatrix} 0 & -det\ V_{2L} \\ det\ V_{2L} & 0 \end{pmatrix} = -i \begin{pmatrix} 0 & -1 \\ 1 & 0 \end{pmatrix} det\ V_{2L}$$

which is consistent with the evaluation of $\bar{\nu}_A \begin{pmatrix} 0 & B_2 \\ 0 & 0 \end{pmatrix} \nu_M$ since the matrix $\begin{pmatrix} 0 & -1 \\ 1 & 0 \end{pmatrix}$ is the 2×2 matrix representation of the imaginary unit i. Then

$$\bar{\nu}_A \begin{pmatrix} 0 & B_2 \\ 0 & 0 \end{pmatrix} \nu_M = i\ det\ V_{2L} \tag{4.41}$$

and

$$m\bar{\nu}\nu = 2m\ Re[\kappa_1^*\kappa_2(\bar{\nu}_M\nu_A + 2i\ det\ V_{2L})]. \tag{4.42}$$

Setting $m\bar{\nu}_M\nu_A$ equal to zero,

$$m\bar{\nu}\nu = 4m\ Re\left[\kappa_1^*\kappa_2\ i\ det\ V_{2L}\right]. \tag{4.43}$$

Since

$$i(\nu_4^*\ -\nu_3^*) \begin{pmatrix} \nu_3 \\ \\ \nu_4 \end{pmatrix} = 2(\nu_{31}\nu_{42} - \nu_{32}\nu_{41}), \tag{4.44}$$

$$(4.45) \qquad det\ V_{2L} = \frac{i}{2}(\nu_4^* \ -\nu_3^*) \begin{pmatrix} \nu_3 \\ \\ \nu_4 \end{pmatrix}$$

By the definition of ν_L,

$$(4.46) \qquad \bar{\nu}_L = \nu_L^\dagger \gamma^0 = (\nu_3^* \ \nu_4^* \ 0 \ 0)$$

and

$$(4.47) \quad \bar{\nu}_L C\gamma_0 \nu_L = (\nu_3^* \ \nu_4^* \ 0 \ 0) \begin{pmatrix} i\sigma^2 & 0 \\ 0 & -i\sigma^2 \end{pmatrix} \begin{pmatrix} \nu_3 \\ \nu_4 \\ 0 \\ 0 \end{pmatrix} = (\nu_4^* \ -\nu_3^*) \begin{pmatrix} \nu_3 \\ \\ \nu_4 \end{pmatrix}.$$

It follows that

$$(4.48) \qquad det\ V_{2L} = \frac{i}{2}\bar{\nu}_L C\gamma^0 \nu_L$$

when $\nu_L = \frac{1}{2}(1-\gamma_5)\nu$, $\nu_R = \frac{1}{2}(1+\gamma_5)\nu$, $\nu_1 = \nu_3$, $\nu_2 = \nu_4$, and

$$(4.49) \qquad m\bar{\nu}\nu = 2m\ Re[-\kappa_1^*\kappa_2 \bar{\nu}_L C \nu_R].$$

Equivalently,

$$(4.50) \quad (\nu_4^* - \nu_3^*) \begin{pmatrix} \nu_3 \\ \\ \nu_4 \end{pmatrix} = \nu_M^T \frac{1}{2}(1-\gamma_5)\frac{1}{2}(1-\gamma_5)\gamma_0 \nu_A = \bar{\nu}_M C^{-1} \frac{1}{2}(1+\gamma_5)\gamma^0 \nu_A$$

and

$$(4.51) \qquad m\bar{\nu}\nu \to 2m\ Re\left[\kappa_1^*\kappa_2 \bar{\nu}_M C \cdot \frac{1}{2}(1+\gamma_5)\gamma^0 \nu_A\right]$$

Now consider

$$(4.52) \qquad 2m\ Re[\kappa_1^*\kappa_2 \bar{\nu}_L^{(8)} C^2 \nu_R^{(8)}],$$

where ν_L and ν_R are chiral projections in an 8-component spinor. The above process of deriving the mass term, and then transforming it to a form such as that given in Eq.(4.51), results in

$$(4.53) \qquad 2^{n-2} m\ Re[\kappa_1^*\kappa_2 \bar{\nu}_L^{(4(n-1))} C^{n-1} \nu_R^{(4(n-1))}]$$

after the $(n-3)^{th}$ iteration, where ν_L^{4k} and ν_R^{4k} are embedded in spinors with 2^{n_k} components with $2^{n_k-1} < 4k \leq 2^{n_k}$ components, if the initial bilinears in the expansion of $\bar{\nu}_L^{4(\ell-1)}\nu_R^{(4(\ell-1)}$ vanish, similarly to $\bar{\nu}_M\nu_A$, for $2 \leq \ell \leq n-1$. The mass may be left in the form

$$2^{n-1}m\ Re[\kappa_1^*\kappa_2\bar{\nu}_M^{(4n)}C^n\Gamma^{(n)}\nu_A^{(4n)}]_{(0)} \tag{4.54}$$

after the $(n-2)^{nd}$ iteration, where $\nu_M^{(4n)}$,$\nu_A^{(4n)}$ are spinors with $4n$ non-zero components, $\Gamma^{(n)}$ is a product of gamma, generalized charge conjugation and transformation matrices, and $[\bar{\nu}_M^{(4n)}\Gamma^{(n)}\nu_A^{(4n)}]_{(0)}$ denotes those terms proportional to a scalar bilinear.

5. The Maximal Iteration of the Transformation of the Scalar Bilinear

The transformation from the bilinear $\bar{\nu}_L\nu_R$ to $\bar{\nu}_M\nu_A + 2\bar{\nu}_M \begin{pmatrix} 0 & B_2 \\ 0 & 0 \end{pmatrix} \nu_A$ reflects the embedding of two-component spinors into four-component spinors and $\mathrm{SL}(2,\mathbb{R})$ into $\mathrm{SL}(4;\mathbb{R})$ and $\mathrm{SL}(2;\mathbb{C})$. Iterations of this transformation similarly would require the embedding of spinors with $4k$ components into spinors with 2^{n_k} components, where $2^{n_k-1} < 4k \leq 2^{n_k}$, characteristic of spinors in $2n_k$ and $2n_k+1$ dimensions.

The spinor space of the standard model $\oplus_{i=1}^{3}(\mathbb{C}\otimes\mathbb{H}\otimes\mathbb{O})_i$ is a direct sum over the three generations of fermions. When a single generation consists of a lepton, lepton neutrino of both chiralities and two quarks with three different colours. amd two chiral lepton neutrinos can be combined in a four-component spinor, the number of particle and antiparticles would equal 16, The automorphism group of the spinor space is the wreath product $\mathrm{G}_2 \times \mathrm{SU}(2) \times \mathrm{SU}(1)\ wr\ S_3$, where S_3 is the symmetric permutation group. The fundamental representation of G_2 is seven-dimensional, and the theory of the strong interactions has this symmetry at higher energies with the charges of the quarks having seven values. The fermions in one generation in a unified model of the fundamental interactions then would consist of 32 particles and antiparticles.

The expectation value of an operator may be given by quotient a sum of over a complete set of states by the quotient of the sum over states of the expectation value of the identity operator

$$\langle 0|\bar{\nu}\nu|0\rangle = \frac{\sum_\alpha \langle 0|\bar{\nu}|\alpha\rangle\langle\nu|\alpha|0\rangle}{\sum_\alpha \langle 0|\alpha\rangle\langle\alpha|0\rangle} \tag{5.1}$$

The physical states must be identified with the fermions and anti-fermions in each generation. In a unified theory with a $G_2 \times SU(2) \times U(1)$ symmetry.

The iteration of the process described in §4 generates a spinor with $4n$ components, which represents all of the quantum states in place of the particle and antiparticles in the fermion multiplets simultaneously when $n = 32$. This spinor, related to the neutrino that will be designated to be ν_1, can be decomposed into a tensor product of four-component spinors. Then the above method is sufficient to generate from ν_1 an entire set of quantum states, $\{\nu_1, \nu_2, ..., \nu_{16}\}$ in place of the particles in one fermion generation and substitute $\{\bar{\nu}_1, \bar{\nu}_2, ..., \bar{\nu}_{16}\}$ for the antiparticles. Setting

(5.2)

$$\begin{aligned}\{|\alpha\rangle\} = &\left[\langle 0\rangle_1 + |\nu\rangle_1 + \ ... \ + |\nu\nu...\nu\rangle_1\right] \otimes \left[|0\rangle_2 + |\nu\rangle_2 + \ ... \ + \ |\nu\nu...\nu\rangle_2\right] \\ &... \otimes \left[|0\rangle_{16} + |\nu\rangle_{16} + \ ... \ + |\nu\nu...\nu\rangle_{16}\right] \\ &\otimes \left[|\bar{0}\rangle_1 + |\bar{\nu}\rangle_1 + \ ... \ + |\bar{\nu}\bar{\nu}...\bar{\nu}\rangle_1\right] \\ &... \otimes \left[|\bar{0}\rangle_{16} + |\bar{\nu}\rangle_{16} + \ .... \ + |\bar{\nu}\bar{\nu}...\bar{\nu}\rangle_{16}\right] ||_{(32)}\end{aligned}$$

where the states are restricted to have a maximum of 32 entries. Decomposing this spinor into a tensor product of four-component spinors, the numerator equals

(5.3)

$$\begin{aligned}\sum_\alpha \langle 0|\bar{\nu}_1...\bar{\nu}_{16}|\alpha\rangle\langle\alpha|\nu_1...\nu_{16}...\rangle = &\langle 0|\bar{\nu}_1...\bar{\nu}_{16}\nu_1...\nu_{16}|\nu_1...\nu_{16}\bar{\nu}_1...\bar{\nu}_{16}\rangle \\ &\langle\nu_1...\nu_{16}\bar{\nu}_1...\bar{\nu}_{16}|\nu_1...\nu_{16}\bar{\nu}_1...\bar{\nu}_{16}|0\rangle\end{aligned}$$

because only the single quantum state consisting of all fermions in the generation will produce a nonvanishing expectation value. The denominator is

$$\begin{aligned}\sum_\alpha \langle 0|\alpha\rangle\langle\alpha|0\rangle = &\langle 0|0\rangle_{1\ 1}\langle 0|0\rangle + ... + \langle 0|0\rangle_{16\ 16}\langle 0|0\rangle \\ &+ \langle 0|\bar{0}\rangle_{1\ 1}\langle\bar{0}|0\rangle + ... + \langle 0|\bar{0}\rangle_{16\ 16}\langle\bar{0}|0\rangle \\ &= 32.\end{aligned} \tag{5.4}$$

The process described in §4 cannot be continued beyond the 30^{th} iteration because the sum is evaluated over the 32 quantum states in one generation. Then, the vacuum expectation value of the mass term would be

$$\frac{1}{32}2^{31}m_\nu\langle 0|Re[\kappa_1^*\kappa_2\bar{\nu}_M^{(4(32))}C^{32}|\nu^{(4(32))}\rangle\langle\nu^{(4(32))}|\Gamma^{(32)}\nu_A^{(4(32))}]_{(0)}|0\rangle. \tag{5.5}$$

Since $C^4 = \mathbb{I}$, the effective mass equals approximately

$$\frac{1}{32}2^{31}m_\nu = 2^{26}m_\nu. \tag{5.6}$$

The mass of the electron [14] is experimentally measured to be

$$m_e = 0.51099895000 \pm 0.00000000015\ MeV/c^2. \tag{5.7}$$

If the electron is the final state of the algorithm, the effective mass of the electron neutrino predicted by this algorithm is

$$m_{\nu_e} \approx 0.0076144777238368 \pm 0.000000000002235\ eV/c^2, \tag{5.8}$$

which coincides with the experimental value.

This method also will provide a connection between mass terms of leptons and neutrinos in the second and third generations. Extra structure in the geometrical models of quarks occurs in these generations. The description of leptons, however, would remain uniform in the absence of this structure. Furthermore, Koide's relation is valid both for leptons [10]

$$m_e + m_{\mu+\tau} = \frac{2}{3}\left(\sqrt{m_e} + \sqrt{m_\mu} + \sqrt{m_\tau}\right)^2 \tag{5.9}$$

and neutrinos [8][11][15]

$$m_e + m_{\nu_\mu} + m_{\nu_\tau} = \frac{2}{3}\left(\sqrt{m_{\nu_e}} + \sqrt{m_{\nu_\mu}} + \sqrt{m_{n_\tau}}\right)^2. \tag{5.10}$$

These numerical equalities are compatible when the proportionality between the masses of the lepton and neutrino continues to hold for the second and third generations. Given the masses of the muon and the τ lepton [14]

$$\begin{aligned} m_\mu &= 105.6583755 \pm 0.0000023\ MeV/c^2 \\ m_\tau &= 1776.82 \pm 0.16\ MeV/c^2, \end{aligned} \tag{5.11}$$

the neutrino masses then would be predicted to be

$$\begin{aligned} m_{\nu_\mu} &= 1.574432484 \pm 0.000000034\ eV/c^2 \\ m_{\nu_\tau} &= 26.47668 \pm 0.00238\ eV/c^2. \end{aligned} \tag{5.12}$$

6. Derivation of the Modified Nonrelativistic Wave Equation

The Schrödinger equation may be derived from the Hamilton-Jacobi equation [13] and the path integral [6]. Given the Hamilton principal function or action

$$S(\vec{q},t) = \int L dt, \tag{6.1}$$

the Hamilton-Jacobi equation is

$$-\frac{\partial S}{\partial t} = H\left(\vec{q}, \frac{\partial S}{\partial \vec{q}}, dt\right) \tag{6.2}$$

where $\frac{\partial S}{\partial \vec{q}} = \vec{p}$. The Hamiltonian of a nonrelativistic particle of mass m in a potential $V(q)$ is

$$H(\vec{q},\vec{p},t) = \frac{1}{2m}|\vec{p}|^2 + V(\vec{q}) \tag{6.3}$$

and

$$H\left(q, \frac{\partial S}{\partial \vec{q}}, t\right) = \frac{1}{2m}\left(\frac{\partial^2 S}{\partial (q^1)^2} + \frac{\partial^2 S}{\partial (q^2)^2} + \frac{\partial^2 S}{\partial (q^3)^2}\right) + V(\vec{q}). \tag{6.4}$$

Then the Hamilton-Jacobi equation is

$$\frac{1}{2m}\left(\frac{\partial^2 S}{\partial (q^1)^2} + \frac{\partial^2 S}{\partial (q^2)^2} + \frac{\partial^2 S}{\partial (q^3)^2}\right) + V(\vec{q}) = -\frac{\partial S}{\partial t}. \tag{6.5}$$

If $\psi(\vec{q},t) = e^{\frac{i}{\hbar}S(\vec{q},t)}$,

$$\begin{aligned}
\frac{\partial S}{\partial q^1} &= -\frac{i\hbar}{\psi}\frac{\partial \psi}{\partial q^1} \\
\frac{\partial S}{\partial q^2} &= -\frac{i\hbar}{\psi}\frac{\partial \psi}{\partial q^2} \\
\frac{\partial S}{\partial q^3} &= -\frac{i\hbar}{\psi}\frac{\partial \psi}{\partial q^3}, \\
\frac{\partial S}{\partial t} &= -\frac{i\hbar}{\psi}\frac{\partial \psi}{\partial t}.
\end{aligned} \tag{6.6}$$

and

$$\frac{1}{2m}\left(-\frac{\hbar^2}{\psi}\right)\nabla^2\psi + V(\vec{q}) = \frac{i\hbar}{\psi}\frac{\partial \psi}{\partial t} \tag{6.7}$$

At points where the wavefunction does not vanish, such as the interior of a potential well, this equation can be multiplied by ψ to give

$$-\frac{\hbar^2}{2m}\nabla^2\psi + V(\vec{q})\psi = i\hbar\frac{\partial \psi}{\partial t}. \tag{6.8}$$

To modify the wave equation, it is necessary to alter the Hamiltonian. Multiplying the kinetic term by 3 in Eq.(5.4),

$$H\left(q, \frac{\partial^2 S}{\partial q}, t\right) = \frac{3}{2m}\left(\frac{\partial S}{\partial (q^1)^2} + \frac{\partial^2 S}{\partial (q^2)^2} + \frac{\partial^2 S}{\partial (q^3)^2}\right) + V(\vec{q}) \tag{6.9}$$

for particles that can be described by Majorana spinors. The Hamilton-Jacobi equation becomes

$$\frac{3}{2m}\left(\frac{\partial^2 S}{\partial (q^1)^2} + \frac{\partial^2 S}{\partial (q^2)^2} + \frac{\partial^2 S}{\partial (q^3)^2}\right) + V(\vec{q}) = -\frac{\partial S}{\partial t}. \tag{6.10}$$

By Eq.(6.6),

$$-\frac{3\hbar^2}{2m}\nabla^2\psi + V(\vec{q})\psi = i\hbar\frac{\partial\psi}{\{}\partial t. \tag{6.11}$$

If ψ is independent of x^1 and x^3, and $\psi(\vec{q}, t) = \psi_0(\vec{q})e^{-\frac{i}{\hbar}Et}$,

$$-\frac{3\hbar^2}{2m}\partial_2^2\psi + V(\vec{q})\psi = E\psi \tag{6.12}$$

which is equivalent to Eq.(2.5).

The path integral over an infinitesimal time integral gives the amplitude [9] from t to $t+\varepsilon$,

$$\psi(y; t+\varepsilon) = \int_{-\infty}^{\infty} Dx\ \psi(x;t) \int_{x(t)}^{x(t+\varepsilon)} e^{iS(x,\dot{x},t)} D[x(t)]. \tag{6.13}$$

Over an infinitesimal time interval, the action of a nonrelativistic particle of mass m in a potential $V(x)$ is

$$\int_{x(t)}^{x(t+\varepsilon)} L(x, \dot{x}, t)dt \approx \left(\frac{1}{2m}\dot{x}^2 - V(x)\right)\varepsilon. \tag{6.14}$$

By the Baker-Campbell-Hausdorff formula,

$$e^{\left(i\left(\frac{1}{2m}\dot{x}^2 - V(x)\right)\varepsilon + \frac{1}{4m}[\dot{x}^2, V(x)]\varepsilon^2 + O(\varepsilon^3)\right)} = e^{\frac{i}{2m}\dot{x}^2\varepsilon}e^{-iV(x)\varepsilon}. \tag{6.15}$$

Then

$$\psi(y; t+\varepsilon) = \int \psi(x;t)e^{-iV(x)\varepsilon}e^{\frac{i}{2m}\frac{(x-y)^2}{\varepsilon}}dx + O(\varepsilon^2) \tag{6.16}$$

Since $e^{\frac{i}{2m}\frac{(x-y)^2}{\varepsilon}} \to 0$ for $x \neq y$ and $e^{\frac{i}{2m}\frac{(x-y)^2}{\varepsilon}} \to 1$ for $x \to y$, it is sufficient to regard $\frac{(x-y)^2}{\varepsilon}$ as an expansion $\frac{1}{\varepsilon}f(x,y) \approx \frac{1}{\varepsilon}\left[f(y,y) + \varepsilon\frac{\partial f}{\partial x}\Big|_{y\approx x}(x-y) + \frac{1}{2!}\frac{\partial^2 f}{\partial y^2}\Big|_{y\approx x}(x-\right.$

$y)^2 + ...\Big]$, where $f(x,y)\Big|_{y\approx x} \approx 0$, $\frac{\partial f(x,y)}{\partial} x\Big|_{y\approx x} \approx 0$ and $\frac{\partial^2 f}{\partial x}\Big|_{y\approx x} \approx 2$. Setting $y - x = \varepsilon$, integration by parts and division by ε by parts yields

$$\frac{\partial \psi}{\partial t} = \frac{i}{2m}\frac{\partial^2 \psi}{\partial x^2} - V(x)\psi \tag{6.17}$$

in the limit $\varepsilon \to 0$. Replacing the Lagrangian by $\frac{3}{2m}\dot{x}^2 - V(x)$, the path integral over the infinitesimal time slice $[t, t+\varepsilon]$ produces the equation

$$-\frac{3}{2m}\frac{\partial^2 \psi(x,t)}{\partial x^2} + V(x)\psi(x,t) = i\frac{\partial \psi(x,t)}{\partial t} \tag{6.18}$$

which is the time-dependent version of the modified nonrelativistic wave equation in §2 in the units with $\hbar = 1$.

7. Conclusion

The generalization of the momentum operator to introduce a real component of the quantum commutation relations requires a matrix term for hermiticity. The resulting nonrelativistic equations are matrix equations for a four-component spinor. It may be reduced to a differential equation for a real-valued Majorana or anti-Majorana spinors. The Schrödinger equation with an effective mass reduced by a factor of 3 is derived for the real-valued Majorana spinors. The second class of real anti-Majorana spinors would solve the standard Schrödinger equation.

These conditions on the spinors may be combined with the Dirac conjugate to prove the vanishing of a set of bilinears, including $\bar{\psi}\psi$ for both classes. Furthermore, it can be checked that an anti-particle is defined by the equivalent of an anti-Majorana condition when the particle is represented by a Majorana spinor. The bilinear representing the current of this anti-Majorana anti-fermion, with a Majorana fermion, may be demonstrated to be zero. This result provides a theoretical explanation of the zero-energy state consisting of negative-energy electron states being filled and essentially no positron current.

Given this discussion of the positron current, and a theoretical prediction for the reaction $e^- \to W^- \nu_e$ in cosmic rays, the electron can be described as a linear combination of Majorana spinor and an anti-Majorana spinor, where the coefficient of the first field being much larger. The neutrino is a nearly massless, chiral spin-$\frac{1}{2}$ field. Since the electron and the chiral neutrino form an SU(2) in the electroweak model, the existence of transformations from Weyl spinors to Majorana spinors is investigated. The matrix may be mapped bijectively to a subset of an $\mathrm{SL}(2;\mathbb{R})$ subgroup of $\mathrm{SL}(2;\mathbb{C})$, the spin covering of the Lorentz group, and it is separate from an isospin rotation. Both the

neutrino and the electron would have a nonvanishing mass by the existence of this transformation.

The mass term of the neutrino is transformed into a bilinear consisting of a Majorana spinor, a product of matrices and anti-Majorana spinors. When the $\mathbb{Z}_2$ transformation is included, the product equals the negative of the identity. If the set of transformation matrices is given by multiplication with γ_5, the product in the bilinear may be equated to the sum of the identity and a nilpotent matrix. The identity yields a scalar bilinear $\bar{\nu}_M \nu_A$ that vanishes. The second matrix gives rise to $2i\ det\ V_{2L}$, where the matrix V_{2L} is composed of the real components of ν_L. This determinant may be reformulated in terms of $\bar{\nu}_L$ and ν_R, the initial chiral spinors. Then, mass term of a new quantum state can be defined by projecting a product charge conjugation and γ matrices to the identity, and replacing the spinors in the bilinear by $\bar{n}u_L^{(4)}$ and $\nu^{(R)}$. These four-component spinors would be the equivalent of the two-component spinors upon the embedding into a general eight-component spinor. The numerical coefficient of the bilinear increases by a factor of 2.

This algorithm then generates a sequence of mass terms of quantum states that stops after a finite number of iterations. The number of iterations can be related to the number of components of spinors representing fermions in a single generations as a result of a completeness relation for the expectation value of an operator. Since the number of spinor components of only particles in one fermion generation is 32, the number of iterations of the initial transformation is 30, and normalization of the expectation value requires a quotient by 32. Then the effective mass of the final state is increased from the neutrino mass by a factor of $\frac{1}{32}2^{31} = 2^{26}$. The final quantum state in the sequence would be the lepton. Recent experimental measurments of the mass of the electron neutrino mass coincide with $\frac{1}{2^{26}}$ of the electron mass. The proportionality between the lepton and neutrino mass in the second and third generations is consistent with the Koide relation. It yields theoretical predictions for m_{ν_μ} and m_{ν_τ} and verifies the direct sum structure of the spinor space of the standard model.

REFERENCES

[1] S. Davis, Quantum Theory of the Fermion Field near Classical Scales, RFSC-17-26.

[2] S. Davis, The Equation for the Wavefunction in Nonrelativistic Quantum Mechanics, Bull. Pure Appl. Sci. **40E** (2021) 127-134.

[3] S. Davis, Relativistic Quantum Scalar Fields, Bull. Pure Appl. Sci. **40D** (2021) 25-33.

[4] S. Davis, The Quantization of a Theory of Charged Scalar Fields, Bull. Pure Appl. Sci. **40D** (2021) 106-120.

[5] P. A. M. Dirac, The Quantum Theory of the Electron, Proc. Roy. Soc. London A117 **117** (1928) 610-624.

[6] R. P. Feynman, Space-time Approach to Nonrelativistic Quantum Mechanics, Rev. Mod. Phys. **20** (1948) 367-387.

[7] R. P. Feynman, The Theory of Positrons, Phys. Rev. bf 76 (1949) 749-759.

[8] J. M. Gérard, F. Goffinet and M. Herquet, A New Look at an Old Mass Relation, Phys. Lett. **633B** (2006) 563-566.

[9] H. Kleinert, Path Integrals in Quantum Mechanics, Statistics, Polymer Physics and Financial Markets, World Scientific Publishing Company, Singapore, 2006.

[10] Y. Koide, A Fermion-Boson Composite Model of Quarks and Leptons, Phys. Lett. **120B** (1983) 161-165.

[11] N. Li and B. Q. Ma, Estimate of Neutrino Masses from Koide's Relation, Phys. Lett. **609B** (2005) 309-315.

[12] M. Schein and P. S. Gill, Burst Frequency as a Function of Energy, Rev. Mod. Phys. **11** (1939) 267-276.

[13] E. Schrödinger, Quantisierung und Eigenwertproblem, Ann. Phys. **79** (1926) 361-376.

[14] R. L. Workman et al. (Particle Data Group), The Review of Particle Physics, Prog. Theor. Exp. Phys. **083C01** (2022).

[15] Z. Xing and H. Zhang, On -like Relations for the Running Masses of Charged Leptons, Neutrinos and Quarks, Phys. Lett. **635B** (2006) 107-111.

HADRONIC JOURNAL 47, 411 - 421 (2024)
DOI 10.29083/HJ.47.04.2024/SC411

WORMHOLES AND NEGATIVE ENERGY

J. J. Bevelacqua
Bevelacqua Resources
7531 Flint Crossing Circle SE.
Owens Cross Roads, AL 35763
bevelresou@aol.com

Received October 2, 2024
Revised October 20, 2024

Abstract

This paper investigates a possible wormhole and associated metrics, and the physical consequences of these geometries. Using the wormhole metric, the solution of Einstein's equation suggests that the energy density component of the energy-momentum tensor is negative. This result implies that a stable wormhole requires negative energy, and is consistent with Penrose's theory.

An evaluation of a representative set of spacetime geometries suggests that the occurrence of negative energy does not universally occur in every theoretical spacetime geometry. It does not occur in flat spacetime or in the Schwarzschild geometry. Negative energies theoretically occur under a limited set of conditions for a general static spherical geometry and the Friedmann-Robertson-Walker spacetime.

Keywords: General Relativity, Wormholes, Negative Energy, Exotic Astrophysical Structures

1.0 Introduction

Following Penrose, a stable wormhole requires the existence of negative energy [1]. It is important to emphasize the original concept of antiparticles and associated negative energies were proposed by Dirac [2]. The reader is also referred to a comprehensive treatment of the negative energy antiparticle concept by Santill [3].

The concept of negative energy has been associated with a number of physical effects. These include the Casimir effect [4], Lamb shift in hydrogen [(5) – (6)], anomalous magnetic moment of the electron [7], and Fulling-Davies-Unruh effect [(8) – (11)].

Associated with negative energy is the zero point energy concept. Related to these concepts are postulated physical effects including fluctuations that are typically quantified in terms of pair production and annihilation in a bubbling quantum foam, the zero-point energy of particle fields [(12)–(14)], virtual particle vacuum bubbles and loops [(15), (16)] , and interacting virtual particles [(17), (18)]. Although these theoretical arguments have been and continue to be made, there is no definitive experimental basis to select if any of these proposed mechanisms occur.

Other work emphasized the importance of negative energy in wormhole dynamics. Ida and Hayward [19] note that a traversable wormhole requires negative energy density, and argues how much negative energy is needed for wormholes. Their local analysis does not assume any symmetry, and allows dynamic (non-stationary) but non-degenerate wormholes. Davis [20] and Garattini [21] address traversable wormhole dynamics and the associated exotic energy requirements.

Of particular importance is the assertion of Penrose [1] that suggests the importance of negative energy in black hole formation, and the associated production of a stable wormhole. The negative energy requirement for wormhole stability [1] is the main objective of this paper. Morris and Thorne (MT) [22] provide additional commentary regarding wormhole stability.

This paper utilizes a set of spacetime geometries including the MT wormhole metric [22] to determine if negative energies occur. The associated Einstein tensor will be shown to exhibit a negative energy density for a subset of these metrics.

2.0 Wormhole Metric

Wormholes are theoretical constructs that have yet to be experimentally observed. The MT wormhole geometry can be represented by a spherically symmetric and time independent metric [(22), (23)]

$$ds^2 = -dt^2 + dr^2 + \left(b^2 + r^2\right)\left(d\theta^2 + \mathrm{Sin}^2\theta\, d\phi^2\right) \qquad (1)$$

where the constant b has the dimension of length.

The coordinates used to define the wormhole geometry are $\{t, r, \theta, \varphi\}$ where t is the time coordinate and (r, θ, φ) are spherical coordinates [23]. An examination of the wormhole geometry indicates that it reduces to flat spacetime in the limit $b \rightarrow 0$ [(22),(23)].

The MT wormhole geometry is a theoretical construct that is not based on experimental evidence. Except for the $b = 0$ metric, the geometry is not flat, but is curved. For $b \neq 0$, an embedding of the (r, φ) slice of the wormhole geometry produces a surface with two asymptotically flat regions connected by a region of minimum radius b [(22),(23)]. This region resembles a tunnel or wormhole connecting the two asymptotically flat regions [(24)- (26)].

The wormhole metric is time independent. It is also spherically symmetric because a surface of constant r and t has the geometry of a sphere. In addition, at very large r ($r \gg b$), the MT wormhole spacetime approaches flat spacetime [(22),(23)].

3.0 Einstein Equation

The Einstein equation can be expressed in the form

$$G_{\mu\nu} = 8\pi G\, T_{\mu\nu} \qquad (2)$$

where $G_{\mu\nu}$ is the Einstein tensor that is a measure of the local spacetime curvature, and $T_{\mu\nu}$ is the energy-momentum tensor that characterizes the matter energy density. The T_{00} component is the energy density, T_{i0} and T_{0i} are the momentum density in the i direction, and T_{ij} are the i component of force per unit area exerted across a surface with a normal in direction j.

The Einstein equation will be used to demonstrate that negative energies result from the wormhole and other metrics. $G_{\mu\nu}$ is calculated and used to determine the coordinate basis components of $T_{\mu\nu}$.

4.0 Results and Discussion

Although the focus of this paper is the wormhole geometry, it is of interest to investigate other geometries to determine if the negative energy result is unique. These geometries include flat spacetime [(23) – (24)], the Schwarzschild geometry [(23), (24), (27), (28)], the Friedmann-Robertson-Walker (FRW) geometry [(23), (24), (28)], and a general static spherical geometry [(23), (24)].

4.1 Wormhole Geometry

The MT wormhole metric [22] was defined in (1). As noted in [23], the G_{00} component of the wormhole geometry is

$$G_{00} = -\frac{b^2}{\left(b^2+r^2\right)^2} \tag{3}$$

(2) and (3) lead to an expression for the energy density

$$T_{00} = -\frac{1}{8\pi G}\frac{b^2}{\left(b^2+r^2\right)^2} \tag{4}$$

T_{00} is the energy density that has a negative value for the MT wormhole geometry. Although the metric is a representation of the theoretical wormhole geometry, it provides an example that a static wormhole represented by (1) requires negative energy. This is consistent with Penrose's assertion [1], and these results can be interpreted to suggest that a wormhole requires negative energy to be stable.

It is of interest to investigate other geometries to determine if the negative energy result is unique. These geometries are addressed in subsequent discussion.

4.2 Flat Spacetime

For the flat spacetime geometry, the scalar curvature will be zero [23]. Zero curvature also suggests the associated tensors (e.g., the Ricci tensor and the Riemann curvature tensor) will also have few, if any, non-zero elements. In a similar fashion, the Einstein tensor in flat spacetime is expected to have few, if any, non-zero elements. This qualitative argument is supported by calculation of the elements of these tensors [23].

The flat spacetime metric has the form

$$ds^2 = -dt^2 + dr^2 + r^2 d\theta^2 + r^2 \mathrm{Sin}^2\theta d\phi^2 \qquad (5)$$

As summarized in [23], the G_{00} component of the flat spacetime geometry is

$$G_{00} = 0 \qquad (6)$$

(2) and (6) lead to an expression for the energy density that is zero. Accordingly, negative energies do not occur in the flat spacetime geometry.

4.3 Schwarzschild Geometry

The simplest curved spacetime geometries of general relativity are those that are the most symmetric. One of the most useful spacetime geometries is the Schwarzschild metric [(24), (27), (28)] that describes empty space outside a static, uncharged, spherically symmetric source of curvature (e.g., a spherical star of mass M that is uncharged and not rotating). In addition, the Schwarzschild geometry is a solution of the vacuum Einstein equation that describes spacetime devoid of matter.

The Schwarzschild metric has the form

$$ds^2 = -\left(1-\frac{2M}{r}\right)dt^2 + \frac{1}{\left(1-\frac{2M}{r}\right)}dr^2 + r^2 d\theta^2 + r^2 \mathrm{Sin}^2\theta d\phi^2 \qquad (7)$$

As calculated in [23], the G_{00} component of the Schwarzschild geometry is

$$G_{00} = 0 \qquad (8)$$

(2) and (8) lead to an expression for the energy density that is zero. Therefore, negative energies do not occur in the Schwarzschild geometry.

4.4 Friedmann-Robertson-Walker (FRW) Geometry

The FRW geometry [(24), (29)] describes the time evolution of a homogeneous, isotropic space that expands in time as the scale factor a(t) increases and contracts as a(t) decreases. The function a(t) contains information about the temporal evolution of the universe. In addition, a constant k is included in the FRW metric. The constant k determines the classification of the universe (i.e., k = +1 indicates a closed universe, k = 0 a flat universe, and k = –1 an open universe). Although the conventional terminology flat, closed, and open are used to distinguish the three possible homogeneous and isotropic geometries of spacetime, it is more physical to distinguish these features in terms of their spatial curvature [(23), (24)].

Homogeneity requires that the spatial curvature be the same at each point in the FRW geometries. The flat case has zero spatial curvature everywhere. The closed and open cases have constant positive and constant negative curvature, respectively.

The FRW metric has the form

$$ds^2 = -dt^2 + \frac{a^2(t)}{1-kr^2}dr^2 + r^2a^2(t)d\theta^2 + r^2a^2(t)\mathrm{Sin}^2\theta d\phi^2 \qquad (9)$$

As summarized in [23], the G_{00} component of the FRW geometry is

$$G_{00} = \frac{3\left(k + \dot{a}^2(t)\right)}{a^2(t)} \qquad (10)$$

(2) and (10) lead to an expression for the energy density

$$T_{00} = \frac{1}{8\pi G}\,\frac{3\left(k + \dot{a}(t)^2\right)}{a^2(t)} \qquad (11)$$

Negative energy density occurs if $k + \dot{a}(t)^2 < 0$. For a flat universe with $k = 0$ and $\dot{a}(t)^2 \geq 0$, a negative energy density does not occur. Negative energy densities do not occur in a closed universe since $1 + \dot{a}(t)^2 \geq 0$.

In an open universe, negative energy densities can occur if $\dot{a}(t)^2 < 1$. Therefore, a negative energy density can only occur in an open universe under a limited set of conditions.

4.5 General Static Spherical Geometry

The rr and tt metric tensor elements of the general static spherical geometry are functions of r, namely exponential functions of $\lambda(r)$ and $\varphi(r)$. The corresponding metric tensor is given by

$$ds^2 = -e^{-2\phi(r)}dt^2 + e^{-2\lambda(r)}dr^2 + r^2 d\theta^2 + r^2 \mathrm{Sin}^2\theta d\phi^2 \quad (12)$$

In subsequent discussion, the derivative with respect to r is indicated by a prime. The general static spherical geometry reduces to the flat spacetime geometry in the limit of $\lambda(r)$ and $\varphi(r) \rightarrow 0$.

As summarized in [23], the G_{00} component of the general static spherical geometry is

$$G_{00} = \frac{1}{r^2} e^{-2\lambda(r)+2\phi(r)} \left(-1 + e^{2\lambda(r)} + 2r\lambda'(r)\right) \quad (13)$$

(2) and (13) lead to an expression for the energy density

$$T_{00} = \frac{1}{8\pi G}\left[\frac{1}{r^2} e^{-2\lambda(r)+2\phi(r)} \left(-1 + e^{2\lambda(r)} + 2r\lambda'(r)\right)\right] \quad (14)$$

In the general static spherical geometry, a negative energy density results if $-1 + e^{2\lambda(r)} + 2r\lambda'(r) < 0$. Therefore, negative temperatures can occur under the special condition

$$\frac{d\lambda(r)}{dr} < \frac{1 - e^{2\lambda(r)}}{2r} \quad (15)$$

Therefore, a negative energy density can occur in a general static spherical geometry under the selective condition noted in (15).

5.0 Wormhole Classifications

In subsequent discussion, we define four classes of theoretical wormholes. A conventional view of a wormhole in spacetime is a theoretical structure that connects two separate spacetime points A (t, r, θ, φ) and A' $(t', r', \theta', \varphi')$ [(1),(22),(23)]. These four classes can be illustrated in terms of a generalized line element

$$ds^2 = -d\tau^2 + dD^2 \qquad (16)$$

where dD represents the spatial distance between A and A' for an arbitrary wormhole metric, and $d\tau$ is the corresponding temporal displacement. dD and $d\tau$ can be complicated functions of (t, r, θ, φ) to ensure stability of the wormhole. These functions would likely differ for each wormhole class and geometry. (16) is the basis for defining the four classes of wormholes.

In a Class I wormhole, there is a finite spatial distance between points A and A', and $d\tau$ is the travel time through the wormhole. Class I wormholes are structures that connect two spatial locations.

A second type of wormhole (Class II) connects points A and A' that are temporally separated. A Class II wormhole is characterized by no change in spatial location ($dD = 0$), but a difference in temporal coordinate ($d\tau \neq 0$). In this case, $d\tau$ is a change in the temporal coordinate that can be either positive or negative. A Class II wormhole connects the same spatial location to either the past or present relative to the entry point A into the wormhole. Theoretically, a Class II wormhole could permit a temporal displacement to the past or future.

Class III wormholes have $dD > 0$ and $d\tau \neq 0$. This classification permits the points A and A' to reside at different spacetime locations. A Class III wormhole allows a displacement to different spatial locations that could occur as either past ($d\tau < 0$) or future ($d\tau > 0$) events relative to the initial temporal coordinate.

A final classification (Class IV) is the null wormhole. Class IV wormholes have $dD = 0$ and $d\tau = 0$. In a Class IV event, no wormhole structure occurs and spacetime is not affected.

These four classes of wormholes outline areas for future research and the development of associated metrics. The validity of these theoretical classes and associated spacetime geometries must be confirmed by experimental observations.

6.0 Conclusions

A candidate wormhole metric is investigated, and its components are used to determine the energy density component of the energy momentum tensor (T_{00}). A negative T_{00} component of the energy momentum tensor suggests the existence of negative energy. Following Penrose, negative energy is required for the wormhole to be stable.

In general, negative energy does not universally occur. No negative energies are predicted for flat spacetime and the Schwarzschild geometry. In addition to the wormhole metric, negative energies are possible under limited conditions for the general static spherical and the closed Friedmann-Robertson-Walker geometries.

References

[1] R. Penrose, Gravitational Collapse and Space - Time Singularities, Phys. Rev. Lett. **14**, (1965) 57-59.

[2] P. A. M. Dirac, The Quantum Theory of the Electron, Proceedings of the Royal Society of London. Series A, Containing Papers of a Mathematical and Physical Character **117**, (1928) 610-624.

[3] R. M. Santilli, Isodual Theory of Antimatter with Application to Antigravity, Grand Unification and Cosmology, Springer, A A Dordrecht, The Netherlands (2006).

[4] M. S. Morris, K. S. Thorne, and U. Yurtsever, Wormholes, Time Machines, and the Weak Energy Condition, Phys. Rev. Lett. **61**, (1988) 1446-1449.

[5] H. A. Bethe, The Electromagnetic Shift of Energy Levels, Phys. Rev. **72**, (1947) 339-341.

[6] S. L. Bu, Negative Energy: From Lamb Shift to Entanglement, arXiv:1605.08268v1 [physics.gen-ph] 18 May 2016 (2016).

[7] R. F. O'Connell, Effect of the Anomalous Magnetic Moment of the Electron on the Nonlinear Lagrangian of the Electromagnetic Field, Phys. Rev. **176**, (1968) 1433- 1437.
[8] S. A. Fulling, Nonuniqueness of Canonical Field Quantization in Riemannian Space-Time, Phys. Rev. **D7**, (1973) 2850-2862.
[9] W. G. Unruh, Notes on black-hole evaporation, Phys. Rev. **D14**, (1976) 870-892.
[10] P. C. W Davies, Scalar production in Schwarzschild and Rindler metrics, J. Phys. A: Math. Gen. **8**, (1975) 609-616.
[11] G. E. A. Matsas and D. A. T. Vanzella, The Fulling-Davies-Unruh Effect is Mandatory: The Proton's Testimony, arXiv:gr-qc/0205078v1 17 May 2002 (2002).
[12] J. J. Bevelacqua, Zero-Point Energy Conundrum, Hadronic Journal **46**, (2023) 305-313.
[13] J. J. Bevelacqua, Zero-Point Energy Conundrum for Spin ½ Particles, Qeios **5VZB0M**, (2023) 1-7. https://doi.org/10.32388/5VZB0M.
[14] J. J. Bevelacqua, Zero-Point Energy Conundrum for Spin 1 Particles, Qeios **8W0RRJ**, (2023) 1-7. https://doi.org/10.32388/8W0RRJ.
[15] J. J. Bevelacqua, Possible Planck-scale Physical Production Mechanisms and Consequences of Negative Energies – Initial Formulation, Physics Essays **34**(3), (2021) 342-351.
[16] J. J. Bevelacqua, Planck-Scale Quantum Field Theory –II- Evaluation of QED Analogue Amplitudes, Hadronic Journal **45**, (2022) 235-252.
[17] J. A. Wheeler, On the Nature of Quantum Geometrodynamics, Annal. Phys. **2**, (1967) 604-614.
[18] S. Weinberg, The cosmological constant problem, Rev. Mod. Phys. **61**, (1989) 1-23.
[19] D. Ida and S. A. Hayward, How much negative energy does a wormhole need?, Phys.Lett. **A260**, (1999) 175-181.
[20] E. W. Davis, Traversable Wormholes, Stargates, and Negative Energy, DIA-08-1004-004, Defense Intelligence Reference Document, Washington DC (2010).
[21] R. Garattini, Casimir wormholes, Eur. Phys. J. C (2019) **79:951**, 1-11.

[22] M. S. Morris and K. S. Thorne, Wormholes in spacetime and their use for interstellar travel: A tool for teaching general relativity, Am. J. Phys. **56**, (1988) 395-412.
[23] J. J. Bevelacqua, Curvature Systematics in General Relativity, FIZIKA A **15**, (2006) 133–146.
[24] C. W. Misner, K. S. Thorne, and J. A. Wheeler, Gravitation, W. H. Freeman and Company, San Francisco (1973).
[25] M. Visser, Lorentzian Wormholes: From Einstein to Hawking, Am. Inst. Phys., Woodbury, NY (1995).
[26] T. Müller, Visual Appearance of a Morris-Thorne-Wormhole, Am. J. Phys. **72**, (2004) 1045-1050.
[27] K. Schwarzschild, On the gravitational field of a mass point according to Einstein's theory I, Sitzber. Deut. Akad. Wiss. Berlin, Math.-Phys. Tech. **1916**, (1916) 189-196.
[28] K. Schwarzschild, On the gravitational field of a mass point according to Einstein's theory II, Sitzber. Deut. Akad. Wiss. Berlin, Math.-Phys. Tech. **1916**, (1916) 424-434.
[29] A. S. Friedmann, On the Curvature of space Z. Phys. **10**, (1922) 377-386.

HADRONIC JOURNAL 47, 423 - 472 (2024)
DOI 10.29083/HJ.47.04.2024/SC423

SPECTROSCOPIC MANIFESTATION OF THE UNUSUAL PROPERTIES OF STRONG NUCLEAR INTERACTION

V. G. Plekhanov
Fonoriton Sci. Lab. Garon Ltd.
Tallinn, 11413, Estonia
vgplekhanov@proton.me

Received September 27, 2024
Revised October 25, 2024

Abstract

The dependence of the proton - neutron interaction in the deuterium nucleus on the distance between nucleons which was not available on accelerators hence it was first - time measured. Experimentally, neutron electron binding energy equal to 106 meV was found in diamonds and LiH which is 128 times less than proton - electron coupling energy (13.6 eV) and its value is perfectly agreed with Breit's theory. The results of our experiments make it possible to determine not only the constant of strong nuclear interaction equal 2.4680, but also to predict the mass of the boson carrying the interaction between neutron and electron equal 3.5 keV. Moreover, the creation of mass in massless Dirac fermions (leptons) in graphene by strong nuclear interaction has been demonstrated for the first time.

Keywords: strong interaction, hadrons, quarks, gluons, excitons, phonons, quantum electrodynamics, quantum chromodynamics

I. Introduction.

Simple atoms, like hydrogen, being essentially quantum electrodynamics (QED) systems, allow highly accurate theoretical predictions. QED is the first successful and still the most successful quantum field theory. The spectacular success of QED gives physicists great confidence in Maxwell's equation on the one hand and Dirac's equation on the other, yet something is missing in relations between them (see, e.g. [1]). After the discovery of the neutron in 1932 by Chadwick, there was no longer doubt that the building block of nuclei are proton and neutron (collectively called nucleons). The discovery of the neutron may be viewed as the birth of the strong nuclear interaction: it indicated that the nuclei consists of protons and neutrons and hence the presence of a force that holds them together, strong enough to counteract the electromagnetic repulsion. Theory strong nuclear interaction is the heart of quantum chromodynamics (QCD) which is part of the Standard Model (SM) [2, 3], therefore the base exchange is the gluon which mediates the forces between quarks. Nucleus is a bound system of strongly interacting protons and neutrons (more generally baryons and mesons - this is the reason for the collective name hadrons) holds atomic nuclei together and, in another context, binds quarks within hadrons. The baryons are bound states of the three quarks and mesons are composed of quark and antiquark (see, e. g. [4]).

The subject of elementary particle physics to have begun with the discovery of the electron more than century ago. In the following 50 years, one new particle after another was discovered, mostly as a result of experiments with cosmic rays, the only source of very high energy particle then available. After second war the accelerator technique was used to study the elementary particle physics. Nuclear and particle physics are essentially at the forefront of nowadays understanding of physics. Nucleus is a bound system of strongly interacting protons and neutrons. Unfortunately, modern

Quantum Electrodynamics (QED) does not provide us with the tools to calculate the bound states properties of the proton (deuteron) from first principles [1]. The present review is devoted to the results of measurements of residual strong nuclear interaction via the study the low - temperature optical spectra (reflection, photoluminescence) of the LiH (without strong interaction in hydrogen nucleus) and LiD (with strong interaction in deuterium nucleus) crystals which are different by term of one neutron from each other as well as very rich of diamond allotropes (diamond, graphite, graphene, fullerene). We should repeat that nowadays in text books and elsewhere the separation of electromagnetic and strong interaction is tacitly assumed. It is very strange because up to present time we do not even know the strong nuclear force very well. The origin of the strong interaction is very important especially in the problem of all force unification (see, also [5]). The results of the paper [6] have shown a new light on some residual strong nuclear interaction (ultimately based in the character of magnetic forces, the electromagnetic or color origin, which by their very nature, are difficult to conceal within the elusive nucleon physical boundary) between both kind of forces which experimentally manifested through isotopic shift of zero phonon line in optical spectra.

As indicated above, there is a common place in Standard Model (SM) of modern physics; that the strong force does not act on leptons (see, also [5]). Following this conclusion we do not must to observe the dependence of the optical properties of solids on addition neutrons in substance. This contradict the history of the development of isotope effect. The first attempt to discover an interaction between neutrons and electrons was made by Dee [7] in the same year, 1932 in which the neutron was discovered by Chadwick [8]. In 1936, Condon [10] pointed out that the existence of a neutron - electron interaction would give rise to an isotope shift in spectral lines of atoms, which was observed for the first time by Aronberg in 1918 [9] in the line spectra of Pb isotopes (see, also review [11]). The existence of a weak attractive interaction between electrons and neutrons has been described in the series papers by Foldy [12]. Foldy has showed that neutron - electron interaction has two contributions - one arising from anomalous magnetic moment of the neutron (see, also [5]) and the other from an intrinsic Darwin coefficient [13] - electric field. This picture was justifiable in meson theory though both of these contributions have a common origin [12, 14]. In all methods of the measurements (see, e.g. [14]) there are principal troubles connected with the necessity of introducing large corrections in size of order of the investigated effect of neutron - electron interaction. Besides there is intrigue in the fact that all known experimental values (see [15] and references quoted therein) were scattered around the so called Foldy scattering length in the interval $\pm$

10%. The main conclusion of the fundamental papers by Foldy is that the intrinsic neutron - electron interaction is essentially an electromagnetic interaction between the neutron and the charge density producing an external electromagnetic field by electron [12, 14].

According to contemporary physics the strong force does not act on lepton (electrons, positrons, muons and neutrinos), but only on protons and neutrons (more generally, on baryons and mesons - this is the reason for the collective name hadrons) (see, however below). It should be add that the forces between the quarks must be long range, because the gluons (as photons) have zero mass. This does not imply that the forces between hadrons are also long - range, because hadrons have zero color charges overall. The forces between the colorless hadrons are the residues of the for as between their quark constituents, and cancel when the hadrons are far apart [2 - 4]. In 1935, Yukawa [16] pointed out that the nuclear force could be generated by the exchange of a hypothetical spinless particle, provided its mass intermediate between the masses of proton and electron - a meson. Yukawa predicted the pion [1 - 4].The macroscopic manifestations of the strong interaction are restricted up to now to radioactivity and the release of nuclear energy. Yutaka's potential has the form

$$V = g\frac{e^{-kr}}{r^n}, \qquad (1)$$

for some n. Here the strength of the force is measured by the constant k (see, also [5]). The most important feature Yukawa's forces is that they have a small range ($\sim 10^{-15}$ m). The central dogma of atomic physics after Yukawa's paper that proton - electron attraction could be explained in terms of classical electrostatic theory, while the strong force effects were essentially new and inexplicable. So, far the best theoretical guess is the Yutaka potential, but it is a static potential not dependent on velocities of the nucleons. A static force is not a complete one because it can not explain the propagation of the nuclear interaction. Moreover, as was indicated above, a phenomenological Yukawa potential can not be directly verified experimentally. We should note that nowadays in text books and elsewhere the separation of electromagnetic and strong interaction tacitly assumed. It is very strange up to present time we do not even know the strong force very well. And what is more we have some contradiction taking into account that the forces between quarks must be long - range, because the gluons have zero mass. But as was mentioned above the force between colorless hadrons is short - range, when the distance between hadrons is more than nuclear size [1]. In connection of our brief analysis, we must emphasize that outsanding works on hadrons mechanics [17] deserve separate and fundamental

study.

One may consider four families of particles in order of increasing rest mass; the first contains only one member, the proton, a boson of spin 1. The second family, leptons, contains fermions of spin 1/2, lighter than proton. Leptons are subject to electromagnetic and Fermi interaction only, not the strong interaction (see however below). The third family, mesons, comprises bosons of spin 0. These are heavier than the leptons, lighter than the protons, and the subject to all three types of interactions; weak, strong and electromagnetic. The fourth family, baryons, comprises the proton and heavier fermions. Baryons are subject to all three types of interactions; those heavier than neutron are called hyperons.

Table 1. The four fundamental forces.

Interaction	FQ	Mass	Range (m)	RS	Spin	TC-S (m^2)	TTS(s)
Str	Gluon	0	10^{-15}	1	1	10^{-30}	10^{-23}
We	W , Z	81, 93 GeV/c2	10^{-18}	10^{-5}	1, 1	10^{-44}	10^{-8}
Elec	Photon	0	∞	1/137	1	10^{-33}	10^{-20}
Gra	Graviton	0	∞	10^{-38}	2	-	-

Here - FQ field quant, RS relative strength, TC - S Typical cross - section, TTS - Typical time scale.

The Table 1 (see also [19]) given for the strength and range of the forces come from a comparison of the effects they produce on two protons. In some respect these resemble an ordinary Newtonian force between the protons, varying with the distance between them as if the force was derived from a potential function (1): for some n. This is an inverse - power force which is diminished by an exponential factor at distances larger than a certain distance R, the range of the force. The strength of the force is measured by the constant k. The unit of strength is $hc/2\pi$ where h is Planck's constant and c the speed of light. Thus nuclear physics was essentially the paradigmatic example of understanding particle physics. The modern quantummechanical view of the three fundamental forces (all except gravity) is that

particles of matter (fermions neutrons, protons, electrons) do not directly interact with each other, but rather carry a charge, and exchange virtual particles (gauge bosons photons, gluons, gravitons) which are the interaction carriers or force mediators. As can be seen from Table 1, photons are the mediators of the interaction of electric charges (protons, electrons, positrons); and gluons are the mediators of the interaction of color charges (quarks). In our days, the accepted view is that all matter is made of quarks and leptons. As can be seen, of the three pairs of quarks and leptons, one pair of each - the quark u and d and the leptons e and ν_e (electrons neutrino) - are necessary to make up the every day world, and a world which contained only these would seem to be quite possible.

As we can see above the method of the scattering particles allows to determine only length of scattering as well as the size and depth (highest) of the neutron's potential. In the present paper we attempt to measure the energy of the neutron - electron interaction via spectroscopic study of the optical characteristics of solids with isotope effect at low temperature. Therefore, it is purpose of our paper to advance a description of the manifestation of strong nuclear interaction in solids, using partly published and new non - accelerator experimental results. Our spectroscopic measurement of the low temperature optical characteristics of LiH_xD_{1-x} crystals is permitted to quantitative study of the dependence of strong coupling constant, α_s, on the proton - neutron distance in the deuteron nuclei. Carbon, being the second element after silicon on Earth, has unusually wide range of allotropic compounds with completely different physical properties [20]. The use of our object allows the investigation of not only the isotope effects in lattice dynamics (vibrational, elastic and thermal properties), but also the influence of such effects on the electronic excitations (for example, the renormalization of the band - to - band transition energy E_g). We emphasize that the study of the isotope effect remains at the forefront not only in materials science, but also nuclear and high energy physics.

Isotopically pure materials represent a separate class of modern materials science, which is an accelerator of the development of the latest fine technology. First of all, it is necessary to remember due to this explosive leap in the development of electronic and optical technologies. It is thanks to isotopically pure silicon used in personal computer processors that it has been possible to step beyond the 3GHz threshold. Moreover, isotopically pure germanium is the best weak signal detector. Low dimensional structures of quantum wires (QW), quantum dots (QD) received a new impetus for development when using isotopically pure materials, as well as artificially regulating the isotopic composition of a material. We emphasize that due to the wide class of allotropic carbon compounds, the physical properties of which vary from

transparent in the ultraviolet (UV) range (diamond) to opaque (graphite, graphene), from dielectric (diamond) to a compound with metallic conductivity (graphene) and also which have extremely different elastic and thermal properties - all of the above mentioned characteristics exhibit isotopic dependence. We must substitute ^{12}C for a heavy isotope ^{13}C. Semiconductor graphene could come to replace all silicon electronics. Of course, the new technology for the development of quantum computer (QC) processors is based on the use of materials with different spin values. Great demand for isotopically pure materials from control agencies. For example, a special requirement for isotopically pure silicon, from which it is planned to make a control sample of 1 kg. We will not at all touch upon the very wide applications of pure isotopes in biophysics and medicine. As an example, let us point out that only one country (USA) uses tens of thounds tons of different isotopes per year.

The present paper reviews of recent research work on the preparation and remarkable properties of isotope - mixed systems, covering wide range of topics from physics of elementary particles, materials science to engineering applications, including in quantum information and quantum computers. Artificial activation of the strong interaction by adding of one neutron to the nucleus causes the global reconstruction of the macroscopic characteristics of solids. The experimental evidence of macroscopic manifestation of the strong interaction in optical spectra of solids which are different by term of one neutron from each other (using LiD crystals instead LiH) has been presented. The initial components of mixed crystals LiH_xD_{1-x} are LiH (no strong interaction in the hydrogen nucleus) and LiD (with strong interaction in the deuterium nucleus) crystals are dielectrics with cubic symmetry. The change of the concentration of deuterium in mixed crystals LiH_xD_{1-x} determines the change in the distance between nucleons, which is directly manifested in the position of the phononless free exciton emission line in the low - temperature luminescence spectrum. A series of such measurements made it possible to construct a function of the dependence of the energy of strong nuclear interaction on the distance between nucleons in the deuterium nucleus. This evidence is directly seen from luminescence (reflection) and scattering spectra. As far as the gravitation, electromagnetic and weak interactions are the same in both of kind crystals, it only emerges the strong interaction in deuterium nucleus. Therefore a sole conclusion is made that the renormalization of the energy of electromagnetic excitations (electrons, excitons, phonons) is carried out by the strong nuclear interaction. The measurements of the dependence of the energy of strong nuclear interaction on the distance between nucleons in a nucleus were performed for the first time and this results allow to find the maximum possible value of $\alpha_s = 2.4680$. Our non - accelerator results opens new

avenue in the investigation of the propagation the force of strong nuclear interaction in the wide value range by means the condensed matter alike traditional accelerator methods. Carbon, being the second element after silicon on Earth, has unusually wide range of allotropic compounds with completely different physical properties. The use of our object allows the investigation of not only the isotope effects in lattice dynamics (vibrational, elastic and thermal properties), but also the influence of such effects on the electronic excitations (for example, the renormalization of the band - to - band transition energy E_g). We emphasize that the study of the isotope effect remains at the forefront not only in materials science, but also nuclear and high energy physics.

II. Experimental.

The apparatus used in our experiments has been described in several previous publications [21 - 23]. For clarity, we should mentioned here that immersion home - made helium cryostat and two identical double - prism monochromators were used. One monochromator was used for the excitation and the other, which was placed at right - angle to the first for analyzing the luminescence and scattering of light. In our experiments we investigated two kinds of crystals (LiH and LiD) which are differ by a term of one neutron. Lithium hydride and lithium deuteride are ionic insulating crystals with simple electronic structure, four electrons per unit cell, both fairly well – described structurally (neutron diffraction) and dynamically (second – order Raman spectroscopy) and through ab initio electronic structure simulation. Among other arguments, LiH and LiD are very interesting systems due to their extremely simple electronic and energy structure and to the large isotopic effects when the hydrogen ions are replaced by the deuterium ones. On the other hand, the light mass of the ions, specially H and D, makes that these solids have to be considered like quantum crystals, and consequently, described theoretically by quantum theory. In a solid one deals with a large number of interacting particles, and consequently the problem of calculating the electronic wave functions and energy levels is extremely complicated. It is necessary to introduce a number of simplifying assumptions. In the first place we shall assume that nuclei in the crystalline solid are at rest. In an actual crystal this is of course never the case, but the influence of nuclear motion on the behavior of electrons may be treated as a perturbation for the case in which they are assumed to be at rest. Even with above assumption, however, we are still with a many – electron problem which can be solved only be approximative methods. In the case of solids, the most

important approximative method which has been applied extensively is the so – called one – electron approximation. In this approximation the total wave function for the system is given by a combination of wave functions, each of which involves the coordinates of only one electron. In other words, the field seen by a given electron is assumed to be that of the fixed nuclei plus some average field produced by the charge distribution of all other electrons.

The difference between a good conductor and a good insulator is striking. The electrical resistivity of a pure metal may be as low as 10^{-10} ohm-cm at a temperature of 1 K, apart from the possibility of superconductivity. The resistivity of good insulator may as high as 10^{22} ohm-cm. The understand the difference between insulators and conductors, we shall use the band – gap picture (Fig. 2 below). The possibility of band gap is the most important property of solids.

The single crystals of LiH and LiD were grown from the melt by the modified method of Bridgeman - Stockbarger (see [24, 25]). The crystals were synthesized from ^{7}Li metal and hydrogen of 99.7% purity and deuterium of 99.5% purity. Virgin crystals had a slightly blue - grey color, which can be attributed to nonstoichiometric excess of lithium present during the grown cycle. On annealing for several days (up to 20) at 500^0C under ~ 3 atm of hydrogen or deuterium, this color could be almost completely eliminated. Because of the high reactivity and high hygroscopy of investigated crystals should be protected against the surrounding atmosphere. Taking into account this circumstance, we have developed special equipment which is allowed to prepare samples with a clean surface cleaving their in the bath of helium cryostat with normal or superfluid liquid helium [22]. The samples with such surface allow to perform measurements during 15 hours. An improved of LiH (LiD) as well as mixed crystals were used in the present study. In spite of the identical structure of all free - exciton luminescence spectra, it is necessary to note a rather big variation of the luminescence intensity of the crystals from the different batches observed in experiment. Experimental set up for diamond and grafene is described in relatively cited below papers. The crystal periodicity leads to the formation of a band energy structure (Fig. 1). An electron from valence band is excited into conduction band.

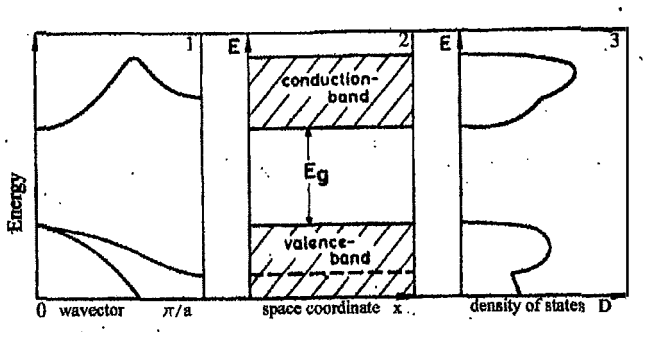

Fig. 1. Various possibilities to present the band - structure of homogeneous undoped insulator (semiconductor). 1 - the dipersion relation, i.e. the energy E as a function of the wave vector $\vec{k}$, 2 - the energy regions of allowed and forbidden states as function of a space coordinate x and 3 - the density of states (all curves are schematic ones) [22].

The attractive Coulomb potential between the missing electron in the valence band, which can be regarded as a positively charged hole, and the electron in the conduction band gives a hydrogen - like spectrum with an infinitive number of bound state and ionization continuum Fig. 2. Below we will briefly describe the results of the optical spectroscopy of isotope - mixed solids. For this purpose we use crystals LiH (without strong interaction in thr nucleus) and LiD (with strong interaction in the deuterium nucleus) which are differ by term of one neutron from each other as well as diamond with different concentration of different isotopes.

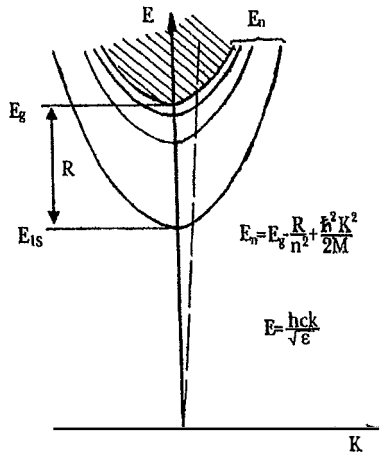

Fig. 2. Discrete and continous (hatched area) Wannier - Mott exciton energy spectrum taking into account its kinetic energy $\hbar^2k^2/2M$. The broken line connects to the dispersion of light in the medium. R - is the exciton binding energy, n = 1, 2, 3, ...

As demonstrated early (see, e.g book [24]) most low - energy electron excitation in LiH (LiD) crystals are the large radius escitons [24, 26].

III. Results.

Photoluminescence is the optical radiation emitted by a physical system (in excess of the thermal equilibrium blackbody radiation) resulting from excitation to a nonequilibrium state by irradiation with light. Photoluminescence is also rapidly evolving into major basic research tool comparable to absorption (reflection) measurements in importance. Two reason for this stand out as significant. First is the sensitivity of the luminescence technique. It often happens that features which are just discernible in absorption will completely dominate the luminescence spectra. The converse is also sometimes true, making luminescence and absorption (reflection)

complementary techniques. Second is the simplicity of data collection. In last half-century the luminescence method has become one of the most common techniques for studying excitons in dielectrics and semiconductors. While the structure of spectra of fundamental reflection (absorption) depends on the internal degrees of freedom of Wannier – Mott exciton, the structure and shape of the luminescence spectrum are determined primarily by its external degrees of freedom. The latter are associated with the translation motion of large – radius exciton as a whole, with the translation mass $M = m_e + m_h$, where m_e and m_h – effective masses of electron and hole, respectively.

Free exciton luminescence is observed when LiH (LiD) crystals are excited in the midst of the fundamental absorption. The spectrum of free exciton photoluminescence of LiH crystals cleaved in superfluid helium consists of a narrow (in the best crystals, its half - width is $\Delta E \leq 10$ meV [27]) phononless emission line and its broader phonon repetitions, which arise due to radiated annihilation of excitons with the production of one to five longitudinal optical (LO) phonons (see Fig. 3).

The phononless emission line coincides in an almost resonant way with the reflection line of the exciton ground state which is indication of the direct electron transition $X_1 - X_4$ of the first Brillouin zone [28].The lines of phonon replicas form an equidistant series biased toward lower energies from the resonance emission line of excitons. The energy difference between these lines in LiH crystals is about 140 meV, which is very close to the calculated energy of the LO phonon in the middle of the Brillouin zone [29] and which was measured in (see, e.g. [24] and references quoted therein). The isotopic shift of the zero - phonon emission line of LiH crystals equals 103 meV. As we can see from Fig. 3 the photoluminescence spectrum of LiD crystals is largely similar to the spectrum of intrinsic luminescence of LiH crystals. There are, however, some distinctions one is related. Firstly the zero - phonon emission line of free excitons in LiD crystals shifts to the short - wavelength side on 103 meV. These results directly show the violation of the strong conclusion (see, e.g. [1 - 4]) that the strong force does not act on leptons. The second difference concludes in less value of the LO phonon energy, which is equal to 104 meV. The simplest approximation, in which crystals of mixed isotopic composition are treated as crystals of identical atoms having the average isotopic mass, is referred to as virtual crystal approximation (VCA) [24].

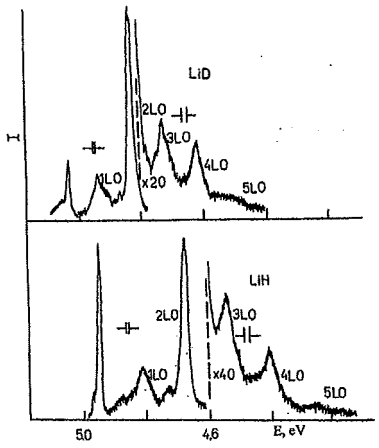

Fig. 3. Photoluminescence spectra of free excitons at 2 K in LiH and LiD crystals cleaved in superfluid helium.

When light is excited by photons in a region of fundamental absorption in mixed LiH_xD_{1-x} crystals at low temperature, lines luminescence of free excitons are observed (Fig. 4), like in the pure LiH and LiD crystals. As before [24], the luminescence spectrum of crystals cleaved in superfluid liquid helium consists of the relatively zero - phonon line and its wide LO replicas. For the sake of convenience, and without scarfing generality, Fig. 4 shows the lines of two replicas. Usually up to five LO repetitions are observed in the luminescence spectrum as described in detail in [30]. In Fig. 4 we see immediately that the structure of all three spectra is the same. The difference is in the distance between the observed lines, as well as in the energy at which the luminescence spectrum begins, and in the half - width of the lines.

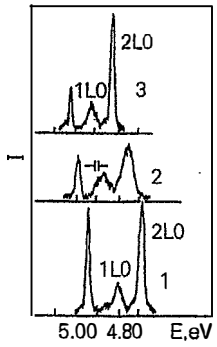

Fig. 4. Photoluminiscence spectra of free excitons in LiH (1), LiH_xD_{1-x} (2) and LiD (3) crystals cleaved in superfluid helium at 2 K. Spectrometer resolution is shown.

The change of the concentration of deuterium in mixed crystals LiH_xD_{1-x} determines the change in the distance between nucleons, which is directly manifested in the position of the phononless free exciton emission line in the low - temperature luminescence spectrum. A series of such measurements made it possible to construct a function of the dependence of the energy of strong nuclear interaction on the distance between nucleons in the deuterium nucleus. This evidence is directly seen from luminescence (reflection [24]) and scattering spectra [30]. The X - ray diffraction investigations show that the LiH_xD_{1-x} mixed crystals [31] form a continuos row of the solid solution and testify themselves like a virtual crystal with a variable lattice constant (and exciton radius, respectively) that obeys Vegard's law (see Fig. 5)

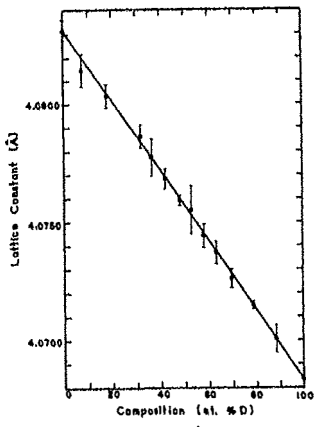

Fig. 5. Lattice constan in the ^{7}Li(H,D) crystals plotted against the isotopic composition [31].

Fig. 6 shows the concentration dependence of the energy of interband transition E_g (see Fig. 1). As can be seen from Fig. 6, VCA method (the straight dashed line) cannot describe observed experimental results. This dependence has a nonlinear character.

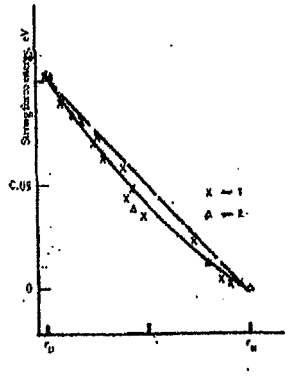

Fig. 6.Dependence of the interband transition (strong interaction) energy E_g in mixed crystals LiH_xD_{1-x} on the concentration x (number of neutrons). Here r_D and r_H are the radii of deuterium and hydrogen nuclei according CODATA recommended values. The stright line is the linear dependence $E_g = f(x)$ in the VCA model. The solid line corresponds to calculation using the polynom of second degree [22].

Comparison the experimental results on the luminescence (reflection) and light scattering in the crystals LiH_xD_{1-x} which differ by a term of one neutron only is allowed to the next conclusions;

1. At the adding one neutron (using LiD crystals instead LiH ones) is involved the increase exciton energy on 103 meV.

2. At the addition one neutron the energy of LO phonons is decreased on the 36 meV, that is direct seen from luminescence and scattering spectra.

Both characteristics are macroscopic.

Another very interesting example is carbon. Carbon atom is built from 6 protons, A neutrons and 6 electrons, where A = 6 or 7, yield the stable isotopes ^{12}C and ^{13}C, respectively, and A = 8 characterizes the radioactive isotope ^{14}C [32]. The isotope ^{12}C , with nuclear spin I = 0, is the most common one in nature with 99% of all carbon atoms, whereas only $\simeq$ 1% are ^{13}C with nuclear spin I = 1/2. There only traces of ^{14}C (10^{-12} of all carbon atoms) which transforms into nitrogen ^{14}N by β - decays [33]. Although ^{14}C only occurs rarely, it is important isotope used for historical dating (see,

e.g. [37]). Carbon, one of the most elements in nature, still gives a lot surprises. It is found in many different forms - allotropes - from zero dimensional fullerene, one dimensional carbon nanotubes, two dimensional graphene and graphite, to three dimensional diamond - and the properties of the various carbon allotropes can vary widely [20, 34]. Fullerenes are essentially hollow carbon shells of various sizes. the most well - known of these is a 60 - carbon unit called buckminster fullerene or C_{60} (more details see below). For instance, diamond is the hardest material, while graphite is one of the softest; diamond is transparent to the visible part of spectrum, while graphite is opaque; diamond is an electrical insulator, while graphite and graphene are a conductors. Very important is that all these different properties originate from the same carbon atoms, simply with different arrangements of the atomic structure. Below we describe the new phenomena of the carbon - isotope effect in diamond. Crystals ^{12}C and ^{13}C diamond differ only one neutron.

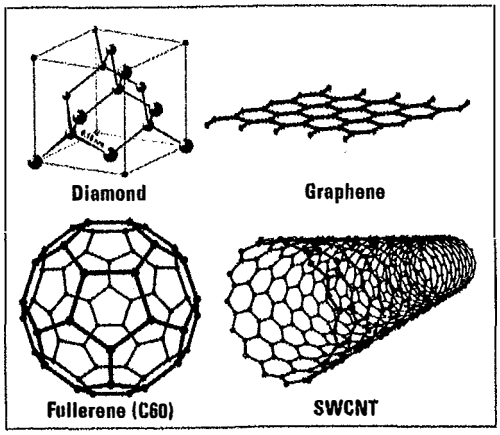

Fig. 7. Structure of some representative carbon allotropes [diamond, graphene, fullerene (C60) and SWCNT].

In the atomic ground state of carbon, the 6 electrons are in the configuration $1s^2 2s^2 2p^2$, i.e. 2 electrons fill the inner shell 1s, which is close to the nucleus and which is irrelevant for chemical reactions, whereas 4 electrons occupy the outer shell of 2s and 2p orbitals. Because the 2p orbitals ($2p_x$, $2p_y$ and $2p_z$) are roughly 4 eV

higher than the 2s orbital, it is energetically favorable to put 2 electrons in the 2s orbital and only 2 of them in the 2 p orbital (see, e.g. [1, 34]). It turns out, however, that in the presence of other atoms, such as e.g. H, O, or other C atoms, it is favorable to excite one electron from the 2s to the third 2p orbital, in order to form covalent bonds with the other atoms. The gain in energy from the covalent bond is indeed larger than the 4 eV invested in the electronic excitation. In the excitation state, we therefore have four equivalent quantum - mechanical states: $|2s\rangle$, $|2p_x\rangle$, $|2p_y\rangle$ and $|2p_z\rangle$. a quantum - mechanical superposition of the state $|2s\rangle$ and $n|2p_j\rangle$ states is called sp^n hybridization, which play an essential role in carbon bonds [34].

In the case of a superposition of the 2s and two 2p orbitals, which we may choose to be the $|2p_x\rangle$ and the $|2p_y\rangle$ states, one obtains the planar sp^2 hybridization. The three quantum - mechanical states are given by

$$|sp_1^2\rangle = \frac{1}{\sqrt{3}} |2s\rangle - \sqrt{\frac{2}{3}} |2p_y\rangle,$$

$$|sp_2^2\rangle = \frac{1}{\sqrt{3}} |2s\rangle + \sqrt{\frac{2}{3}} \left(\frac{\sqrt{3}}{2} |2p_x\rangle + \frac{1}{2} |2p_y\rangle\right), \qquad (2)$$

$$|sp_3^2\rangle = -\frac{1}{\sqrt{3}} |2s\rangle + \sqrt{\frac{2}{3}} \left(-\frac{\sqrt{3}}{2} |2p_x\rangle + \frac{1}{2} |2p_y\rangle\right).$$

These orbitals are oriented in the xy - plane and have nutual 120^0 angles (Fig. 8^a). The remaining unhybrized $2p_z$ orbitalis perpendicular to the plane A prominent chemical example for such hybridization is the benzene molecule [35]. This molecule consists of a hexagon with carbon atoms at the corner linked by σ bonds (Fig 8^b). Each carbon atom has, furthermore, a covalent bond with one of the hydrogen atoms which stick out from the hexagon in a star like manner. In addition to the 6 bond, the remaining $2p_z$ orbitals form 3π bonds, and the resulting double bonds alternate

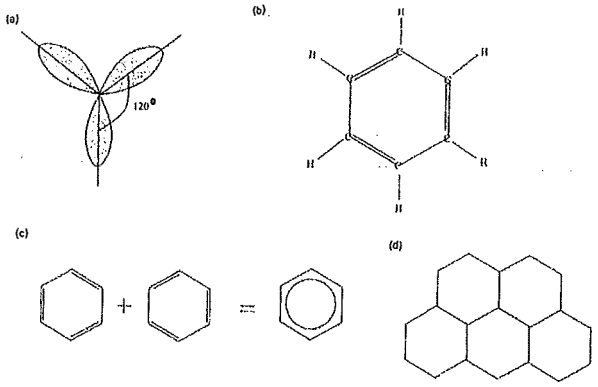

Fig. 8. (a) Schematic view of the sp^2 hybridization. The orbitals form angles of 120^0. (b) Benzene molecule - C_6H_6. The 6 carbon atomsare situated at the corners of a hexagon and form covalent bonds with the H atoms. In addition to the 6 covalent σ bonds between C atoms, there are three π bonds indicated by the doubled line. (c) The quantum - mechanical ground state of the benzene ring is a superposition of the two configurations which differ by the position of the π bonds. The π electrons are, thus, delocalized over the ring. (d) Graphene may be viewed as a tiling of benzene hexagons, where the H atoms are replaced by C atoms of neighbouring hexagons and where the π electrons are delocalized over the whole structure.

with single σ bonds around hexagon. Because a double bond is stronger than a single σ bond, one may expect that the hexagon is nor perfect. A double bond (C = C) yields a carbon - carbon distance of 0.135 nm, whereas it is 0.147 nm for a single σbond (C - C). However, the measured carbon - carbon distance in benzene is 0.142 nm for all bonds, which is roughly the average length of a single and a double bond. The ground state a quantum - mechanical superposition of the two possible configurations for the double bonds shown schematically in Fig. 8[c]. These chemical considerations indicate the way towards carbon - based condensed matter physics - any graphitic compound has been a sheet of graphene as its basic constituent. Such a graphene sheet may be viewed simply as a tiling of benzene hexagons, where one has

replaced the hydrogen by carbon atoms to form a neighboring carbon hexagon (see Fig 8[d]). However, graphene has remained the basic constituent of graphitic systems during a long time only on the theoretical level. From experimental point of view, graphene is the youngest allotrope and accessible to physics measurements only since 2004. Graphite may be viewed as a stacking sheets (Fig.8[c]) that stick together due to the van der Waals interaction, which is much weaker than in plane covalent bonds.

If one superimposes the 2s and all three 2p orbitals, one obtains the sp^3 hybridization, which consist of four club - like orbitals that mark a tetrahedron. The orbitals forma angles of 109.5^0 degrees (Fig 9[a]). A chemical example for this hybridization is methane (CH_4), where the four hybridized orbitals are used to form covalent bonds with the 1s hydrogenatoms. In condensed matter physics, the $2p^3$ hybridization is at the origin of the formation of diamonds, when liquid carbon condenses under high pressure. The diamond lattice consists of two interpenetrating face - center - cubic (fcc) lattice as, with a lattice spacing of 0.357 nm as shown in Fig. 9[b].

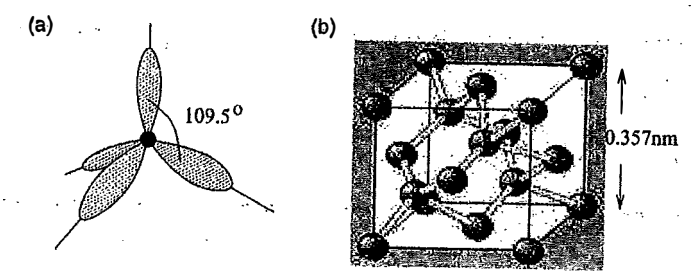

Fig. 9. (a) sp^3 hybridization with 109.5^0angle between the four orbitals. (b) Crystal structure of diamond.

Although they consist of the same atomic ingredient, namely carbon, the 3D graphite and diamond crystals are physically extremely different. Graphite, as described above [1] is a very soft material due to its layered structure, whereas diamond is one of the hardest natural materials because all bonds are covalent σ bonds. The fact that all 4 valence electrons in the outer atomic shell are used in the

formation of the σ bonds is also the reason for diamond being an insulator with a large band gap of 5.47 eV (see above). In contrast to insulating diamond, the electrons in the weaker π bonds in graphite are delocalized and thus, yield good electronic conduction properties. The fbsorption spectrum demonstrating an indirect electronic transition in diamond is presented in Fig. 10.

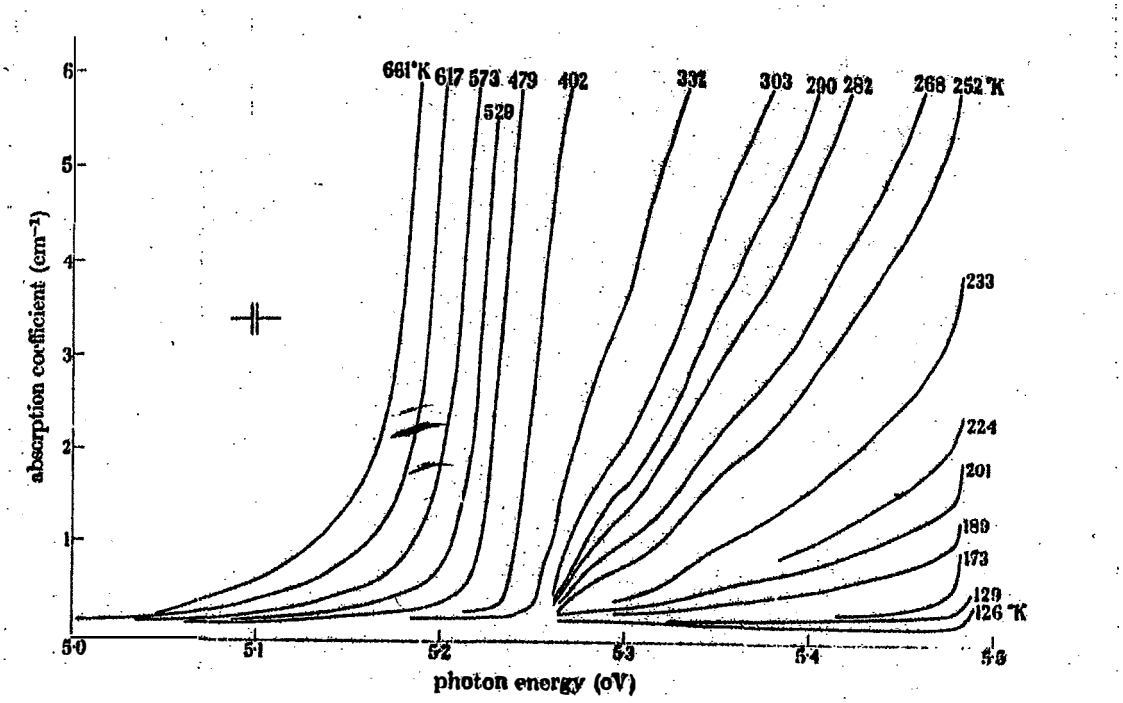

Fig. 10 Absorption edge spectrum of diamond at various temperature [36].

The indirect transition diagram is shown in Fig. 11. In diamond , we have seen (Fig. 2.5 in [37]) that excitation across the minimum separation of filled and empty states demands a large change in wave vector, and such a transition cannot be initiated by a photon unless it has access to a source of crystal momentum. We should repeat that it is the phonons that provide the required momentum (see, also Fig.11).

We write the conservation laws in the form

$$E_f - E_i = h\nu + \hbar\omega_f,$$
$$\vec{k}_f - \vec{k}_i = 0 + \vec{q}, \qquad (3)$$

here $\vec{q}$ and ω_f apply to the phonon involved in the transition. Now $E_f - E_i = E_g$ and it is clear that the inclusion of phonons produces an absorption edge at a somewhat lower energy, namely $E_g - \hbar\omega_f$. These indirect or phonon - assisted transitions produce only weak absorption compared with that associated with direct transitions (see, e.g. [38]).

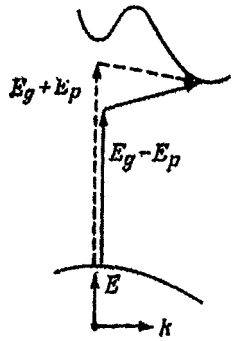

Fig. 11. Schematic of two - step transition in the case of the indirect bandgap of material, where E_p is the phonon energy and E_g is the energy of interband transition.

Due to the indirect gap of $E_g = 5.47 \pm 0.005$ eV (295 K), at K = 0.76 X, diamond has intrinsic phonon - assisted free exciton luminescence lines (see, e.g. [30]). The change of the indirect gap of diamond between pure ^{12}C and ^{13}C crystals has been determined by Collins et al. [39]. The luminescence spectra of the natural (^{12}C) and synthetic (^{13}C) diamond at electron excitation were investigated by Collins et al. [39] (Fig. 12), Ruf et al. [40], Watanabe et al. [41]. Fig. 12 compares the free exciton luminescence for a natural diamond with that for a synthetic diamond.

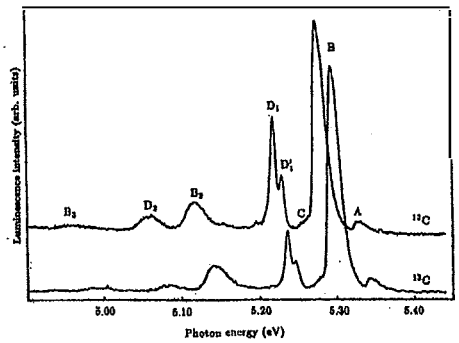

Fig. 12. Spectra measured at 77K phonon - assisted free cathodoluminescence feature (A, B and C) and the phonon assisted bound - exciton feature (D) from natural semiconducting ^{12}C diamond and a ^{13}C synthetic diamond (after [39]).

The peaks labeled A, B and C are due, respectively, to the recombination of a free exciton with the emission of transverse - acoustic, transverse - optic and longitudinal - optic phonons having wavevector $\pm k_{min}$ and quanta in ^{12}C [30, 42].

$$\hbar\omega_{TA} = 87 \pm 2;\ \hbar\omega_{TO} = 141 \pm 2;\ \hbar\omega_{LO} = 163 \pm 1 \text{ meV}. \qquad (4)$$

Features B_2 and B_3 are further free exciton processes involving the above TO phonon with one and two zone - center optic phonons respectively. As we can see from Fig. 12 the isotope shift of the free exciton luminescence spectrum of ^{13}C diamond is equal 16.5 ± 2.5 meV [30]. The more detailed and quantitative investigation of $E_g \sim f(x)$, where x is the isotope concentration was done by Ruf et all. [40] (Fig. 13) and Watanabe et all. [41] (Fig. 14) where five samples of diamond with different concentrations x were studied.

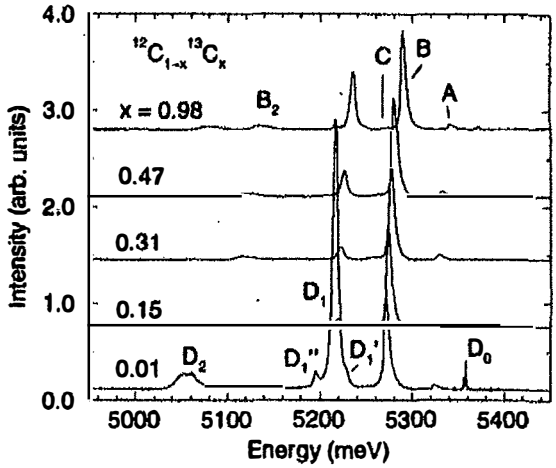

Fig. 13. Cathodoluminescence spectra of isotopically modified diamond at 36 K. Intrinsic phonon - assisted recombination peaks are labeled in the top spectrum, those from boron - bound excitons in that at the bottom. The spectra are normalized to the intensity of the B peak and vertically offset for clarity (after [40]).

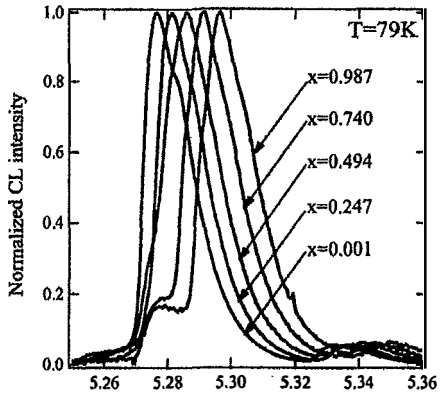

Fig. 14. luminescence spectra of free excitons in homoepitaxial diamond films

grown from mixture of methane in hydrogen by means of a microwave plasma - assisted CVD. The spectra illustrate the effect of isotope composition $^{12}C^{13}_{1-x}C_x$ mixed in the CVD gas phase. All spectra ate normalized to the same height (after [41]).

Watanabe et al. have concluded that the maximum change of the band gap due to substitution of ^{12}C by ^{13}C is ΔE_g = 15.4 meV. The dependence of the change exciton energy on the isotopic concentration in a diamond is depicted on the Fig. 15.

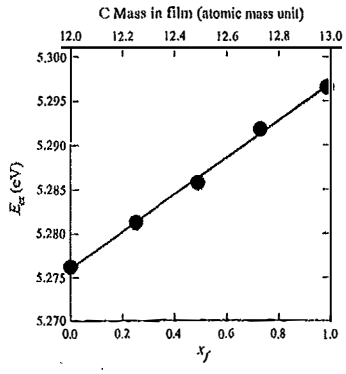

Fig. 15. Excitonic band - gap energy E_{exc} obtained for the CL peak energes in Fig. 14 as a function of the ^{13}C concentration of the films (x_f). The solid line is a linear regression fit of the data (after [41]).

This value (15.4 meV) is in good agreement with the estimate of 16.5 ± 2.5 meV by Collins et all. [36] using a zero - point renormalization obtained from a fit of the experimental temperature dependence of the band gap (see, also [39]). We should stress that the isotope shift in $^{12}C^{13}_xC_{1-x}$ diamond cryatals approximately 15 meV per one neutron and on seven neutrons we get 15 • 7 = 105 mev. This value is very lose to the observed one (0.103 meV) in LiH_xLiD_{1-x} crystals. As will be shown below this value is the maximum value of the neutron - electron binding energy.

It is clear that the lattice - dynamic properties of a crystal are directly affected by the atomic mass. To a first approximation, phonon behave like harmonic oscillators

with frequencies [39]

$$\omega \propto m^{-1/2}. \qquad (5)$$

Crystals containing various isotopes are usually described within virtual crystal approximation (VCA) [44] where m in Eq. (4) is replaced by the average atomic mass

$$\overline{m} = \sum_i c_i m_i. \qquad (6)$$

It is obtained from the sum over the isotopes masses m_i and concentration c_i. In spite of VCA simplicity, the model describes the general feature of the lattice dynamics of mixed alkali - halide crystal sufficiently well (for details see [39, 42]). Isotopes are ideal for lattice - dynamitic investigations of crystals. One can make use of the unique isotopic properties by varying the isotopic composition. Isotope substitution helps to disentangle the individual contributions of anharmonic and disorder - induced effects and to clarity the origin of phonon broadening mechanisms. Due to the fact that substitution of the isotopic mass in semiconducting crystals a small variation of E_g [42], perturbation theory is applicable (excluding LiH crystals [24]).

Raman spectroscopy is a powerful means to gain experimental access to phonons and their interaction and scattering mechanisms. All studies presented in this paragraph are restricted to stable, i.e. non - radioactive isotopes. About 300 stable and 1000 radioactive isotopes are known today. Some elements are isotopically pure (for example, Co), while others may contain numerous isotopic modifications (for example, Sn has 10 stable isotopes with atomic masses ranging from 112 to 124, while Xe has 23 isotopes, 9 of which are stable (see, Table 1 in [42]).

In this part, the modern understanding of first - order Raman slight scattering spectra in isotopically mixed elementary and compound (CuCl, GaN, GaAs, GaP) semiconductors having a zinc blende structure is described. It is well - known that materials having a diamond structure (C, Si Ge, α - Sn) are characterized by the triply degenerate phonon states in the Γ - point of the Brillouin zone ($\vec{k} = 0$) (see, e.g. [37]). Isotope effect in light scattering spectra in Ge crystals was first investigated by Agekyan et al. [46]. A more detailed study of Raman light scattering spectra in

isotopically mixed Ge crystals has been performed by Cardona and coworkers [42].

The cubic modifications of crystalline carbon, diamond, is characterized by a tetrahedral coordination underlying its structure dictated by sp^3 bonding (see Fig. 9) between the nearest neighbor atoms. Diamond has two atoms per primitive (Bravais) cell. The strong covalent bonding and the light mass of the constituent atoms result in a large frequency (see, Eq. (3)) for zone center, Raman active, triply degenerate F_2 mode [47]. Its crystalline perfection and transparency [36] make diamond ideally suited for inelastic light scattering. First Raman study of the dependence the frequencies of phonons on the isotopic composition was conducted on diamond by Chrenko [49] in 1988. Several publications on diamond by other groups followed later [50 - 52]. Most clear results was obtained by Hanzawa et al. [48] (see Fig. 16).

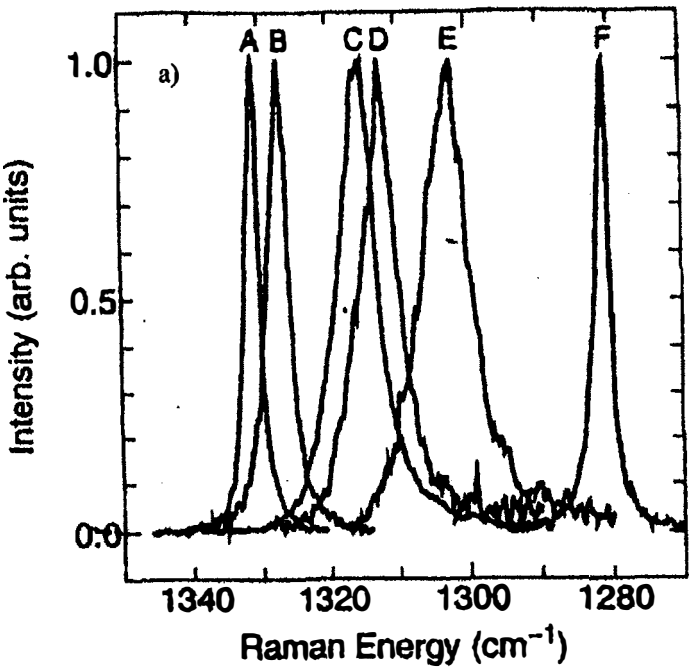

Fig. 16. First - order Raman scattering in isotopically mixed diamond crystals $^{12}C_x^{13}C_{1-x}$. The peaks A, B, C, D, E and F correspond to x = 0.989; 0.90; 0.60; 0.50; 0.30 and 0.001(after [48]).

First - order Raman light scattering spectrum in diamond crystals also includes one line with maximum $\omega_{LTO}(\Gamma) = 1332.5\ cm^{-1}$ [51]. In Fig. 16 the first - order scattering spectrum in diamond crystals with different isotope concentrations is shown [48]. As was shown in [42], the maximum and width of the first - order scattering line in isotopically - mixed diamond crystals are nonlinearly dependent on the concentration of isotopes x. The maximum shift of this line is 52.3 cm^{-1}, corresponding to the two limiting values of x = 0 and x = 1. The effect of the isotopic ^{12}C to ^{13}C ratio on the first - and second - order Raman scattering of light in the diamond has been investigated in [52]. As ^{13}C content is increased from the natural ratio ($^{12}C/^{13}C = (1 - x)/x$, where x = 0.011 to the almost pure ^{13}C (x = 0.987) the whole spectrum has shifted towards longer wavelength (Fig. 17) in good agreement with the expected $M^{-0.5}$ frequency dependence on the reduced mass M. For an approximately equal mix of the two isotopes, the authors reported that the feature seen in the above two - phonon spectra were either broadened or unresolved.

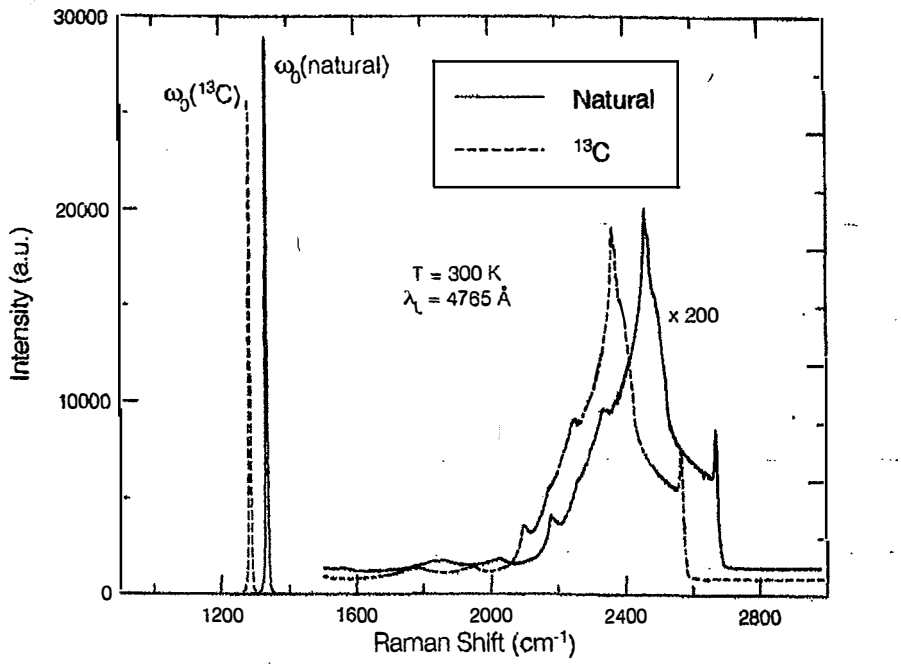

Fig. 17. The Raman spectra of natural and a ^{13}C diamond. The spectra show the dominant first - order Raman - active F_{2g} line and the significantly weaker quasi - continuous multiphonon features (after [52]).

The measured dependence on average mass mainly reflects the isotope effect on the harmonic frequency (Eq. (5)) which is, however, modified by anharmonic and disorder - induced contributions [30, 42]. Isotope renormalization frequencies of phonons of other semiconducting crystals (GaP, GaAs, α - Sn, ZnS, ZnO, CuCl, CuBr) was published in the next reviews [38]. We should highlight that addition one next neutron in nuclei is called the change in more or less of energy of elementary excitations in solids.

The science of the nuclear, atoms, simple molecules and the science of matter from microstructuree to larger scales are well established. A remaining, extremely important [30, 42], size related challenge is at the atomic scale, roughly the dimensional scale between 1 and 10 molecular sizes, where the fundamental properties of materials are determined and can be engineered (see also [37]. This field of science - isotopetronics - is a broad and interdisciplinary field of emerging research and development. Isotopetronics is connected to materials, structures and systems which components, as in nanoscience, exhibit novel and significantly modified physical properties due to their small sizes [37]. The method of the isotope renormalization of the energy of elementary excitations in bulk solid and low - dimensional structures very often used in the last five decades and well documented in the scientific literature (see [30, 42] and refrences quoted therein). In this paper, curent understanding of the band - gap opening in graphene is discussed along with associated experimental and theoretical investigations..

As was shown above, carbon, one of the second basic elements in nature after silicon, still gives a lot surprises. It is found in many different forms - allotropes - from zero dimensional fullerene, one dimensional carbon nanotubes, two dimensional graphene and graphite, to three dimensional diamond (Fig. 9) - and the properties of the various carbon allotropes can vary widely [20]. For instance, diamond is the hardest material, while graphite is one of the softest: diamond is transparent to the visible part of spectrum, while graphite is opaque; diamond is an electrical insulator, while graphite is a conductor. Very important is that all these different properties originate from the same carbon atoms, simply with different arrangements of the

atomic structure.

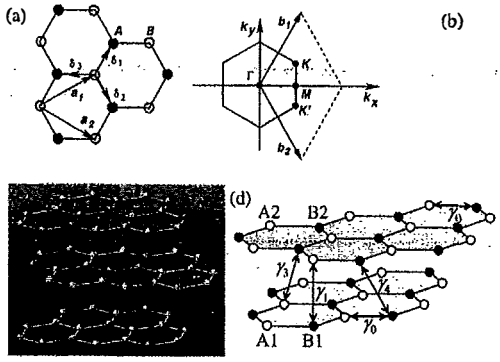

Fig.18. (a) Graphene honeycomb lattice showing the two triangular sublattices. (b) The graphene Brillouin zone in momentum space. (c) Lattice structure of graphite, graphene multilayer. (d) Lattice structure of bilayer graphene (explanation in text).

In two-dimensional graphene, carbon atoms are periodically arranged in an infinite honeycomb lattice Fig.18[a]. Such an atomic structure is defined by two types of bonds within the sp^2 hybridization. From the four valence orbitals of the carbon atom (the 2s, $2p_x$, $2p_y$, and $2p_z$ orbitals, where z is the direction perpendicular to the sheet), the (s, p_x, p_y) orbitals combine to form the in plane σ (bonding or occupied) and σ* (antibonding or unoccupied) orbitals. Three σ –bonds join a C atom to its three neighbors. They are quite strong, leading to optical - phonon frequencies much higher than observed in diamond (see below). Such orbitals are even with respect to the planar symmetry. The σ bonds are strongly covalent bonds determining the energetic stability and the elastic properties of graphene. The remaining p_z orbital, pointing out of the graphene sheet is odd with respect to the planar symmetry and decoupled from the σ states. From the lateral interaction with neighboring p_z orbitals (called the ppπ interaction), localized π (bonding) and π* (antibonding) orbitals are formed [54]. Graphite consists of a stack of many graphene layers. The unit cell in graphite can be primarily defined using two graphene layers translated from each other by a C-C

distance ($a_{c\text{-}c}$ =1.42 Å). The three-dimensional structure of graphite is maintained by the weak interlayer van der Waals interaction between π bonds of adjacent layers, which generate a weak but finite out-of-plane delocalization [35]. The bonding and antibonding σ bands are actually strongly separated in energy > 12 eV at , and therefore their contribution to electronic properties is commonly disregarded, while the bonding and antibonding π states lie in the vicinity of the Fermi level (Fig. 19) . The two remaining π bands completely describe the lowenergy electronic excitations in both graphene and graphite (see [35] and references therein). The bonding π and antibonding π* orbitals produce valence and conduction bands (Fig. 19) which cross at the charge neutrality point (Fermi level of undoped graphene) at vertices of the hexagonal Brillouin zone. Carbon atoms in a graphene plane are located at the vertices of a hexagonal lattice.

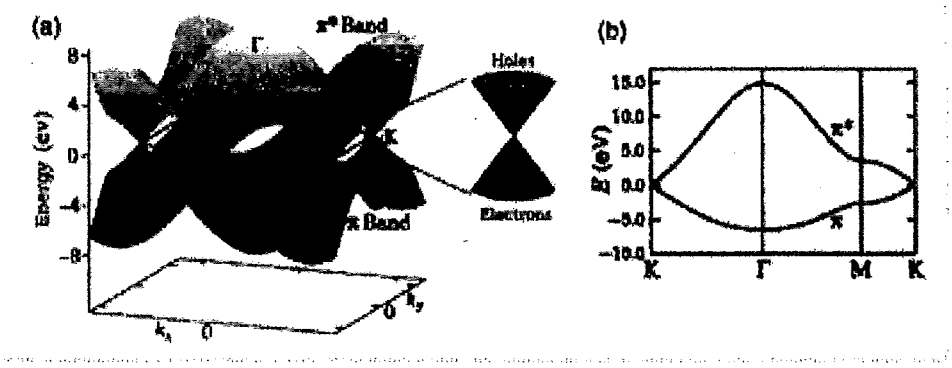

Fig. 19. Energy dispersion of graphene obtained within the tight - binding approximation. a) Energy dispersion relation for graphene, drawn in the entire region of the Brillouin zone. Since in this approximation to ignore the coupling between the graphene sheets, the bands depend only on k_x and k_y. The π band is completely filled and meets the totally empty π^* band at the K points. Near these points both bands linear dispersion as described in the literature. b) The dispersion along the high symmetry points ΓMK.

This graphene network can be regarded as a triangular Braves lattice with two

atoms per unit cell (A and B). Each A- or B - type atom is surrounded by three atoms of the opposite type. In a simple neighbor model graphene is a semimetal with zero - overlap between valence and conduction bands. The energy dispersion of π electrons in graphene was first derived in 1947 by Wallace [54] within the tight - binding approximation. In this case, the wave function of graphene is a linear combination of Bloch function for sublattice A

$$\Phi_A = \frac{1}{\sqrt{N}} \sum_{\vec{R}_A} e^{i\vec{k}\vec{R}_A} \varphi(\vec{r} - \vec{R}_A), \qquad (7)$$

and equilibrium function Φ_B for the B sublatice. Here N is the number of unit cells, $\vec{R}_A$ are the position of the atom A and $\varphi(\vec{r} - \vec{R}_A)$ is the $2p_z$ orbital of the atom at $\vec{R}_A$. The sum runs over all unit cells, i.e. all possible lattice vectors. In the nearest neighbor approximation (every A site has three nearest B sites, and vice versa), the energy eigenvalues can be obtained in a closed form [35]

$$\varepsilon(k_x, k_y) = \pm \gamma_0 \left[1 + 4\cos\frac{\sqrt{3}k_x a}{2}\cos\frac{k_y a}{2} + 4\cos^2\frac{k_y a}{2}\right]^{1/2}, \qquad (8)$$

where γ_0 is the transfer integral between the nearest neighbors. The energy dispersion of two - dimensional graphene according to this formula is plotted in Fig. 2(a) as a function of the wave vector $\vec{k}$. The upper half of the curves is called the π^* or the antibonding band while the lower one is π or the bonding band. The two bands degenerate at the two K points given by the reciprocal space vectors $\vec{K} = (2\pi/a)(1/3, 1/\sqrt{3})$ and $\vec{K}' = (2\pi/a)(-1/3, 1/\sqrt{3})$ points where the dispersion vanishes (see above).

Basically, graphene has redefined the limits of what a material can do: it boasts record thermal conductivity and the highest current density at room temperature ever measured (a million times that of copper!); it is the strongest material known (a hundred times stronger than steel!) yet is highly mechanically flexible; it is the least permeable material known (not even helium atoms can pass through it!); the best transparent conductive film; the thinnest material known; and the list goes on ...[34]. In the vicinity of K - points (as it can be see from Fig. 19), the low - energy electron/hole dispersion relation is proportional to momentum, rather than its square. This is analogous to the energy dispersion relation of massless relativistic electrons, so

the electrons/holes of graphene are described as Dirac fermions having no mass. In a simple neighbor model graphene is a semimetal with zero - overlap between valence and conduction bands. In order to make graphene a real technology, a special issue must be solved: creating an energy gap at K - points in the Brillouin zone [35]. Different attempts have been made by researches, such as patterning graphene into nanoribbon, forming graphene quantum dots], making use of multilayer graphene sheetsand applying an external electric field [55 - 58] It was shown that the uniaxial strain can open a band - gap in a metallic carbon nanotubes as well as carbon nanoribbon [59 - 61].

As it can be seen from Fig. 12 the band gap of ^{13}C has increased by 13.6 meV. Numerous examples of band gap increasment at hard isotope substitution were collected in the papers [30, 42]. The effect of the isotopic ^{12}C to ^{13}C ratio on the first and second - order Raman scattering of light in the diamond has been investigated in [41, 52]. As the ^{13}C content is increased from the natural ratio ($^{12}C/\ ^{13}C = (1 - x) / x$, where $x = 0.011$), to the almost pure ^{13}C ($x = 0.987$), the whole spectrum has shifted towards longer wavelengths (see Fig. 16) in good agreement with the expected $M^{-0.5}$ frequency dependence on the reduced mass M. For an approximately equal mix of the two isotopes, the authors reported that the features seen in the above two - phonon spectra were either broadened or unresolvable. We should stress that the main line in the first - order Raman scattering spectrum of light at ω 1332 cm^{-1} also shifts to the short-wavelength side on the 52.3cm^{-1} [30, 42].

Elastic and inelastic light scattering are powerful tools for investigating graphene [62 - 67]. Raman spectroscopy allows monitoring of doping, defects, disorder, chemical and isotope [1] modifications, as well as edges and uniaxial strain (see Fig. 20).

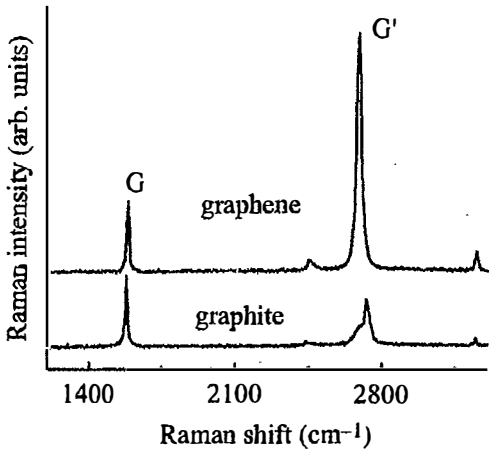

Fig. 20. Comparison of the Raman spectra of graphene and graphite measured at room temperature and at the excitation at E_{laser} = 2.41 eV (514.5 nm).

All sp^2 - bonded carbons show common features in their Raman spectra, the so - called G and D peaks (see, Fig. 20), around 1580 and 1360 cm^{-1} (see, e.g. [34]). The G peak (see, also below Fig. 22) corresponds to the E_{2g} phonon at the Brillouin zone center (Γ - point). The D peak is due to the breathing modes of six - atom rings and requires a defect for its activation. It comes from TO phonons around the Brillouin zone K point and it is activated by an intravalley scattering process. The 2D peak is the second order of the D peak. This is a single peak in monolayer graphene, whereas it splits into four bands in bilayer graphene, reflecting the evolution of the band structure [1, 34]. The Raman spectrum of graphene also shows significantly less intensive defect - activated peaks such as the D' peak , which lies at ~ 1620 cm^{-1}. This is activated by an intravalley process i.e. connecting two points belonging to the same cone around K (see, Fig. 6 in [1]). The second order of the D' peak is called 2D' peak. Since 2D and 2D' peaks originate from a Raman scattering process where momentum conservation is obtained by the participation of two phonons with opposite wave vector ($\vec{q}$ and $-\vec{q}$), they do not require the presence of defects. Thus, they are always visible in the Raman spectrum (see cited papers [19 - 25] and references therein).

Graphene is one unique material which shows properties not fond in other

materials. One of these unique features of graphene is the influence of long range strains on the electronic properties. The possibility of tuning the dynamics of carriers as well as phonons by appropriately designed strain patterns opens the way for novel applications of graphene, not possible with any other materials (see, e.g. [25] and references therein). At present time we have several reports, which have examined graphene properties under uniaxial deformation [1, 34, 68, 69].

Strain can be very efficiently studied by Raman spectroscopy since this modifies the crystal phonon frequency, depending on the anharmonicity of the interatomic potentials of the atoms. Raman spectra of strained graphene show significant redshifts of 2D and G band (see Table 2) because of the elongated of the carbon - carbon bonds.

Table 2. Red shift of the G and 2D bands in the Raman spectra in graphene monolayers under uniaxial tensile stress.

Ref.	Shift of G (G^+ and G^-) band $cm^{-1}/\%$	Shift of 2D band $cm^{-1}/\%$	E_g, meV
15	14.2	27.8	300
25	5.6; 12.5	21	
27	10.8; 31.7	64	
26 theory			$\simeq$ 500

The authors of the paper [68] have proposed that by applying uniaxial strain on graphene, tunable band - gap at K - point can be realized. First principle calculations predicted a band - gap opening of $\simeq$ 300 meV for graphene under 1% uniaxial tensile strain (Fig. 21). Thus, the strained graphene provides an alternative way to experimentally tune the band - gap of graphene, which would be more efficient and more contollable than other methods (see, above) that are used to open band - gap in graphene.

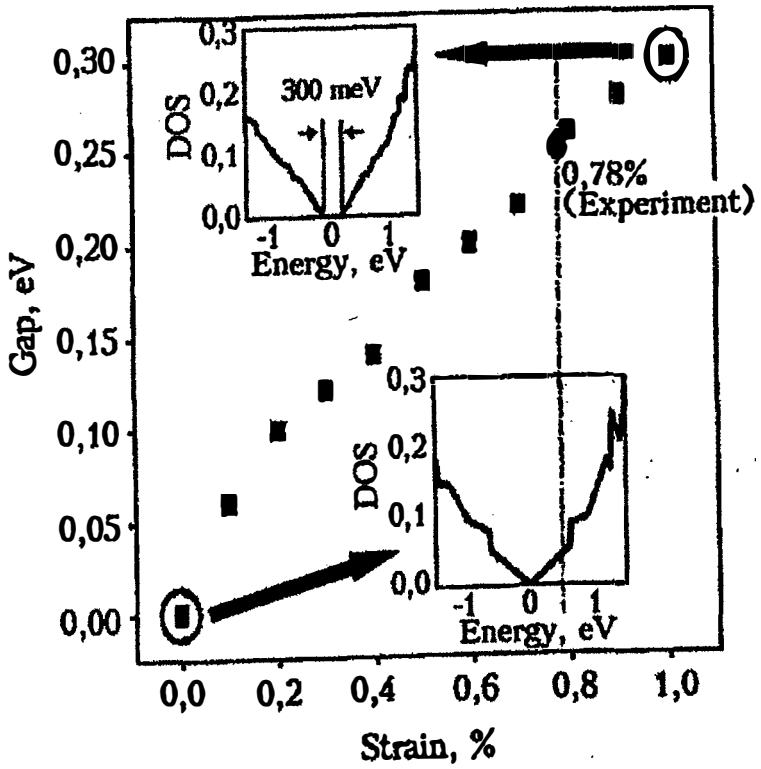

Fig. 21. The band - gap of strained graphene with the increase of uniaxial tensile strain on graphene. The magnitude of gap is determined by the gap opening of density of states. The insert show the calculated density of states of unstrained and 1% tensile strained graphene. The dash line and solid dot indicate the calculated bandgap of graphene under the highest strain (0.78 %) [68].

The method of the isotope renormalization of the energy of elementary excitations in solid very often used in last five decades and well described in the scientific literature (see, for example reviews [24, 30, 42]). At now there is a large list of the paper devoted to investigation of the isotope - mixed graphene [1, 34, 70]. Chen at al. [65] have reported the first experimental study of the isotope effect on the thermal properties of graphene. The thermal conductivity K, of isotopically pure ^{12}C (0.01 of ^{13}C) graphene determined was higher than 4000 W/mK (approximately two times

more than it in diamond [41, 51]) at the measured temperature $T_m \sim 320K$, and more than a factor of two higher than the value of K in a graphene sheets composed of a 50% - 50% mixture of ^{12}C and ^{13}C. Raman spectroscopy transferred to the 285 nm SiO_2/Si wafer was performed under 532 nm laser excitation [65]. The G peak and 2D band positions in Raman spectra of graphene with 0.01%, 1.1% , 50% and 99.2% ^{13}C - isotope are presented in Fig. 22.

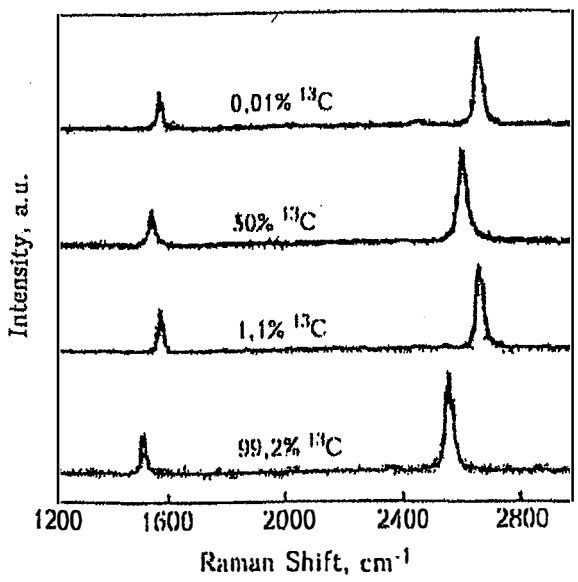

Fig. 22. Raman spectra of graphene with different isotope concentration at room temperature [65].

Isotope shift of the G and 2D bands in the Raman spectra depicted on the Fig. 23 [33].

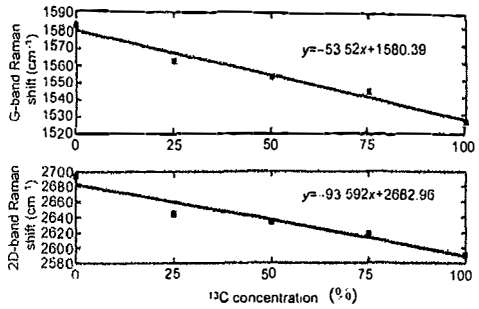

Fig. 23. Peak position of G and 2D bands in Raman spectra as a function of the concentration of ^{13}C [70].

As in the case of isotope - mixed diamond [30, 34, 42] the Brillouin - zone - center optical - phonon frequency ω varies with the atomic mass M as $\omega \sim M^{-1/2}$ making the Raman shift for ^{13}C approximately $(12/13)^{-1/2}$ times smaller than that for ^{12}C. The experimental difference between the lowest 99.2% ^{13}C and the highest 0.01% ^{13}C peak is ~ 64 cm^{-1} which is according [42] in agreement with the theory, and attests for the high quality of isotopically modified graphene. By the way we should indicate that in the Raman spectra in diamond (with sp^3 - bond) analogous shift of first - order line in Raman spectrum is equal 52.3 cm^{-1} [34], which is consistent with the isotope mass ratio. Substituting a light isotope (^{12}C, H) with a heavy one increases the interband transition energy in the case $^{12}C_x^{13}C_{1-x}$ on 14.7 meV and LiH_xD_{1-x} on 103 meV [24]. Taking into account a more soft bond (sp^2 - bond instead sp^3 - bond in diamond) isotope - induced band - gap opening in graphene of some hundreds meV (up to E_g of Si) was predicted in paper [71]. Such estimation of the value of isotopical band - gap opening in graphene agrees with not only the results of paper [34] but with very small value $C_{44} = 0.5 \cdot 10^{10}$ dyn/cm^2. Such small value indicates on the strong electron - photon interaction - main reason renormalization of electron excitation energy (for the details, see, e.g. [1]). Very close to isotopically renormalization of electronic excitation energy is the hydrogenation of graphene [71]. In last mechanism there is observable band - gap opening in graphene. We should add that use deuteriun instead of hydrogen we may increase the value of E_g [30, 42]. Thus, isotope substitution will be very useful method for renormalization of the band - gap in graphene - future semiconducting material. Moreover, this method allows to control not only of the

strong nuclear interaction (quantum chromodynamics) but taking it into account at the renormalization of the electromagnetic interaction (quantum electrodynamics) [1]. Adding ^{13}C makes magnetic materials isotope out of graphene.

IV. Discussion.

Traditionally nuclear - electron interaction (in our case neutron - electron interaction) taking into account the solving of Schrödinger equation using Born - Oppenheimer (adiabatic) approximation [72]. Since electrons are much faster and lighter than the nuclei by a factor nearly 2000 the electron charge can quickly rearrange itself in response to the slower motion of the nuclei, and this is the essence of the Born - Oppenheimer approximation. This approximation results the omission of certain small terms which result from the transformation. As was shown in [30] the eigenvalue (energy) of the electronic Schrödinger equation (equation 6 in [73]) depends on the nuclear charges through the Coulomb potential, but it doesn't include any references to nuclear mass and it is the same for the different isotopes. The independent of the potential energy (the eigenvalue of the Schrödinger equation) is the essence adiabatic approximation. However, we must repeat, that the Born - Oppenheimer approximation is the standard anzatz to the description of the interaction between electrons and nuclei in solids (see, e.g. [74]). The last result is forcing us to search for new models and mechanisms of nuclear - electron interaction including results of subatomic physics, e.g. hadron - lepton interaction.

Out of four known interactions, three are described by SM - the electromagnetic, weak and strong ones [1 - 5]. The first two of them have a common electroweak gauge interaction behind them. The symmetry of this interaction $SU(2)_L \times U(1)_Y$ manifests itself at energies higher than ~ 200 GeV. At lower energies, this symmetry is broken down to $U(1)_{EM} \neq U(1)_Y$ (the electroweak symmetry breaking): in SM this breaking is related to the vacuum expectation value of a scalar field [75]. The strong interaction in SM is described by the QCD, a theory with the gauge group $SU(3)_C$. The effective coupling constant of this theory grows when the energy decreased. As a result, particles which feel this interaction cannot exist as free states and appear only in the form of bound states called hadrons (see, also [1]). Most of modern methods of quantum field theory work at small values of coupling constant, α_s, [75], that is, for

QCD, at high energies. Quarks and leptons, the so - called SM matter fields, are described by fermionic fields. Quarks take part in strong interactions and compose observable bound state hadrons. Both quarks and leptons participate in the electroweak interaction. The matter fields constitute three generation: particles from different generation interact identically but have different masses (see, e.g. [4]). For the case of neutrino, Yukawa interactions are forbidden as well, so neutrinos are strictly massless in SM (see, however [73] and references therein)). The gauge bosons, which are carriers of interactions, are massless for unbroken gauge groups $U(1)_{EM}$ (electromagnetism - photons) and $SU(3)_C$ (QCD - gluons), masses of $W^{\pm}$ and Z_0 bosons are determined by the mechanism of electroweak symmetry breaking. It should noted that the forces between the quarks must be long rang, because the gluons have zero mass. This does not imply that forces between hadrons are also long range, because hadrons have zero color charges overall. The forces between the colorless hadrons are the residues of the forces between their quark constituents, and cancel when the hadrons are far apart.

Returning to our non - accelerator experimental results, we should underline that in this paper we measure the strong nuclear interaction in crystals which differ by term of one neutron from each other. When we add one neutron in the hydrogen nucleus, we artificial activated of the strong interaction. As far as the gravitation, electromagnetic and weak interactions are the same in both kind crystals (LiH and LID), it only changes the strong interaction. Therefore a logical conclusion is made that the renormalization of the energy of electromagnetic excitations (isotopic shift equals 0.103 eV) is carried out by strong nuclear interaction. The short range character of the strong interaction of nucleons does not possess direct mechanism of the elementary excitation (electrons, excitons, phonons) energy renormalization, which was observed in our low temperature experiments. Second reason that the interpretation of our experimental results is very difficult task because they are first demonstration of the violation of the strong conclusion in nuclear and particles physics that the strong nuclear force does not act on the colorless leptons (see, e.g. [1, 73]). Moreover we have some contradictions taking into account that the forces between quarks must be long range, because the gluons have zero mass. But as was mentioned above, the short range when forces between the colorless hadrons are the residues of the forces between their quark constituents, and cancel when the distance between hadrons is more than nuclear size [5]. We can see that the nuclear size transforms long range interaction in the short range strong one. It is very old question which up to present time has not any theoretical explanation.

In spite of above discussion, at present time we can distinguish the following

mechanisms of the isotopic shift zero phonon line in LiD crystals:

1. Long range electric field of the neutron's quarks. This mechanism owing to the confinement quarks is limited by the boundary of the neutron.

2. The possible new structure of the quarks and leptons - so - called preons (see e.g. [75] and references quoted therein).

3. The most likely mechanism of the neutron - lepton interaction is connected to the magnetic - like strong field of neutron 's quarks. Taking into account anomalous magnetic moment of the neutron [14] in the paper [6] was obtained the value of strong coupling constant $\alpha_s = 2.4680$. Quite large value in comparison with the accelerator technique value $\alpha_s(M_Z) = 0.1198$ [76]. The large value α_s is thus justified to think that residual strong forces acting beyond nucleon could exist. Besides that our experimental results to allow the neutron electron binding energy equal 106 meV was found in diamond and LiH which is 128 times less than proton - electron coupling energy (13.6 eV) and its value is perfectly agree with Breit's theory. The results of our experiments make it possible to determine not only the constant of strong nuclear interaction equal 2.4680, but also to predict the mass of the boson carrying the interaction between neutron and electron equal 3.5 keV [21].

An another possible interpretation is to assume that in addition to the 8 gluons predicted by QCD $SU(3)_c$ group there is a ninth gluon color singlet [4]

$$g_9 = \frac{1}{\sqrt{3}} \cdot (r\bar{r} + g\bar{g} + b\bar{b}) \qquad (9)$$

This massless photon - like gluon may be strongly interacts between nucleons (neutrons) and leptons (electrons) (see, also [1]). Returning to Fig. 6 we can note that our measurements permit value obtainment of strong coupling constant from $\alpha_s = 2.4680$ (pure LiD crystals) to $\alpha_s = 0$ (pure LiH crystals).

The remarkable properties of the graphene promise unheard of applications, especially in the semiconductor state. Especially graphene nanostructures are promising candidates for future nanoelectronics and solid - state quantum information technology. As was shown numerously, in the vicinity of K - points (see, Fig. 6 in [1]), the low - energy electron/hole dispersion relation is proportional to momentum, rather than its square (see, e.g. [78]). This is analogous to the energy dispersion relation of massless relativistic electrons, so the electrons/holes of graphene are described as Dirac fermions having no mass. In a simple neighbor model graphene is a semimetal with zero - overlap between valence and conduction bands. In order to make graphene a real technology, a special issue must be solved: creating an energy gap at K - points in the Brillouin zone (see, Fig. 24).

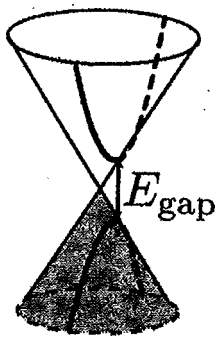

Fig. 24. The energy dispersion of semimetal (solid line) and semiconductor (dashed line).

Different attempts have been made by researches, such as patterning graphene into nanoribbon, forming graphene quantum dots, making use of multilayer graphene sheet and applying an external electric field [79]. It was shown that the uniaxial strain can open a band - gap in a metallic carbon nanotubes as well as carbon nanoribbon . As an example Fig. 25 shows the dependence of the energy of interband transition on the width of the graphene nanoribbons. The observed dependence is well described by the following expression $E_g = \alpha^*/ (W - W^*)$, where $\alpha^* = 0.38$ eV/nm, and $W^* = 16$ nm accounts for inactive edges (see [80] and references quoted therein). This formula gives value of E_g equal to several eV, if W is reduced to a size , for example, ^{13}C, but it is impossible. The isotopic transformation of graphene, a semimetal into semiconductor deserves special attention. This means of the cones dispersion pattern $E(\vec{k})$ at the K point of the Brillouin zone of graphene reformes into the usual parabolic dispersion of band structure pattern (see Fig. 24).

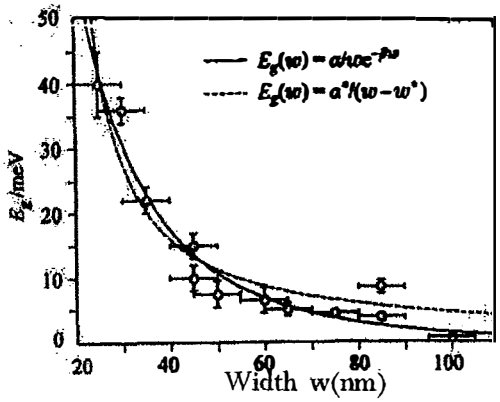

Fig. 25. The dependence of E_g as a function of width of the graphene nanoribbons (after [80]).

According to the results of Ref. 79 this method can be used to obtain E_g of several hundred meV. Since value of E_g depends on the concentration of ^{13}C in graphene, this mechanism is easily realized either chemically or technologically. With the opening E_g of massless fermions (leptons = electrons) acquire mass. estimates of different ways of opening E_g in graphene give the following equality: $E_g = 2m$ [78]. When E_g = 1 eV [71] leptons acquire a mass equal 0.5 eV - the value is not large, but finite. One of the mechanisms of acquire mass in elementary particle physics is considered in the paper [81]. This paper predicts that both quarks and gluons acquire running mass distribution in QCD, which are large at infrared momenta. The current quark of perturbative QCD evolves into a constituent quark as its momentum becomes smaller. The constituent quark mass arises from a cloud of low - momentum gluons attaching thenselves to the current quark. This is DCSB [82]: an essentially nonperturbative effect that generates a quark mass from nothing; namely it occurs even in the chiral limit. DCSB namely the generation of mass from nothing is a theoretically established nonperturbative feature of QCD. The solution of a gap equation shows that gluons are cannibals: they are paricle species whose members become massive by eating each other (the details see [79, 81, 82]).

Thus, the tentative interpretation of describing non - accelerator experimental results does not find consistent explanation at the change of strong interaction leaving to another mystery of SM [3]. We should remind that intrinsic contradiction of Standard Model is already well - known. Really, the Lagrangian of quantum chromodynamics (theory of the strong interaction) has the next form (see, e.g. [2 - 4]):

$$L = i\sum_{q} \overline{\Psi}^{a}_{q}(\nabla_{\mu}\gamma_{\mu} + im_{q})\Psi^{a}_{q} - \tfrac{1}{4}G^{n}_{\mu\nu}G^{n}_{\mu\nu}, \quad (10)$$

where

$$\nabla_{\mu} = \partial_{\mu} - ig\tfrac{\lambda^{n}}{2}A^{n}_{\mu},$$

$$G^{n}_{\mu\nu} = \partial_{\mu}A^{n}_{\mu} - \partial_{n}A^{n}_{\mu} + gf^{nml}A^{n}_{\mu}A^{l}_{\nu}. \quad (11)$$

Ψ^{a}_{q} and A^{n}_{μ} are quark and gluon fields, a=1,2,3,...8 are color indices , λ^{n} and f^{nml} are Gell - Mann matrices and f symbols, m_{q} - are bare (current) masses, q = u, d, s, c, ... different quarks. It is common place [1, 76] that the Lagrangian (10) contains the members which describe both free motion and interaction between quarks and gluons, which is defined by the strength couple g. Spacing of which it is necessary to remark that although the Lagrangian (10) possesses rather attractive peculiarities (see, also [1, 2]), its eigenstates are the quarks and the gluons which are not observed in free states [79, 83]. The observed hadrons in the experiment don't eigenstates in quantum chromodynamics. It is obvious to expect that the modern theory of QCD should finally overcome these difficulties, for example inserting QCD in QED.

V. Conclusion.

The artificial activation of the strong nuclear interaction by adding one (two or more) neutrons in atomic nuclei leads it to the direct observation of the long - range strong interaction in low - temperature optical spectra of solids. This conclusion opens new avenue in the investigation of the constant of strong nuclear interaction in the wide value range by means the condensed matter alike traditional methods. Our experimental nonaccelerator results may shed light on a number of fundamental puzzles in modern physics, particularly on the unification of forces. Experimental observation of the renormalization of the elementary excitation energy of solids by the

strong nuclear interaction stimulates its count in the process of description of the elementary excitations dynamics in quantum electrodynamics. Besides, we should highlight that such important information has been obtained via rather simple and inexpensive experimental physics equipment. Present article continuous to develop between nuclear, high energy and condensed matter physics taking into account that our result does not available on accelerators.

Acknowledgements.

Many thanks to Dr. K. Walker for reading my manuscript, G. Tumar and G.A. Plehhanov for improving my English.

References.

1. V.G. Plekhanov, Hadron - Lepton Interaction (LAMBERT Academic Publishing, Germany, 2021)

2. D.H. Perkins, Introduction to High Energy Physics (CUP, Cambridge, 2000).

3. W.N. Cottingham, D.A. Greenwood, An Introduction to the Standard Model of Particle Physics (CUP, Cambridge, 2007).

4. G. Griffiths, Introduction to Elementary Particles (Wiley - VCH, Weinheim, 2008).

5. E.M. Henley, A. Garcia, Subatomic Physics (World Scientific Publishing Co., Singapore, 2007).

6. V.G. Plekhanov, J.G. Buitrago, Evidence of residual strong interaction in nuclear atomic level via isotopic shift in LiH - LiD crystals, Prog. Phys. **15** (2019) 68 - 71.

7. P.I. Dee, Attempts to detect the interaction of neutrons with electrons, Proc. Roy. Soc. (London) **A136** (1932) 727 - 736.

8. J. Chadwick, The existence of a neutron, Proc. Roy. Soc. (London) A**136** (1932) 692 - 708.

9. Aronberg, Astrophys. J., **47** (1918) 96 (cited in [11]).

10. E.U. Condon, Note on electron - neutron interaction, Phys. Rev. **49** (1936) 459 - 461.

11. A.P. Striganov, Ju.P. Donzov, Isotope effect in atomic spectra, Uspekhi Fiz. Nauk (Moscow) **55** (1955) 315 - 330 (in Russian).

12. L.L Foldy, The electromagnetic propertis of Dirac particles, Phys. Rev. **87** (1952) 688 - 696.

13. C.G. Darwin, The wave equations of electron, Proc.Roy. Soc. (London) **A118** (1928) 654 - 680.

14. Yu.A. Alexandrov, The Fundamental Properties of Neutron (Energoizdat, Moscow, 1982) (in Russian).

14. L.L. Foldy, Neutron - electron interaction, Rev. Mod. Phys. **30** (1958) 471 - 481.

15. L.V. Mitsyna, V.G. Nikovenko, S.S. Parzhitski, et al.,Extraction of the neutron - electron scattering length, Eur. Phys. J. **C40** (2005) 473 - 482.

16. Y. Yukawa, On the interaction of elementary particles, Proc. Phys. Math. Soc. **17** (1935) 48 - 57.

17. R.M. Santilli, The physics of new clean energy anf fuels according to hadronic mechanics, J. New Energy **1** (1998) 5 - 314.

18. S. Beghalla - Bartoli, A. Muktibodh and R.M. Santilli, Problematic aspects of generalized quantum theories and their apparent resolution via hadronic mechanics, Ratio Matematca **52** (2024) 21 - 42.

19. V.G. Plekhanov, Macroscopic manifestation of the strong nuclear interaction in the optical spectra of solids, in, Proc. 25 ISINN, Dubna, Russia, 2018, 49 - 56.

20. J.E. Field, The Properties of Natural and Synthetic Diamond (Academic Press, New York, 1982).

21. V.G. Plekhanov, Solid - state manifestation of quantum chromodynamics, Hadronic Journal **46** (2023) 359 - 457.

22. V.G. Plekhanov, Experimental manifestation of the effect of disorder on exciton binding energy in mixed crystals, Phys. Rev. B**53** (1996) 958 - 9561.

23. V.G. Plekhanov, A possible signature of neutron quarks - leptons via gluon interaction in solids, in, Proc. 21th Int. Conf. Cond. Matter Nucl. Sci., Fort Collins, Colorado, USA, June 2018.

24. V.G. Plekhanov, Giant Isotope Effect in Solids (Stefan University Press, La Jola, CA, 2004).

25. O.I. Tyutyunnik, V.I. Tyutyunnik, F.F. Gavrilov, and G.I. Pilipenko, Lithium hydride growth by Bridgmen - Stockbarger method, J. Crystal Growth **68** (1984) 741 - 749.

26. R.S. Knox, Theory of Excitons (Academic Press, New York - London, 1963).

27. V.G. Plekhanov, Isotopic and disorder effects in large exciton spectroscopy,

Phys. - Uspekhi **40** (1997) 553 - 568.

28. S. Baroni, G. Pastori Parravicini, G. Pezzica, Quasipparticle band structure of lithium hydrude, Phys. Rev. **B32** (1985) 4077 - 4083.

29. J.L. Verble, J.L Warren and J.L. Yarnell, Lattice dynamics of lithium hydride, ibid **168** (1968) 980 - 989.

30. V.G. Plekhanov, Elementary excitations in isotope - mixed crystals, Phys. Reports **410** (2005) 1 - 235.

31. W.B. Zimmerman, Lattice constant dependence on isotopic composition in the ^{7}Li(H,D) system, Phys. Rev. B**5** (1972) 4704 - 7.

32. C.M. Lederer, V.S. Shirley, Table of Isotopes (Wiley, New York, 1978).

33. Ju.M. Shirokov, N.P. Judin, Nuclear Physics (Science, Moscow, 1980) (in Russian).

34. A.C. Ferrari, F. Fal'ko, Jari Kinaret et al., Science and technology road map for graphene, related two - dimensional crystals, and hybrid systems, Nanoscale **7** (2015) 4598 - 4810.

35. W.A. Harrison, Electronic Structure and Properties of Solids (W.F. Freeman and Co., San Fransicko, 1980).

36. C.D. Clark, P.J. Dean and P.V. Harris, Intrinsic edge absorption in diamond, Proc. Roy. Soc. (London) A**277** (1964) 312 - 329.

37. V.G. Plekhanov, Introduction to Isotopic Materials Science (Springer, Heidelberg, 2018).

38. V.G. Plekhanov, Isotope - based material science, Universal J. Mater. Sci. **1** (2013) 87 -147.

39. A.T. Collins, S.C. Lawson and K. Kanda, Indirect energy gap of ^{13}C, Phys. Rev. Lett. **65** (1990) 891 - 893.

40. T. Ruf, M. Cardona, P. Pavone et al., Cathodoluminescence investigation of isotope effect in diamond, Solid State Commun. **105** (1998) 311 - 316.

41. H. Watanabe, T. Koretsune, S. Nakashina et al., Isotopecomposition dependence of the band - gapenergy in diamond, Phys. Rev. B**88** (2013) 205420 - 5.

42. M. Cardona, M.L.W. Thewalt, Isotope effects on the optical spectra of semiconductors, Rev. Mod. Phys. **77** (2005) 1173 - 1224.

43. D.W. Taylor, Phonon response theory and the infrared and Raman measurements, in R.J. Ellott, I.P. Ipatova (eds.), Optcal Propertes of Mxed Crystals (elsever Sci. Pub. B.V., Amsterdam, 1988).

44. I. Nordheim, Zur Elektornentheorie der Metalle, Ann. Phys. (Lepzg) **401** (1931) 641 - 678.

45. V.G. Plekhanov, Expermental evdence of strong phonon scatteirng in isotope

dsordered systems:The case of LH, Phys. Rev. B**51** (1995) 8874 - 8878.

46.V.F. Agekyan, V.M. Asnin, A.M. Kryukov et al., Isotope effect in germanium, Fiz. Tverd. ela (St. Petersburg) **31** (1989) 101 - 104 (in Russian).

47. H. Bilz, W. Kress, Phonon Dispersion Relation in Insulators (Springer - Verlag, Berlin - Heidelberg, 1979).

48. H. Hanzawa, N. Umemura and Y. Nisida et al., Direct effects of nitrogen impurities, and ^{13}C isotope composition on the Raman spectrum 1b diamond, Phys. Rev. B**54**, (1996) 3793 - 3799.

49. R.M. Chrenko, ^{13}C - doped diamond: Raman spectra, J. Appl. Phys. **63** (1988)5873 - 5875.

50. J. Spitzer, P. Etchegoin and M. Cardona et al., Isotopic - disorder induced Raman scattering in diamond, Solid State Commun. **88** (1992) 509 - 514.

51. K.C. Hass, M.A. Tamor and T.R. Anthony et al., Lattice dynamics and Raman spectra of isotopically mixed diamond, Phys. Rev. B**45** (1992) 7171 - 7182 .

52. A.K. Ramdas and S. Rodriguez, Lattice vibrations and electronic excitation in isotopically controlled diamonds, phys. stat. sol. (b) **215** (1999) 71 - 80.

53. F. Widule, T. Ruf, M. Konuma et al., Isotope effects in elemental semiconductors: a Raman study of silicon, Solid State Commun. **118** (2001)1 - 23.

54. P.R. Wallace, The band theory of graphite, Phys. Rev. **71** (1947) 622 - 629.

55. M.Y. Han B. Ozyilmaz, Y. Zhang et al. , Energy band - gap engineering of graphene nanoribbons, Phys. Rev. Lett. **98** (2007) 206805 - 4.

56 L.A. Ponomarenko, F. Schedin, M. Katsnelson et al., Chaotic Dirac billiard in graphene quantum dots, Science **320** (2008) 356 - 358.

57. A. Savchenko, Transforming graphene, Science **323** (2009) 589 - 590; D.C. Elias, R.R. Nair, T.M.G. Mohiuddin et al., Control of graphene properties by reversible hydrohenation: Evidence for graphane, ibid, **323** (2009) 610 - 613.

58. V.G. Plekhanov, Nuclear technology creation the quantum dots in graphene, Transactions Humanitar Institute, Tallinn, 2011, p. 66 - 70 (in Russian); V.G. Plekhanov, 2015 (unpublished results).

59. See special issue Nature, June 11 (2009).

60. K.F. Mak, C.H. Lui, T.F. Heinz, Observation of an electric - field - induced band gap in bilayer graphene by infrared spectroscopy, Phys. Rev. Lett. **102** (2009)256405 - 4.

61. E.V. Castro, K.S. Novoselov, S.V. Morozov, et al., Biased bilayer graphene: semiconductor with a gap tunable by the electric field effect, ibid **99** (2007) 216802 - 4.

62. S. Prawer and R.J. Nemanich, Raman spectroscopy of diamond and doped

diamond, Phil. Transac. R. Soc. (London) **362** (2004) 2537 - 2565.

63. M.S. Dresselhaus, G. Dresselhaus and M. Hofman, Raman spectroscopy as a probe of graphene and carbon nanotubes, ibid, **366** (2008) 231 - 236.

64. C. Casiraghi, A. Hartschuh, H. Qian et al., Raman spectroscopy of graphene edges, Nano Lett. **9** (2009) 1433 - 1441.

65. Sh. Chen, Q. Wu, C. Mishra et al., Thermal properties of isotopically engineered graphene, Nature Mater. **11** (2012) 203 - 207; ArXiv:cond - mat/1112.5752 (2011).

66. A. Ferrari, Raman spectroscopy of graphene and graphite: Disorder, electron - phonon coupling, doping and nonadiabatic effects, Solid State Commun. **143** (2007) 47 - 57.

67.M. Huang, H. Yan, C. Chen et al., Raman spectroscopy of graphene under uniaxial stress: phonon softening and determination of crystallographic orientation, Proc. Natl. Acad. Sci. USA **106** (2009)7304 - 7315.

68. Zh.H. Ni, T. Yu, Y.H. Lu, et al., Uniaxial strain on graphene: Raman spectroscopy study and band - gap opening, ACS Nano **3** (2009) 483 - 492.

69. T.M. Mohiuddin, A. Lombarto, R.R. Nair et al., Uniaxial strain in graphene by Raman spectroscopy: G peak splitting, Grűneisen parameter and sample orientation, Phys. Rev. B**79** (2009) 205433 - 8.

70. C. Kun, L.Q. Yu, T. Bo, et al., Isotope effect of the phonons mean free path in graphene by micro - Raman measurement, Science China, Phys., Mech. and Astro., **57** (2014) 1817 - 1821.

71. V.G, Plekhanov, Renormalization of the band - gap by isotope in graphene, Nano Technol. and Nano Sci. J. **3** (2020) 121 - 130.

72. M.Born and J.R. Oppenheimer, On the quantum theory of molecules, in, Quantum Chemistry (Classic Scientific Paper) (World Sci. Publ. Co., Singapore, 2000).

73. V.G. Plekhanov, Measurements of the wide value range of strong interaction coupling constant, SSRG - IJAP **6** (2019) 32 - 37.

74. R.M. Martin, Electronic Structure - Basic Theory and Practical Methods (CUP, Cambridge, 2004).

75. V.G. Plekhanov, Isotope effect is the paradigm of a non - accelerator study of the residual nuclear strong interaction, Edelweiss Chemical Science J., **3** (2020) 8 - 14.

76. A. Deur, S.J. Brodsky, G.F. Teramond, THe QCD running coupling, Prog. Part. Nucl. Phys. **90** (2016)1 - 74.

77. V.G. Plekhanov, Fundamental and applications of isotope effect in solids, Prog. Mater. Sci. **51** (2006) 287 - 426.

78. V.G. Plekhanov, Remarkable properties of isotope effect, J. Phys. Opt. Sci. **3** (2021)1 - 6 (2021).

79. V.G. Plekhanov, Experimental study of the long - range quark - lepton strong interaction in solids, in, Understanding Quarks (Nova Science Publishers, Inc., New York, 2021) chapter 1.

80. C. Stampher, S. Fringes, J. Güttinger et al, Transport in graphene nanostructures, Front. Phys. **6** (2011) 271 - 293.

81. C.D. Roberts, Hadron physics and QCD: Just the basic facts, ArXiv:nucl. - th/1501.06581.

82. C.D. Roberts, Empirical consequences of emergent mass, Symmetry, **12** (2020) 1468 - 1506.

83. I.M. Dremin, A.B. Kaidalov, Quantum Chromodynamics and the phenomenology of strong interaction, Phys. Uspekhi (Moscow) **49** (2006) 263 - 273; 50 Years of Quantum Chromodynamics.

HADRONIC JOURNAL 47, 473 - 477 (2024)
DOI 10.29083/HJ.47.04.2024/SC473

A SIMPLE EXPLANATION OF WHY TIME STOPS AT THE SPEED OF LIGHT

Farzad Haghmoradi-Kermanshahi
Electrical Engineering Department
Faculty of Engineering, Razi University
Kermanshah 67149, Iran
f.haghmoradi@yahoo.com

Received November 1, 2024

Abstract

According to Einstein's theory of special relativity, the elapsed time for two observers with different speeds in an inertial frame of reference will be measured unequally. The faster the speed of observer, the slower the passage of time. This paper explains why time stops at the speed of light in an understandable manner.

Keywords: Relativity, Elapsed time, Observer

1. Introduction

What is time? There are maybe many definitions for time that are all correct but in order to have a fair judgment, the historical process of time must be considered.

Until a few hundred years ago, it was thought that the earth is the center of the universe and the sun is rotating around it [1]. Imagine a situation where the sun is in the middle of the sky. After a while, the sun moves a little and this movement continues until it reaches the corner of the sky and night falls. The next day, after sunrise, the sun begins to move and will be transferred to the middle of the sky (we look at this matter from the point of view of those who defined time hundreds of years ago). From this issue it can be concluded that the best definition of time is a relative motion between two objects. So, if it is assumed that the earth is the origin of the universe just like olden days, the movement of the sun around it is called the passage of time.

2. The true perception of time

The interval between two consecutive observation of the sun in the middle of the sky is divided into 24 equal parts and each part is named an hour. Similarly, we divide every hour into 60 equal parts and call them minutes and every minute into 60 parts and call them seconds. We invented the clock that simple!

Now, consider a person wearing a watch in the northern hemisphere during summer and looking at the sky while the sun is in the middle of it. In this case, his watch shows 12 noon (Suppose it is always 12 o'clock when the sun is in the middle of the sky). He decides to travel clockwise on the earth at the same speed and direction of the sun (Fig.1).

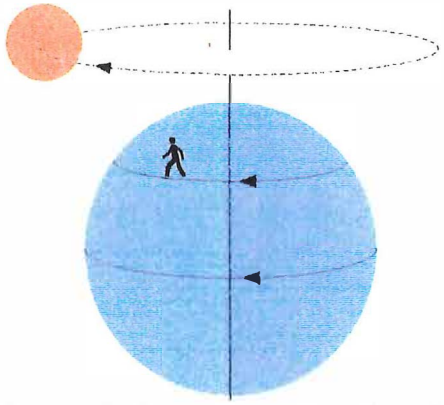

Fig.1. A person moving clockwise on the earth and parallel to the equator

One hour later, his watch shows 1 pm. When he looks at the sky, the sun is exactly in the middle of it, so he must set the watch back an hour. This person keeps moving and it is always 12 noon for him, whereas if he had remained in his original place,

he would have perceived morning, noon, evening and night. This person is so pleased that he has managed to stop time. He keeps to the path consistently and passes the original place many times. After a few months of movement, he notices the change of season and asks himself that I have stopped time and it is always 12 noon, so why is the season changing and transiting from summer to autumn?

After a while of reflection, he decides to deflect his way and incline to the south at a tiny angle of less than 0.5 degrees with respect to the equator. In this case, for instance, if his original place is Helsinki (Finland), the next day he will arrive in Tallinn (Estonia) instead of Helsinki, in Bucharest (Romania) after one month and finally in Cape Town (South Africa) after 6 months (Fig.2).

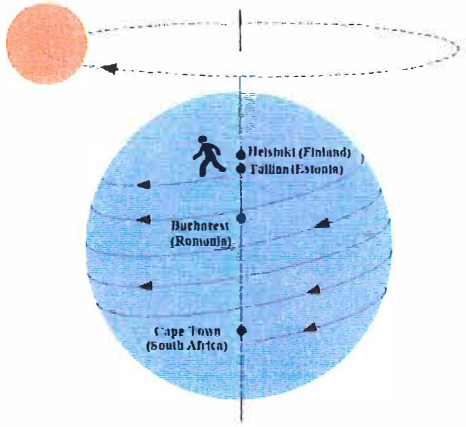

Fig.2. A person moving clockwise on the earth at a tiny angle to south with respect to the equator

Afterwards, he deviates from his path less than 0.5 degrees to the north and will reach the original place in 6 months (Fig.3).

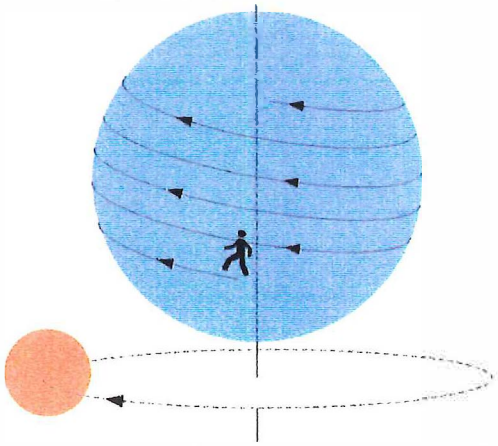

Fig.3. A person moving clockwise on the earth at a tiny angle to north with respect to the equator

At this time, he is pleased again that he has managed to stop time because it is always summer and 12 noon for him. If he had remained in the original place, he would have perceived nights, days, summers, winters and different hours but now, time has stopped for him and it is 12 noon in summer. After a few years of motion, this person feels that he is growing old and asks himself again: if time has stopped for me, so why is my hair turning white?

He is absorbed in thought again and after a while, the question arises in his mind is that he may have chosen the origin and the velocity incorrectly at first.

The human body is made up of cells. A cell is constituted of molecules and a molecule is formed by atoms. The atom, in turn, is composed of nucleus with electrons rotating around it in different directions. On the other hand, the highest speed in the universe belongs to light which is exactly equal to 299,792,458 (m/s) in a vacuum.

Assume that the universe is traveling at the speed of light in all directions relative to an unknown origin. In this case, if a person travels in an arbitrary direction at the speed of light, his relative velocity equals zero with respect to the motion of the universe and time will stop for him in the full sense of the word. To put it another way, since a person traveling at the speed and direction of sun will not observe night, then if he moves at the speed of universe he will not perceive aging.

According to the special relativity, the time interval measured by person A who is moving with constant speed of v relative to person B is given as [2]:

$$\Delta t' = \frac{\Delta t}{\sqrt{1-\frac{v^2}{c^2}}} \rightarrow \Delta t = \Delta t' \sqrt{1-\frac{v^2}{c^2}}$$

where Δt is the time period for person A, $\Delta t'$ is the time period for person B and c is the speed of light. So if $v = c$ then $\Delta t = 0$ which means the elapsed time will be zero for person A.

3. Conclusion

The most accurate definition of time is a relative motion with respect to the universe and since the universe is moving at the speed of light in all directions, so if someone travels at the speed of light in an arbitrary direction, time will stop for him. Suppose that the universe is a moving bus which is traveling at a speed of 100 (km/h). For an observer stationary on the ground, the bus passes him and over time, will be getting further and further away, but for the one riding in the moving bus there will be no distance between the bus and him and there will be no passage of time!

References

[1] Thomas S. Kuhn, *The Structure of Scientific Revolutions*, University of Chicago Press, 1962.

[2] D. Halliday, R. Resnick, and J. Walker, *Fundamentals of Physics*, 10th ed. (John Wiley & Sons Inc, New York, 2014), Vol. 2, p. 1122.

HADRONIC JOURNAL 47, 479 - 487 (2024)
DOI 10.29083/HJ.47.04.2024/SC479

APPARENT MEANING OF ONE KILOGRAM & ONE MOLE VOLUME

Francis V. Fernandes
Independent Researcher
137 Bethany, Kodaikanal, TN, India
aither137@gmail.com

Received September 30, 2024

Abstract

There is one particle type in the universe I call the aitheron whose frequency gives the measure of mass in kilograms. Frequency is intrinsic to the definition of a time interval of one second. Examples of a proton mass and an electron mass serve a fresh understanding of the true meaning of mass as that of an aitheron frequency. Moreover, the term quantum is fully revealed in this respect. One mole volume solved for Hydrogen and a computer chip respectively at a particular temperature and pressure derives from the foundational empirical evidence of aitheron frequency as the source of mass. It is an exciting revelation in this paper to reveal the photon source of molar volume independent of two different materials namely Hydrogen gas and a chip. The volume of a gas being what is measured for equal moles is worked out with three defined length parameters which draws closer to the structure of space.

Keywords: 186-ether, Graviton, 737 Aitheron, Quantum, Hall, Boltzmann constant, Electron Volt, Current, Wavelength, Frequency, Charge, Mass, Molar Volume, Magnetic Pressure, Temperature, Ideal Gas Equation, Avogadro, Klaus Von Klitzing, Josephson

1 Introduction

The terms of one mole mass and one mole volume of an ideal gas have perplexed philosophers from the time of Avogadro. A Socratic question follows: how is it that an Avogadro number of 6.02214076e23 particles of any gas occupy the same volume at a particular temperature and pressure? The answer lies in this paper.

The frequency of a proton or an electron is defined by NIST. This conventional idea is a false assumption. The frequencies are that of a 737 Aitheron and not that of a proton or electron. The frequency of the 737 Aitheron produces a measurement of mass that we call an electron or proton.

The frequency of a photon too is that of an Aitheron. The frequency of emanating electromagnetic radiation is the same frequency of the 737 mass. (*Ch. IV, The Speed of Light Ch. XII, A Story of Creation, 2008*). [2]

The 737 Aitheron mass is in the10e-51Kg range. The so-called Higgs Boson God Particle is in the 10e-25Kg range. There are 26 decimal places between my algebraic calculations of two lines and a complex statistical calculation of a mass created artificially by smashing protons under a magnetic field and acceleration.

Mass of a God Particle Higgs Boson near 125 GeV so named for the public imagination to suggest that God is an objective reality that can be measured as another material particle object that is one of many particle masses. In other words, a senseless play in nomenclature to subtly deceive the world at large that something great has been observed of statistical significance but for a fleeting moment. Over the years several Higgs Bosons have been observed and the theory has now evolved to a Higgs Field that gives mass.

Now, let us deal with molar volume. Millions of students in high school over centuries have studied the mole concept. The experimental evidence that one mole of an ideal gas occupies a fixed volume at a particular temperature and pressure is measured and done. No further discussion was required nor revisited in classrooms even though the experimental observation is inexplicable until now.

The number of atoms or molecules do dictate the Avogadro number for one mole. However, photons dictate molar volume about one particle of say an atom or molecule or ion in a gas.

2 Literature review

2.1 A brief history on one kilogram

NIST has revised the definitions of fundamental units of measurements several times over the past decades. Nobel laureate Von Klitzing humorously describes these developments in lectures that entertain and yet point to the landscape of ever-changing accuracy and definitions of fundamental constants in Physics. Rather than providing citations on the topic, Klitzing's video narrations bring out with images what one kilogram looks like in a vault in Paris. The history as well as the most recent definition of one kilogram is described at, Kilogram - Wikipedia.

2.2 A brief history on one mole volume

NIST has defined one mole substance. The definition is easily understood in the following link, Molar volume - Wikipedia. The development of the Ideal Gas Equation via the works of namely Charles, Gay Lussac and Kelvin have yielded important industrial outcomes in terms of reaction kinetics and yield of products in synthesis of chemicals and pharmaceuticals. For example, it is a fact that one molar volume of Hydrogen gas at a particular temperature and pressure occupies the molar volume as say Nitrogen gas under similar conditions of pressure and temperature. One would expect 28g of molecular Nitrogen to occupy a larger volume than 2g of molecular Hydrogen. And this is where the history of molar volume and inexplicable understanding ends.

3 Method

Employing ratio and proportion where dimensional homogeneity is maintained on both sides of an empirical equation, I present this Fernandes Ether Model utilizing algebraic computation. The method entails asking the right questions about a seemingly well-done science on one kilogram mass and molar volume.

4 Data Processing and Analysis

In the Ether Model, there are two particle types described namely a Graviton and an Aitheron. An Aitheron is a Graviton point particle at 10e7 Hz. [1]

An interval in math is measured in terms of numbers. An interval includes all the numbers that come between two particular real numbers. In the Fernandes Ether Model mass, length and frequency are measurements as defined by NIST in a time interval of one second.

NIST has defined intervals of mass, length & frequency respectively in a time interval of one second, measured with a Cs atomic clock based on a defined speed of light *c*.

a. Graviton:

$$1.859222909\times10^{-9}\times V_{Rk}=7.372497321\times10^{-58}\times\frac{c^2}{1.380668031\times10^{-36}}\times1.0 \qquad (1)$$

$$V_{Rk}=25812.807\text{m/s}$$

b. Aitheron: The energy of 737 Aitheron equals the Planck's constant times one second.

$$7.372497321\times10^{-51}\times c^2=h\times1.0 \qquad (2)$$

$$1.859222909\times10^{-9}\times V_{Rk}=7.372497321\times10^{-51}\times\frac{c^2}{1.380668031\times10^{-29}}\times1.0 \qquad (3)$$

So, the imposed condition is 1 second for the wave-maker measurement.

ELECTRON MASS

An electron is 737 Aitheron frequency that produces a measure an electron mass.

$$7.372497321\times10^{-51}\ \text{Kg} \times 1.0\ \text{s} \times f = 9.10938356 \times 10^{-31}\ \text{Kg} \quad (4)$$

$$f = 1.235589945 \times 10^{20}\ \text{Hz}\ \textit{[NIST]} \quad (5)$$

PROTON MASS

A proton is 737 Aitheron frequency that produces a measure of proton mass.

$$7.372497321 \times 10^{-51}\text{Kg} \times 1.0\ \text{s} \times f = 1.672622 \times 10^{-27}\ Kg \quad (6)$$

$$f = 2.26873262\times10^{23}\ \text{Hz}\quad \textit{[NIST]} \quad (7)$$

NIST frequency depicted above is of the 737 Aitheron and not that of a proton or electron. The measurement of 737 Aitheron frequency is what we think of as mass of an electron or proton or photon.

The next computation is the application of this understanding of mass in defining one Kilogram.

737 AITHERON & ONE KILOGRAM MASS

$$\text{Photon frequency of Cs atom } f1 = 9192631770\ Hz \quad (8)$$

$$t = \frac{1}{f1} = 1.087827757 \times 10^{-10}\ \text{s} \quad (9)$$

$$\text{Photon mass, } m^* = 7.372497321^{-51}\ \text{Kg}\times 1.0\ \text{s}\times f1 = 6.77726531\times10^{-41}\ \text{Kg} \quad (10)$$

Fernandes Ether Model Dogma - *737 Aitheron frequency produces a measure of a virtual photon mass, m^**

$$FTL = r\times f1 \qquad r = 378.76191\ \text{lm} \qquad e^2 = m^*\times r = m^*\times R \times 10^7 \quad (11)$$

$$\text{Wavelength, } \lambda = 2\pi \times R \times 137.036 \quad (12)$$

$$1.4755214 \times 10^{40}\text{photons} \times 6.77726531 \times 10^{-41}\ \text{Kg} = 1\ \text{Kg} \quad (13)$$

Same outcome as the new kilogram definition by NIST

$$e^2 = m^{**} \times 1.163131281 \times 10^{-13} \quad (14)$$

Atomic mass of Cs is 132.9055u

Mass of one Cs atom $m^{**}= 2.2069393e^{-25}$ Kg (15)

$$v^* = R \times fl = 1.069223757 \times 10^{-3} m/s \quad (16)$$

$$v^2 = V_{RK} \times v^* = 27.599\ m^2/s^2 \quad (17)$$

$$R = 1.163131281 \times 10^{-13} m$$

$FTL = R \times f$ $\quad f = 2.993558762 \times 10^{25} Hz$ frequency of a Cs atom (18)

Frequency f times Aitheron mass in 1 second gives the measure of mass of a Cs atom.

$E = m^{**} \times v^2 = h\,fl =$ mass of photon, $m^* \times c^2$ See (8) (10) (15) (17) (19)

[Depicts two particles namely a Cs atom, m^{**} and a photon, m^* at the same energy]

<u>One second NIST definition</u> - "The second is the duration of 9192631770 cycles (periods) of the radiation corresponding to the transition between the two hyperfine levels of the ground state of the Cesium 133 atom.

<u>One kilogram NIST kilogram definition</u> -

(a) the mass difference between 1.4755214×10^{40} cesium atoms in the ground state and the same number in the excited hyperfine state or as (b) the mass of 1.4755214×10^{40} photons at the Cs hyperfine frequency trapped in a microwave cavity.

Boltzmann Constant factored as Q

For the photon,

Current, $I = \frac{m^*_o}{e} = 1.268132978 \times 10^{-13}$ amp (20)

Note: $1.268132833e\text{-}13 / fl = 1.379510095e\text{-}23 = 2Pi \times 10^{-7} \times 137.036 \times e = Q$ (21)

Notice that the Boltzmann constant is now factored by me and renamed as Q.

For the Cs atom,

Current, $I = \frac{m^{**}v}{e}$ Velocity $v = 9.206257483 \times 10^{-8}$ m/s (22)

$v = r \times fl$ The drift velocity of a Cs atom at the same frequency fl of the photon

$r = 1.001482243e\text{-}17m$ (23)

$e^2 = m \times r$ (24)

$m = 2.563170392e\text{-}21$ Kg (25)

$m^{**}/m = 2Pi \times 10^{-7} \times 137.036$ (26)

A precession factor is involved in Cs drift velocity v

ONE MOLE VOLUME

A photon contribution to one mol volume of an ideal Hydrogen gas and a specimen is explained here. In childlike terms, one elephant and one ant as gas each occupy the same volume at a particular temperature and pressure. Here is the volume of one molecule of Hydrogen gas at 1.01325 × 10e5 Pa and 300K. [3]. Utilizing the magnetic flux quantum phi, magnetic field B, magnetic pressure B squared, temperature T, charge squared equations one can arrive at the table below. There is a faster than light FTL component too.

Table 1: The three lengths that produce the empirical volume of molecular Hydrogen gas.

			$A = R_1 \times R_3$
$R_1 = 0.278731462$ m	$2m$	Used to calibrate voltmeters	BA is the magnetic flux quantum Pressure = Current squared per area, A
$R_2 = 0.557462906$ m	m	The photon mass measured due to 737-frequency	The FTL Component velocity of speed of light squared
$R_3 = 2.6287224 \times 10^{-25}$ m	m^*	Measured in magnetism	The source of magnetism

Utilizing the modified Ideal Gas Equation PV = QT for one particle (27)

Volume of one molecule of H_2 (g) = 4.0845734217398595393909 12e-26m^3 at 300K, 1.01325e5 Pa (28)

Vol at 300K at 0.0025 Pa = 1.655477607831165071315136633 6e-18 m^3 (29)

Pressure = B squared = 0.0025 Pa (30)

Vol at 6.968 K and 0.0025Pa = 3.8451226571225194056412906876416e-20 m^3 Vol of one molecule $H_{2(g)}$ (31)

Example – A slice of semi conducting material 0.5 mm thick is placed at right angles to a magnetic field of flux density 0.05 T. A Hall voltage of 0.3 mV is generated across the specimen when a current of 100 mA flows through it.

I will now show how the volume of this material specimen at 6.968 K and 0.0025 Pa is the same as that of Hydrogen gas in the previous example. This is – *An amazing depiction of the true meaning of one mole volume & Magnetic field pressure* B^2. [3]

Phi = h/2e = BA B = 0.05T

Area A = 4.135649296939619520264681555004 1e-14 m^2 (32)

Magnetic Pressure P = B squared

A = $2R_2 \times R_2$ = 1.080596e-13 m^2 of this specimen semiconductor See Table 2. (33)

Vol/A = 3.55833508278997831348745570744 44e-7 m (34)

where Vol at 6.968 K and 0.0025Pa is

Vol = 3.84512265712251940564129068764 16e-20 m^3 the Vol of one molecule $H_{2(g)}$

R_1 = 0.0000003558439279601505 / 8.610225e-5 m (35)

R_1 = 0.004132806378m (36)

A* = Pi × 10e-7 × R_1 × R_2 ×137.036 m^2 See Table 2 below

R_2 = 2.3244275e-7 m R_1 = 0.004132806378 m (37)

A* = Pi × 10e-7 × 9.6064088e-10 × 137.036 = 4.135667453183351338e-14 m^2 (38)

Table 2: The volume occupied by photons obey the ideal gas equation.

Current amps I A	Photon mass m Kg	R = I / B meters m	Ohms c/e Ω	Charge Squared e^2 C^2
2.066403189e-4 R × B = I	m = 6.2112e-36	R_1 = 0.004132806378 R_1 /2 × f_J = c	I / m = v/e I / m = c/e	m × R 2m × R/2
I 1.16221378e-8 Q × **f** = **I**	m = 5.5217e-32	$R_2 \times f_J$ = 33722.794 = v R_2 = 2.3244275e-7	I / m = v/e I / m = c/e	2m ×R

The reason for the Josephson frequency f_J and Cooper pairs in the table are dealt with in Ref. 3. A curious observation is that the 2m Cooper pairs are not electrons.

The source of R_2 can be calculated from the Hall Quantum frequency **f** related to **I.**

eV = 0.0003eV $2 \times eV = 8.610025e\text{-}5 \times T$ T = 6.96845839 K (39)

Quantized Hall Resistance

0.0003eV = I × 25812.807 Ω I = 1.16221378e-8A (40)

The same method can be used for material superconductivity.

One has to look at the data from a distance as a snapshot of an invisible physical reality. This gives a chance for the brain to design a structure of the invisible.

5 Results and Discussions

Mass:

The empirical data from this paper and several others in the reference section prompted me to formulate the following scientific dogmas.

DOGMA - An aitheron is a graviton point particle at f1 = 10e7 Hz.

DOGMA – Aitheron mass × f2[Codata] = anti-matter mass [photon, atoms, electrons, protons etc] *in one second*

DOGMA – anti-matter mass × f3 = 186-ether mass *in one second*

NOTE: f2 × f3 events are simultaneous because their product is a constant.

DOGMA – 186-ether × f3 = Toroid mass simultaneous in one second with f1 and f2 and f3

The Ether toroid mass = $4.688656088 \times 10^{39}$ kg

The Major Axis Radius, $R = 1.380668031 \times 10^{-29}$m [Note: Symbol R is for this image only]

The Minor Axis Radius, $r = 1.380668031 \times 10^{-36}$m [Note: Symbol r is for this image only]

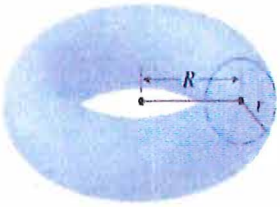

Molar Volume

The molar volume of Hydrogen gas and the specimen at a particular temperature and pressure for one particle is the same. The volume is the product of three lengths. The three lengths are that of three measured photon masses. This is the reason why molar volume is independent of the mass of individual particles such as atoms, molecules in an idealized gas phase state. The meaning of an idealized gas state is yet to be determined over time. The answer lies in the Fernandes Ether Model.

6 Conclusion

The new kilogram definition by NIST is defined by the atomic mass difference between 1.4755214×10^{40} cesium atoms in the ground state and the same number in the excited hyperfine state or the mass of 1.4755214×10^{40} photons at the Cs hyperfine frequency trapped in a microwave cavity. By mass defect each photon has a mass of 6.777264095 × 10e-41 Kg. One kilogram mass measured here is by mass defect. However, on deeper

inspection there is one particle type in the universe I call the aitheron whose frequency gives the measure of mass of one kilogram. The frequency is intrinsic to the definition of a time interval of one second. "One second is the duration of 9192631770 cycles (periods) of the radiation corresponding to the transition between the two hyperfine levels of the ground state of the cesium 133 atom as defined by NIST. Examples of mass of a proton and mass of an electron serve as a fresh understanding of the true meaning of frequency as that of an aitheron. Moreover, the term quantum is fully revealed in this respect. One mole volume solved for Hydrogen and a computer chip respectively at a particular temperature and pressure derives from the foundational empirical evidence of aitheron frequency the true source of mass. It is an exciting revelation in this paper to reveal the photon source of molar volume independent of two different materials namely Hydrogen gas and a chip. The volume of a gas being what is measured for equal moles is worked out with three defined length parameters which draws closer to the structure of space.

Understanding of the interconnectedness of aitheron frequency and measurements of mass and volume is key to unlocking the true meaning of data from secondary units in Physics. The Boltzmann constant, k of the Ideal Gas Equation is empirically factored and called Q. There is a beautiful connection between Kelvin Temperature, and eV and Electric current with the Hall frequency and Quantum Hall Resistance.

TECHNOLOGICAL SIGNIFICANCE – In Chemistry

Free energy generators – By utilizing VRK in the design of a generator.
Quantum computing chips – By utilizing the true meaning of molar volume
Superconductors – By utilizing the Quantum Hall Resistance in relation to eV and T.
Weather predictions – By measurement of magnetic field B squared as pressure and T.
Pressure sensors - By measurement of magnetic field B squared as pressure and molar volume relationships.

References

[1] Francis V. Fernandes, The Hand of God Alpha Represents Radial Pulsation Limits of Fernandes-186 Ether to the Planck Ether Length, Sips23_70_407FS
[2] Francis V. Fernandes, Mark Antrobus, *The Ether Model & The Hand of God*, Lulu Press, 2008.
[3] Francis V. Fernandes, Electrodynamic Treatment of Infectious Diseases - The Realm of Biophysics, Crete SIPS 2024

HADRONIC JOURNAL 47, 489 - 500 (2024)
DOI 10.29083/HJ.47.04.2024/SC489

FOURIER TRANSFORM OF SCHWARTZ ALGEBRAS ON GROUPS IN THE HARISH-CHANDRA CLASS

Olufemi O. Oyadare
Department of Mathematics
Obafemi Awolowo University
Ile-Ife, 220005, Nigeria
femi_oya@yahoo.com

Received April 8, 2024

Abstract

It is well-known that the Harish-Chandra transform, $f \mapsto \mathcal{H}f$, is a topological isomorphism of the spherical (Schwartz) convolution algebra $\mathcal{C}^p(G//K)$ (where K is a maximal compact subgroup of any arbitrarily chosen group G in the Harish-Chandra class and $0 < p \leq 2$) onto the (Schwartz) multiplication algebra $\tilde{\mathcal{Z}}(\mathfrak{F}^\epsilon)$ (of $\mathfrak{w}-$invariant members of $\mathcal{Z}(\mathfrak{F}^\epsilon)$, with $\epsilon = (2/p) - 1$). The same cannot however be said of the full Schwartz convolution algebra $\mathcal{C}^p(G)$, except for few specific examples of groups (notably $G = SL(2,\mathbb{R})$) and for some notable values of p (with restrictions on G and/or on $\mathcal{C}^p(G)$). Nevertheless the full Harish-Chandra Plancherel inversion formula on G is known for all of $\mathcal{C}^2(G) =: \mathcal{C}(G)$. In order to then understand the structure of Harish-Chandra transform more clearly and to compute the image of $\mathcal{C}^p(G)$ under it (without any restriction) we derive an absolutely convergent series expansion (in terms of known functions) for the Harish-Chandra transform by an application of the full Plancherel inversion formula on G. This leads to a computation of the image of $\mathcal{C}(G)$ under the Harish-Chandra transform which may be seen as a concrete realization of Arthur's result and be easily extended to all of $\mathcal{C}^p(G)$ in much the same way as it is known in the work of Trombi and Varadarajan.

2010 Mathematics Subject Classification: $43A85$, $22E30$, $22E46$
Keywords: Fourier Transform; Reductive Groups; Harish-Chandra's Schwartz algebras.

§1. Introduction. Let G be a reductive group in the *Harish-Chandra class* where $\mathcal{C}^p(G)$ is the *Harish-Chandra-type* Schwartz algebra on G, $0 < p \leq 2$, with $\mathcal{C}^2(G) =: \mathcal{C}(G)$. The image of $\mathcal{C}^p(G)$ under the (Harish-Chandra) *Fourier transform* on G has been a pre-occupation of harmonic analysts since the emergence of Arthur's thesis [1*a*], where the Fourier image of $\mathcal{C}(G)$ was characterized for connected non-compact semisimple Lie groups of real rank one. Thereafter Eguchi [3*a*.] removed the restriction of the real rank and considered non-compact real semisimple G with only one conjugacy class of *Cartan subgroups* as well as the Fourier image of $\mathcal{C}^p(G/K)$, [3*b*.], while Barker [2.] considered $\mathcal{C}^p(SL(2,\mathbb{R}))$ as well as $\mathcal{C}^0(SL(2,\mathbb{R}))$. The complete $p = 2$ story for any real reductive G is contained in Arthur [1*b*, *c*]. The most successful general result along the general case of p is the well-known *Trombi-Varadarajan Theorem* [9.] which characterized the image of $\mathcal{C}^p(G//K)$, $0 < p \leq 2$, for a maximal compact subgroup K of a connected semisimple Lie group G as a (Schwartz) multiplication algebra $\tilde{\mathcal{Z}}(\mathfrak{F}^\epsilon)$ (of $\mathfrak{w}-$invariant members of $\mathcal{Z}(\mathfrak{F}^\epsilon)$, with $\epsilon = (2/p) - 1$); thus subsuming the works of Ehrepreis and Mautner [4.] and Helgason [6.]. However the characterization of the image of $\mathcal{C}^p(G)$ for reductive groups G in the Harish-Chandra class has not yet been achieved due to failure of the method (successfully employed in [1*b*, *c*] and [10.]) of generalizing from the real rank one case. Nevertheless the *Plancherel inversion formula* is already known for $\mathcal{C}(G)$, where G is a reductive group in the Harish-Chandra class, [10.].

This paper contains a derivation of an absolutely convergent series expansion (in terms of known functions) for the *Harish-Chandra transform* and its application in constructing an explicit image of $\mathcal{C}(G)$ under it, for reductive groups, G, in the Harish-Chandra class. These results give explicit realization of the *abstract* computations of Arthur [1.] and show the direct contributions of the Plancherel inversion formula to the understanding of Harish-Chandra transform. As a Corollary we deduce a more explicit form of the $p = 2$ Trombi-Varadarajan Theorem.

§2. Preliminaries. Let G be a group in the Harish-Chandra class. That is G is a locally compact group with the properties that G is reductive, with Lie algebra $\mathfrak{g}$, $[G : G^0] < \infty$, where G^0 is the connected component of G containing the identity, in which the analytic subgroup, G_1, of G defined by $\mathfrak{g}_1 = [\mathfrak{g}, \mathfrak{g}]$ is closed in G and of finite center and in which, if $G_{\mathbb{C}}$ is the adjoint

group of $\mathfrak{g}_{\mathbb{C}}$, then $Ad(G) \subset G_{\mathbb{C}}$. Such a group G is endowed with a *Cartan involution,* θ, whose fixed points form a *maximal* compact subgroup, K, of G [5.]. K meets all connected components of G, in particular G^0.

We denote the *universal enveloping algebra* of $\mathfrak{g}_{\mathbb{C}}$ by $\mathcal{U}(\mathfrak{g}_{\mathbb{C}})$, whose members may be viewed either as left or right invariant differential operators on G. We shall write $f(x;a)$ for the left action $(af)(x)$ and $f(a;x)$ for the right action $(fa)(x)$ of $\mathcal{U}(\mathfrak{g}_{\mathbb{C}})$ on functions f on G. Let $\mathcal{C}(G)$ represents the space of $C^\infty-$functions on G for which

$$\sup_{x\in G} \mid f(b;x;a) \mid \Xi^{-1}(x)(1+\sigma(x))^r < \infty,$$

for $a, b \in \mathcal{U}(\mathfrak{g}_{\mathbb{C}})$ and $r > 0$. Here Ξ and σ are well-known *elementary* spherical functions on G. $\mathcal{C}(G)$ is known to be a Schwartz algebra under convolution while $\mathcal{C}(G//K)$, consisting of the spherical members of $\mathcal{C}(G)$, is a closed commutative subalgebra.

Let $\hat{G}$ represent the set of equivalence classes of *irreducible unitary representations* of G. If G_1 is non-compact then the support of the Plancherel measure does not exhaust $\hat{G}$. We write $\hat{G}_t$ for this support, which generally contains a discrete part, $\hat{G}_d$ ($\neq \emptyset$, if $rank(G) = rank(K)$), and a continuous part, $\hat{G}_t \setminus \hat{G}_d$ ($\neq \emptyset$, always). G has finitely many conjugacy classes of *Cartan subgroups,* which may be represented by the set $\{A_1, \cdots, A_r\}$.

We can write

$$A_i = A_{i,I} \cdot A_{i,\mathbb{R}},$$

where $A_{i,I} = A \cap K$ is a maximal compact subgroup of A_i and $A_{i,\mathbb{R}}$ (whose Lie algebra shall be denoted as $\mathfrak{a}_{i,\mathbb{R}}$) is a vector subgroup with $\theta(a) = a^{-1}$, $a \in A_{i,\mathbb{R}}$. There are parabolic subgroups P_i of G whose *Langlands decompositions* are of the form $P_i = M_i A_{i,\mathbb{R}} N_i$. Each of the subgroups M_i satisfies all the requirements on G.

The *full* Harish-Chandra Plancherel inversion formula on G states that there are uniquely defined non-negative continuous functions, C_i, on $(\hat{M}_i)_d \times \mathfrak{a}_{i,\mathbb{R}}$ such that each C_i is of at most polynomial growth in which $C_i(s\omega : s\nu) = C_i(\omega : \nu)$, $s \in W(G, A_i)$ (the Weyl group of the pair (G, A_i)) and, for $f \in \mathcal{C}(G)$, we have

$$f(1) = \sum_{i=1}^{r} (\sum_{\omega \in (\hat{M}_i)_d} \int_{\mathfrak{a}_{i,\mathbb{R}}^*} C_i(\omega : \nu) \Theta_{\omega,\nu}(f) d\nu),$$

with absolute convergence, [10.]. Here $\Theta_{\omega,\nu}$ represents the *distributional characters* of irreducible unitary representations, $\pi_{\omega,\nu}$, on G.

More explicitly, the support of the *reduced dual* $\widehat{G}_r$ of G split as $\widehat{G}_r^d \bigsqcup \widehat{G}_r^M$, it is populated only by the *discrete,* π_ω, $\omega \in \widehat{G}_r^d$ and *principal series,* $\pi_{(\sigma,\lambda)}$, $(\sigma,\lambda) \in \widehat{M} \times \mathbb{R} = \widehat{G}_r^M$ of representations of G and there exist a number $\beta(\omega)$, $\omega \in \widehat{G}_r^d$ (called the *formal degree* of ω) and a non-negative function $\beta : \widehat{M} \times \mathbb{R} \to [0,\infty) : (\sigma,\lambda) \mapsto \beta(\sigma,\lambda)$ such that, for any $f \in \mathcal{C}(G)$, the split version of the full Harish-Chandra Plancherel inversion formula on G is given as

$$f(1) = \sum_{\omega \in \widehat{G}_r^d} \beta(\omega)\Theta_\omega(f) + \sum_{\sigma \in \widehat{M}} \int_0^\infty \beta(\sigma,\lambda)\Theta_{\sigma,\lambda}(f)d\lambda.$$

The first form of the Plancherel inversion formula given above (which bears a striking resemblance with members of the space $L^2_{\wp}(\hat{G})$ given in [1*b*, *c*]) may be re-written as $f(1) = \sum_{i=1}^r (\sum_{\omega \in (\hat{M}_i)_d} \int_{\mathfrak{a}_{i,\mathbb{R}}^*} C_i(\omega : \nu)\Theta_{\omega,\nu}(f)d\nu)$

$$= \sum_{i=1}^r (\sum_{\omega \in (\hat{M}_i)_d} \int_{\mathfrak{a}_{i,\mathbb{R}}^*} \|a_{\wp_i}(\omega,\nu)\|^2 \mu_\omega(\nu)d\nu),$$

where the measurable functions

$$(\omega,\nu) \mapsto a_{\wp_i}(\omega,\nu)$$

(of Arthur [1*b*, *c*]) on $(\hat{M}_i)_d \times \mathfrak{a}_{i,\mathbb{R}}$ are realizable as those for which

$$\|a_{\wp_i}(\omega,\nu)\|^2 \mu_\omega(\nu) = C_i(\omega : \nu)\Theta_{\omega,\nu}(f) \text{ and } \|a_\wp\|^2 = f(1),$$

for any $f \in \mathcal{C}(G)$ and μ_ω−almost everywhere. This gives a first suggestion that the Plancherel inversion formula may contribute to the realization of the image of $\mathcal{C}(G)$. It then means that Arthur's map $(\omega,\nu) \mapsto a_{\wp_i}(\omega,\nu)$ are functions whose L^2−norm satisfies the above prescriptions of being realizable in terms of members of $\mathcal{C}(G)$. This remark may prove useful in the eventual realization of these functions. It will however be clear from our main Theorem that an explicit expression for $a_{\wp_i}(\omega,\nu)$ (though of interest in its own right) would not be necessary in the computation of $\mathcal{H}(\mathcal{C}(G))$.

We shall denote the (elementary) spherical functions on G by φ_λ, $\lambda \in \mathfrak{a}_{\mathbb{C}}^*$. We know that the *functional equation*

$$\varphi_{s\lambda}(x) = \varphi_\lambda(x)$$

holds ([10.], *p.* 365) for all $s \in \mathfrak{w} = \mathfrak{w}(\mathfrak{g}_{\mathbb{C}}, \mathfrak{a}_{\mathbb{C}})$, $x \in G$. Since

$$\mathcal{C}(G) * \mathcal{C}(G) \twoheadrightarrow \mathcal{C}(G)$$

is a continuous map, then the function $x \mapsto s_{\lambda,f}(x)$, $x \in G$, given as

$$s_{\lambda,f}(x) := (f * \varphi_\lambda)(x)$$

is a Schwartz function on G. It is also clear that $s_{\lambda,f}(1) = (\mathcal{H}f)(\lambda)$, [8.] and [9.].

§3. Harish-Chandra Fourier Transform on $\mathcal{C}(G)$. We shall start by introducing the following space of functions on $\mathfrak{a}^*$.

Definition 3.1 *Let $\{A_1, \cdots, A_r\}$ be a complete set of representatives in the conjugacy classes of Cartan subgroups of G and let $\mathcal{C}_G(\mathfrak{a}^*)$ represents the space of functions on $\mathfrak{a}^*$ that are topologically spanned by maps of the form*

$$\lambda \mapsto g_{i,f}(\lambda) := \int_{\mathfrak{a}^*_{i,\mathbb{R}}} C_i(\omega : \nu)\Theta_{\omega,\nu}(f * \varphi_\lambda)d\nu,$$

where $i = 1, \cdots, r$, and $f \in \mathcal{C}(G)$.

It is clear (from the fact that $\hat{G}_t \setminus \hat{G}_d \neq \emptyset$) that $\mathcal{C}_G(\mathfrak{a}^*) \neq \emptyset$ for any reductive group, G, in the Harish-Chandra class. We endow $\mathcal{C}_G(\mathfrak{a}^*)$ with the basic operations of a function space which convert it into a multiplication algebra. Since $f \in \mathcal{C}(G)$ and $\varphi_\lambda \in \mathcal{C}(G//K)$, the algebra $\mathcal{C}_G(\mathfrak{a}^*)$, consisting of absolutely convergent integrals whose decay estimates follow from the above Plancherel inversion formula, is therefore a Schwartz algebra on $\mathfrak{a}^*$.

Lemma 3.2 *$\mathcal{C}_G(\mathfrak{a}^*)$ is invariant under the action of the Weyl group $\mathfrak{w} = \mathfrak{w}(\mathfrak{g}_{\mathbb{C}}, \mathfrak{a}_{\mathbb{C}})$ defined as $(s \cdot g)(\lambda) = g(s^{-1}\lambda)$, $s \in \mathfrak{w}$, $g \in \mathcal{C}_G(\mathfrak{a}^*)$.*

Proof. Note that $(s \cdot g_{i,f})(\lambda) = g_{i,f}(s^{-1}\lambda) = \int_{\mathfrak{a}^*_{i,\mathbb{R}}} C_i(\omega : \nu)\Theta_{\omega,\nu}(f * \varphi_{s^{-1}\lambda})d\nu$

$$= \int_{\mathfrak{a}^*_{i,\mathbb{R}}} C_i(\omega : \nu)\Theta_{\omega,\nu}(f * \varphi_{s_1\lambda})d\nu$$

(since there exists $s_1 \in \mathfrak{w}$ such that $s_1 \cdot s = 1$ and so that $s^{-1} = s_1$)

$$= \int_{\mathfrak{a}^*_{i,\mathbb{R}}} C_i(\omega : \nu)\Theta_{\omega,\nu}(f * \varphi_\lambda)d\nu = g_{i,f}(\lambda). \square$$

It may also be shown that, if $g \in \mathcal{C}_G(\mathfrak{a}^*)$ and $\lambda_1, \lambda_2 \in \mathfrak{a}^*$ are such that $s\lambda_1 = \lambda_2$, for some $s \in \mathfrak{w}$, then $g(\lambda_1) = g(\lambda_2)$. The above Lemma implies

that $\mathcal{C}_G(\mathfrak{a}^*)^{\mathfrak{w}} = \mathcal{C}_G(\mathfrak{a}^*)$ and that we do not have to consider the $\mathfrak{w}-$invariant subspace of $\mathcal{C}_G(\mathfrak{a}^*)$. Indeed $\mathcal{C}_G(\mathfrak{a}^*)$ is the $\mathfrak{w}-$invariant subspace of a larger space of functions on $\mathfrak{a}^*$ spanned by maps of the form

$$\lambda \mapsto g(\lambda) := \int_{\mathfrak{a}_{i,\mathbf{R}}^*} C_i(\omega : \nu)\Theta_{\omega,\nu}(h_\lambda)d\nu,$$

for *arbitrary chosen* $h_\lambda \in \mathcal{C}(G)$, $i = 1, \cdots, r$, indexed by $\lambda \in \mathfrak{a}^*$.

Lemma 3.3 *The Harish-Chandra Fourier transform* $f \mapsto \mathcal{H}f$ *is a map of* $\mathcal{C}(G)$ *into* $\mathcal{C}_G(\mathfrak{a}^*)$

Proof. As $f \in \mathcal{C}(G)$ we have that $f * \varphi_\lambda \in \mathcal{C}(G)$ for $\lambda \in \mathfrak{a}^*$. Hence by the above Plancherel inversion formula we conclude that

$$(f * \varphi_\lambda)(1) = \sum_{i=1}^{r}(\sum_{\omega \in (\hat{M}_i)_d} \int_{\mathfrak{a}_{i,\mathbf{R}}^*} C_i(\omega : \nu)\Theta_{\omega,\nu}(f * \varphi_\lambda)d\nu).$$

That is,

$$(\mathcal{H}f)(\lambda) = \sum_{i=1}^{r}(\sum_{\omega \in (\hat{M}_i)_d} \int_{\mathfrak{a}_{i,\mathbf{R}}^*} C_i(\omega : \nu)\Theta_{\omega,\nu}(f * \varphi_\lambda)d\nu),$$

which show that $\mathcal{H} : \mathcal{C}(G) \to \mathcal{C}_G(\mathfrak{a}^*)$, with all its known properties still intact.□

A more importatnt realization of the algebra $\mathcal{C}_G(\mathfrak{a}^*)$ is derived as follows.

Lemma 3.4 *The algebra* $\mathcal{C}_G(\mathfrak{a}^*)$ *is the topological linear span of maps of the form*

$$\lambda \mapsto \int_{\mathfrak{a}_{i,\mathbf{R}}^*} C_i(\omega : \nu)\pi_{\omega,\nu,\mathfrak{d}_i}(f)d\nu$$

where $f \in \mathcal{C}(G)$ *and* $\mathfrak{d}_i$ *is the singleton set consisting of the trivial representation of each* M_i *corresponding to the elementary spherical function* φ_λ.

Proof. We only need to show that

$$\Theta_{\omega,\nu}(f * \varphi_\lambda) = \pi_{\omega,\nu,F_i}(f).$$

Indeed, we have that

$$\Theta_{\omega,\nu}(f * \varphi_\lambda) = \int_G \Theta_{\omega,\nu}(x)(f * \varphi_\lambda)(x)dx$$

$$= \int_G \Theta_{\omega,\nu}(x)(\int_G f(y)\varphi_\lambda(y^{-1}x)dy)dx$$

$$= \int_G f(y)(\int_G \Theta_{\omega,\nu}(x)\varphi_\lambda(y^{-1}x)dx)dy$$

$$\int_G f(y)(\Theta_{\omega,\nu} * \varphi_\lambda)(y)dy = \int_G f(y)\Phi_{\pi_{\omega,\nu,\mathfrak{d}}}(y)dy =: \pi_{\omega,\nu,\mathfrak{d}}(f)$$

(in the notation of [5.], *p.* 22), since the function $\Phi_{\pi_{\omega,\nu,\mathfrak{d}}}$ given above as $\Phi_{\pi_{\omega,\nu,\mathfrak{d}}} = \Theta_{\omega,\nu} * \varphi_\lambda$ is a spherical function of type $\mathfrak{d} = \{1\}$ which is associated with $\pi_{\omega,\nu}$.□

Corollary 3.5 *The Harish-Chandra Fourier transform $f \mapsto \mathcal{H}f$ of $\mathcal{C}(G)$ into $\mathcal{C}_G(\mathfrak{a}^*)$ is given by an absolutely convergent series as*

$$(\mathcal{H}f)(\lambda) = \sum_{i=1}^{r}(\sum_{\omega\in(\hat{M}_i)_d}\int_{\mathfrak{a}_{i,\mathbb{R}}^*} C_i(\omega:\nu)\pi_{\omega,\nu,\mathfrak{d}_i}(f)d\nu).\square$$

The above function $\Phi_{\pi_{\omega,\nu,\mathfrak{d}}}$ is worthy of an independent study. It is a spherical function (being a convolution of two spherical functions) and is continuous (due to the continuity of convolution in $\mathcal{C}(G)$). We may normalize it in order to have $\Phi_{\pi_{\omega,\nu,\mathfrak{d}}}(1) = 1$. We shall denote the *isotypical subspace* of $\mathcal{C}(G)$ with respect to $\mathfrak{d} = \{1\}$ as $\mathcal{C}_1(G)$.

Lemma 3.6 *There exists $f \in \mathcal{C}_1(G)$ such that $\pi_{\omega,\nu,\mathfrak{d}}(f) = 1$.*

Proof. Since $\pi_{\omega,\nu,\mathfrak{d}}$ is an irreducible representation on G in which the isotypical subspace $\mathcal{C}_1(G)$ satisfies $dim(\mathcal{C}_1(G)) < \infty$ ([11], *p.* 114), our result follows from using Lemma 1.3.2 of [5]. *p.* 22.□

Theorem 3.7 *Arthur's Fourier image $\mathcal{C}(\widehat{G})$ of $\mathcal{C}(G)$ coincides with the algebra $\mathcal{C}_G(\mathfrak{a}^*)$.*

Proof. The representation $\pi_{\omega,\nu,\mathfrak{d}}$ satisfies all the requirements in Lemma 1.3.3 of [5], *p.* 22. Hence, the topological linear span of the functions

$$\lambda \mapsto \int_{\mathfrak{a}_{i,\mathbb{R}}^*} C_i(\omega:\nu)\pi_{\omega,\nu,\mathfrak{d}_i}(f)d\nu$$

(in Lemma 3.4 above), which is $\mathcal{C}_G(\mathfrak{a}^*)$, gives the same algebra as that of $\pi_{\omega,\nu}(f)$, $f \in \mathcal{C}(G)$, which we already know to be $\mathcal{C}(\widehat{G})$.□

We have therefore proved the main Theorem of this paper.

Theorem 3.8 *The Harish-Chandra Fourier transform, $f \mapsto \mathcal{H}f$, is a topological algebra isomorphism of $\mathcal{C}(G)$ onto the multiplication algebra $\mathcal{C}_G(\mathfrak{a}^*)$.*
Proof. Combine Corollary 3.5 with Theorem 3.7.□

Corollary 3.9 *The map $I_{\mathfrak{d}} : \mathcal{C}(\widehat{G}) \to \mathcal{C}_G(\mathfrak{a}^*)$ defined as*

$$I_{\mathfrak{d}}(\pi_{\omega,\nu}(f)) = \sum_{i=1}^{r}(\sum_{\omega \in (\hat{M}_i)_d} \int_{\mathfrak{a}_{i,\mathbb{R}}^*} C_i(\omega : \nu)\pi_{\omega,\nu,\mathfrak{d}_i}(f)d\nu)$$

is a topological isomorphism.□

An immediate consequence of our results is the following which gives an explicit realization of the celebrated Trombi-Varadarajan Theorem when $p = 2$.

Corollary 3.10 (p=2 **Trombi-Varadarajan Theorem**) *Let $\mathfrak{F}^\epsilon$ be the Trombi-Varadarajan tubular region in $\mathfrak{a}^*$ containing $\mathfrak{a}_{i,\mathbb{R}}^*$, where $\epsilon = (2/p) - 1$ with $0 < p \leq 2$. Then the Trombi-Varadarajan image, $\tilde{\mathcal{Z}}(\mathfrak{F}^0)$, is a closed subalgebra of $\mathcal{C}_G(\mathfrak{a}^*)$ and*

$$\tilde{\mathcal{Z}}(\mathfrak{F}^0) = \mathcal{C}_{G//K}(\mathfrak{a}^*).$$

Proof. Since $\mathcal{C}(G//K)$ is a closed subalgebra of $\mathcal{C}(G)$ and the map $\mathcal{C}(G//K) * \mathcal{C}(G//K) \to \mathcal{C}(G//K)$ is continuous, Theorem 3.8 implies that we only need to show that $\mathcal{H}f \in \mathcal{C}_G(\mathfrak{a}^*)$, for $f \in \mathcal{C}(G//K)$. Now let $f \in \mathcal{C}(G//K)$ and $\lambda \in \mathfrak{a}^*$, then $f * \varphi_\lambda \in \mathcal{C}(G//K)$, so that the map

$$\lambda \mapsto g(\lambda) := \int_{\mathfrak{a}_{i,\mathbb{R}}^*} C_i(\omega : \nu)\Theta_{\omega,\nu}(f * \varphi_\lambda)d\nu,$$

is well-defined on $\mathfrak{a}^*$. Hence $g \in \mathcal{C}_G(\mathfrak{a}^*)$ and $\mathcal{H}f \in \mathcal{C}_G(\mathfrak{a}^*)$. □

The proof of the above Theorem 3.8 contains a new *formula-representation* of the Harish-Chandra transform as an absolutely convergent series expansion in terms of the Harish-Chandra c–functions and global distributions. *This formula shows (for the first time) the direct dependence of the transform on the uniquely defined non-negative continuous functions, C_i, and characters, $\Theta_{\omega,\nu}$, of the irreducible unitary representations on G.* This expansion may further expose other properties of the transform on a closer look. The importance of our approach to harmonic analysis of Schwartz algebra on G is that the (*character form* of) Plancherel inversion formula of any reductive (Lie) group leads directly to the computation of the Fourier image of this algebra, an image that would be as explicit as the Plancherel inversion formula itself.

An analogous realization of $\mathcal{C}_G(\mathfrak{a}^*)$ may still be sought through an explicit derivation of the combined decay properties of

$$C_i(\omega:\nu)\Theta_{\omega,\nu}(f*\varphi_\lambda) = C_i(\omega:\nu)\pi_{\omega,\nu,\vartheta_i}(f),$$

for $f \in \mathcal{C}(G)$, especially for specific G. The continuous inclusion $\mathcal{C}^p(G) \subset L^2(G)$ makes the above (L^2-) Plancherel inversion formula and absolutely convergent series expansion of the Harish-Chandra transform available for use in extending Theorem 3.8 from $\mathcal{C}(G)$ to all of $\mathcal{C}^p(G)$ (and hence Corollary 3.10 from $\bar{\mathcal{Z}}(\mathfrak{F}^0)$ to all of $\bar{\mathcal{Z}}(\mathfrak{F}^\epsilon)$), in exactly the same way that the results on $\mathcal{C}(SL(2,\mathbb{R})//SO(2))$ was extended to all of $\mathcal{C}^p(SL(2,\mathbb{R})//SO(2))$ in [9.].

A close comparison with formula (15.1) of [2] leads to the following.

Conjecture 3.11 *The map I_0 in Corollary* 3.9 *is an explicit realization of the inverse Fourier transform.*

§4. The Example of $SL(2,\mathbb{R})$. The elementary spherical functions on $G = SL(2,\mathbb{R})$ are given as the matrix coefficients of class 1 members of the principal series $\pi_{\omega\nu}$ ([5], *p.* 103) and are found to be the *Legendre functions*

$$\varphi_\nu(a_t) = P_{i\nu+\frac{1}{2}}(\cosh t) = \frac{1}{2\pi}\int_0^{2\pi}(\cosh t + \sinh t\cos u)^{i\nu+\frac{1}{2}}du,$$

$t \in \mathbb{R}$ ([6*b*], *p.* 406). Distributional characters of G are $G-$invariants defined as

$$\Theta_\pi(f) = tr\pi(f),$$

for all f for which $\pi(f) := \int_G f(x)\pi(x)dx$ is of *trace class.* These characters are completely defined on the only two non-conjugate Cartan subgroups of $G = SL(2,\mathbb{R})$ namely the non-compact type $T = MA$ (with $M = \{\pm I\}$ and $A = \{a_t := \begin{pmatrix} e^t & 0 \\ 0 & e^{-t} \end{pmatrix} : \ t \in \mathbb{R}\}$) and the compact type given as $B := K = \{k_\theta := \begin{pmatrix} \cos\theta & \sin\theta \\ -\sin\theta & \cos\theta \end{pmatrix} : \theta \in [0, 2\pi)\}$, with corresponding Haar measures of $d(\pm)dt$ and $\frac{1}{2\pi}d\theta$, where both of functions $(e^{i\theta} - e^{-i\theta})\Theta_\pi(\theta)$ and $\pm \mid e^t - e^{-t} \mid \Theta_\pi(\pm a_t)$ are locally integrable functions with respect to $(B, d(\pm)dt)$ and $(K, \frac{1}{2\pi}d\theta,)$ respectively.

These facts suggest exponential expressions for both $(e^{i\theta} - e^{-i\theta})\Theta_\pi(\theta)$ and $\pm \mid e^t - e^{-t} \mid \Theta_\pi(\pm a_t)$, where $\pi = \pi_{\sigma,\nu}$ is the principal series representations (in which we now write $\Theta_{\pi_{\sigma,\nu}}$ simply as $\Theta_{\sigma,\nu}$) and $\pi = \pi_n^\pm$ is the principal

series representations (in which we now write $\Theta_{\pi_n^{\pm}}$ simply as Θ_n) of G. Indeed we have that $\widehat{M} = \{\sigma_{\pm}\}$ (with $\sigma_+(\pm I) = 1$ and $\sigma_-(\pm I) = \pm 1$) and $\widehat{K} = \mathbb{Z}^* = \mathbb{Z} \setminus \{0\}$, so that

$$\Theta_{\sigma,\nu}(x) = \begin{cases} 0, & \text{if } x \text{ is conjugate to } k_\theta, \\ \frac{\sigma(\pm)(e^{\nu(\log a_t)} + e^{-\nu(\log a_t)})}{|e^t - e^{-t}|}, & \text{if } x \text{ is conjugate to } \pm a_t, \end{cases}$$

and

$$\Theta_n(x) = \begin{cases} \frac{\alpha e^{-\alpha(n-1)i\theta}}{(e^{i\theta} - e^{-i\theta})}, & \text{if } x \text{ is conjugate to } k_\theta, \\ (\pm)^n \frac{e^{(n-1)t}(1 - sgn\, t) + e^{-(n-1)t}(1 + sgn\, t)}{2|e^t - e^{-t}|}, & \text{if } x \text{ is conjugate to } \pm a_t, \end{cases}$$

(Here $\alpha = 1$ when $\pi = \pi_n^-$ and $\alpha = -1$ when $\pi = \pi_n^+$) [7], $p.$ 342, 343.

With $f \in \mathcal{C}(SL(2,\mathbb{R}))$ we have the Plancherel inversion formula given as

$$f(1) = \frac{1}{2\pi} \sum_{k \in \mathbb{Z}^*} \mid k \mid \Theta_k(f) + (\frac{1}{2\pi})^2 \sum_{\sigma \in \widehat{M}} \int_{Re\nu = 0} \beta(\sigma, \lambda) \Theta_{\sigma,\lambda}(f) d\nu.$$

with

$$\beta(\sigma, \nu) = \begin{cases} (\frac{\lambda\pi i}{2}) \tan(\frac{\lambda\pi}{2}), & \text{if } \sigma = \sigma_+, \\ (-\frac{\lambda\pi i}{2}) \cot(\frac{\lambda\pi}{2}), & \text{if } \sigma = \sigma_-, \end{cases}$$

Hence, from Corollary 3.5, we have

$$(\mathcal{H}f)(\lambda) = \frac{1}{2\pi} \sum_{k \in \mathbb{Z}^*} \mid k \mid \pi_{k,1}(f) + (\frac{1}{2\pi})^2 \sum_{\sigma \in \widehat{M}} \int_{Re\nu = 0} \beta(\sigma, \nu) \pi_{\sigma,\nu,1} d\nu,$$

which by Lemma 3.3, becomes

$$(\mathcal{H}f)(\lambda) = \frac{1}{2\pi} \sum_{k \in \mathbb{Z}^*} \mid k \mid \Theta_k(f * \varphi_\lambda) + (\frac{1}{2\pi})^2 \sum_{\sigma \in \widehat{M}} \int_{Re\nu = 0} \beta(\sigma, \nu) \Theta_{\sigma,\nu}(f * \varphi_\lambda) d\nu.$$

Hence

$$(\mathcal{H}f)(\lambda) \leq \mid \frac{1}{2\pi} \sum_{k \in \mathbb{Z}^*} \mid k \mid \Theta_k(f * \varphi_\lambda) + (\frac{1}{2\pi})^2 \sum_{\sigma \in \widehat{M}} \int_{Re\nu = 0} \beta(\sigma, \nu) \Theta_{\sigma,\nu}(f * \varphi_\lambda) d\nu \mid$$

$$\leq \frac{1}{2\pi} \sum_{k \in \mathbb{Z}^*} \mid k \mid \cdot \mid \Theta_k(f * \varphi_\lambda) \mid + (\frac{1}{2\pi})^2 \sum_{\sigma \in \widehat{M}} \int_{Re\nu = 0} \mid \beta(\sigma, \nu) \mid \cdot \mid \Theta_{\sigma,\nu}(f * \varphi_\lambda) \mid d\nu.$$

By a calculation similar to that of [11], $p.$ 271, there exist continuous seminorms, $\lambda \mapsto v_1(\lambda) := v_1(\varphi_\lambda)$ and $\lambda \mapsto v_2(\lambda) := v_2(\varphi_\lambda)$ such that

$$\mid \Theta_{\sigma,\nu}(f * \varphi_\lambda) \mid \leq (1+\mu^2)^{-2} \cdot v_1(\varphi_\lambda)$$

and

$$\mid \Theta_k(f * \varphi_\lambda) \mid \leq m^{-4} \cdot v_2(\varphi_\lambda).$$

Thus

$$(\mathcal{H}f)(\lambda) \leq v_2(\lambda) \cdot \sum_{m \neq 0} \mid m \mid^{-3} + c v_1(\lambda) \cdot \int_0^\infty \mu(1+\mu^2)^{-2} d\mu,$$

proving that $\mathcal{H}f$ is a continuous seminorm on $\mathbb{R}$, as expected in Theorem 3.8. A similar computation suggests Conjecture 3.11.

References.

[**1.**] Arthur, J. G., (*a.*) *Harmonic analysis of tempered distributions on semisimple Lie groups of real rank one,* Ph.D. Dissertation, Yale University, 1970; (*b.*) *Harmonic analysis of the Schwartz space of a reductive Lie group I,* mimeographed note, Yale University, Mathematics Department, New Haven, Conn; (*c.*) *Harmonic analysis of the Schwartz space of a reductive Lie group II,* mimeographed note, Yale University, Mathematics Department, New Haven, Conn.

[**2.**] Barker, W. H., L^p harmonic analysis on $SL(2,\mathbb{R})$, *Memoirs of American Mathematical Society, vol.* **76** , no.: **393**. 1988

[**3.**] Eguchi, M., (*a.*) The Fourier Transform of the Schwartz space on a semisimple Lie group, *Hiroshima Math. J., vol.* **4**, (1974), pp. 133 – 209. (*b.*) Asymptotic expansions of Eisenstein integrals and Fourier transforms on symmetric spaces, *J. Funct. Anal.* **34**, pp. 167 – 216.

[**4.**] Ehrenpreis, L. and Mautner, F. I., Some properties of the Fourier transform on semisimple Lie groups, I, *Ann. Math., vol.* **61** (1955), pp. 406-439; II, *Trans. Amer. Math. Soc., vol.* **84** (1957), pp. 1 – 55; III, *Trans. Amer. Math. Soc., vol.* **90** (1959), pp. 431 – 484.

[**5.**] Gangolli, R. and Varadarajan, V. S., *Harmonic analysis of spherical functions on real reductive groups,* Ergebnisse der Mathematik und iher Genzgebiete, *vol.* **101**, Springer-Verlag, Berlin-Heidelberg. 1988.

[**6.**] Helgason, S., (*a*) A duality for symmetric spaces with applications to group representations, *Advances in Mathematics, vol.* **5** (1970), pp. 1 – 154. (*b*) *Differential geometry and symmetric spaces,* Academic Press, New York, 1962.

[**7.**] Knapp, A.W., *Representation theory of semisimple groups; An overview based on examples,* Princeton University Press, Princeton, New Jersey. 1986.

[**8.**] Oyadare, O. O., On harmonic analysis of spherical convolutions on semisimple Lie groups, *Theoretical Mathematics and Applications, vol.* **5**, no.: **3**. (2015), pp. 19 – 36.

[**9.**] Trombi, P. C. and Varadarajan, V. S., Spherical transforms on semisimple Lie groups, *Ann. Math., vol.* **94**. (1971), pp. 246-303.

[**10.**] Varadarajan, V. S., Eigenfunction expansions on semisimple Lie groups, in *Harmonic Analysis and Group Representation,* (A. Figà Talamanca (ed.)) (Lectures given at the 1980 Summer School of the *Centro Internazionale Matematico Estivo (CIME)* Cortona (Arezzo), Italy, June 24 - July 9. vol. **82**) Springer-Verlag, Berlin-Heidelberg. 2010, pp. 351 – 422.

[**11.**] Varadarajan, V. S., *An introduction to harmonic analysis on semisimple Lie groups,* Cambridge Studies in Advanced Mathematics, **161**, Cambridge University Press, 1989.

INDEX
HADRONIC JOURNAL, VOLUME 47, 2024